GRAIN GROWTH CHARACTERISTICS IN THREE NICKEL-COBALT ALLOYS

By

DIPTI GUPTA

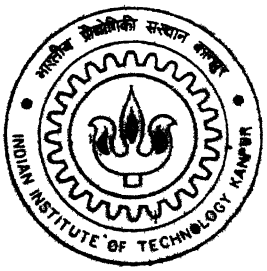

DEPARTMENT OF MATERIALS AND METALLURGICAL ENGINEERING

Indian Institute of Technology Kanpur

FEBRUARY, 2002

GRAIN GROWTH CHARACTERISTICS IN THREE NICKEL-COBALT ALLOYS

A Thesis Submitted

in Partial Fulfilment of the Requirements

for the Degree of

MASTER OF TECHNOLOGY

By

DIPTI GUPTA

To the

DEPARTMENT OF MATERIALS AND METALLURGICAL ENGINEERING

Indian Institute of Technology, Kanpur

FEBRUARY, 2002

CERTIFICATE

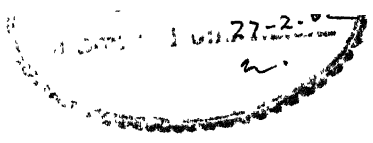

This is to certify that the present work, entitled **"GRAIN GROWTH CHARACTERISTICS IN THREE NICKEL-COBALT ALLOYS"** by Ms. Dipti Gupta has been carried out under my supervision and to the best of our knowledge it has not been submitted elsewhere for a degree.

Dr. R.K.Ray
Professor
Deptt. Of Materials & Metallurgical Engg.
Indian Institute of Technology, Kanpur
Date:

Dedicated to my parents....

Acknowledgement

At the very onset, I wish to express my earnest respect, deep sense of indebtedness and gratitude to my thesis supervisor **Prof. R.K. Ray** for his invaluable guidance, constant encouragement and endless cooperation throughout my tenure without which this work would never have been materialized successfully.

I am truly thankful to all the staff members of the Department of Materials and Metallurgical Engineering; technicians and operators of Phase Stability Lab, Metallography Lab & Physical Metallurgy Lab.

I warmly acknowledge the cooperation extended to me by Dr. M. N. Mungole and Mr. V. Kumar for their help in my experimental work.

I can not forget association and cooperation of my friends Pinaki Prasad Bhattarcharya, Suhash Ranjan Dey, Krishnendu Mukherjee and Arijit Saha Poddar without whose names my thesis is incomplete.

I would like to express my sincere thanks to my friend Manish for his constant support, inspiration and willingness to extract best out of me.

There are the pleasant tasks of acknowledging a number of friends from inside the campus, to be candid; itemizing their names would be nothing compared to what I have received from them.

At last but not the least , I would like to acknowledge my grandparents, my parents, my loving brother and my uncle without whose patience and constant inspiration, I could not become what I am.

February 27,2002 Dipti Gupta
I.I.T. Kanpur

ABSTRACT

Four different heat treatments were given to three Nickel-Cobalt alloys in order to make the grain size distribution uniform and crystallographically random. However, for all the samples and for all the heat treatments, microscopic observations showed invariably a duplex microstructure consisting of colonies of small grains embedded in a matrix of big grains . It was then decided to carry out a detailed statistical analysis of grain size distribution in all the samples to study their grain growth characteristics. For this purpose, the frquency of grain size distribution was determined considering (I) the big grains alone, (ii) the small grains in the coloies alone and also taking (iii) the duplex distribution of grains as a single entity.

From the results of this study some important conclusions could be arrived at. Most importantly it was found that the growth rate of small grain in the colonies is higher than that of the big matrix grains. Not only that, even within the small grain colony, the ones which are relatively finer in size grow faster than their counterparts that are relatively coarse. This is contrary to our usual observations during grain growth, where the bigger grains are known to grow at the expense of the smaller ones. This has been suggested to be due to the possible effect of grain orientations on the relative mobility of grain boundaries. In general, the finer sizes of the grains in the Ni-40Co and Ni-60Co alloys, has been ascribed to the effect of the substantial solutes like Co on the movement of grain boundaries.

INDEX

LIST OF FIGURES

S.No. **TITLE**

(a) 50pct.820°C-3h(i)

(b) 50pct.820°C-3h(ii)

(d) Annealed-820°C-10h

(d) Annealed-850°C-3h

Figure 38. . Histograms for Big Grains for Ni-60Co Samples for the heat treatments

(a) 50pct.820°C-3h(i)

(b) 50pct.820°C-3h(ii)

(e) Annealed-820°C-10h

(d) Annealed-850°C-3h

Figure 39. Histograms for Small Grains for Ni-30Co Samples for the heat treatments

(a) 50pct.820°C-3h(i)

(b) 50pct.820°C-3h(ii)

(f) Annealed-820°C-10h

(d) Annealed-850°C-3h

.Figure 40. Histograms for Small Grains for Ni-40Co Samples for the heat treatments

(a) 50pct.820°C-3h(i)

(b) 50pct.820°C-3h(ii)

(g) Annealed-820°C-10h

(d) Annealed-850°C-3h

Figure 41. Histograms for Small Grains for Ni-60Co Samples fo the heat treatments

(a) 50pct.820°C-3h(i)

(b) 50pct.820°C-3h(ii)

(h) Annealed-820°C-10h

(e) Annealed-850°C-3h

Figure 42. Histograms for Mixed Grains for Ni-30Co Samples for the heat treatments

(a) 50pct.820°C-3h(i)

(b) 50pct.820°C-3h(ii)

(i) Annealed-820°C-10h

(f) Annealed-850°C-3h

Figure 43. Histograms for Mixed Grains for Ni-40Co Samples for the heat treatments

(a) 50pct.820°C-3h(i)

LIST OF TABLES

Chapter 1

INTRODUCTION

The common metals and alloys which are used during familiar industrial practices are the polycrystalline aggregates in which grain size distribution is supposed to be random. Control of grain size is usually affected by applying the empirical 'Laws of Recrystallisation'. For instance, if a coarse grained material is required, either the process schedule is arranged so that a low total reduction precedes the final anneal or a long annealing treatment is given as to allow extensive growth. However this generalisation is too simple and many other factors like orientation dependence of grain boundary mobility, stacking fault energy, activation energy of grain growth, composition, annealing time, annealing temperature etc. play very important role in deciding the grain growth characteristics.

The anisotropy of boundary migration rate can be interpreted as due to the orientation dependence of either the driving force or the boundary mobility. In highly deformed materials which show a complex dislocation substructure, the anisotropy of driving force can be ruled out as a possibility and hence an orientation dependence of boundary mobility is quite expected. The influence of orientation of grain boundary on its migration rate can be approached from two points of view , phenomenological-geometric and structural-atomistic. Both these considerations should be co-ordinated with one another in order to have a complete picture of grain boundary migration.

In the present work, different combinations of cold rolling and annealing have been applied to three Nickel-Cobalt alloys and the microstructures so obtained in each case is found to be of duplex type containing colonies of small grains in a matrix of large grains. In order to understand the grain growth characteristics in these three alloys, statistical analysis of the grain size distribution of small, big and mixed grains has been carried out. The results have been analysed in the light of the existing knowledge on the subject and attempts have been made to understand the basic mechanisms of grain growth in these alloys.

Chapter 2

LITERATURE REVIEW

2.1 The Cold –Worked State

The cold –worked state is usually taken as any strained or damaged condition of a crystalline material brought about by processes such as plastic deformation, particle bombardment, quenching from a high temperature or phase transformations.The principal entities responsible for the cold worked state are point defects such as vacancies and interstitials as well as linear and planar defects like dislocations and stacking faults etc. Plastic deformation of a material involves a permanent shape change produced by stressing the material beyond its elastic limits, during which any or all of the types of the defects mentioned above may be produced in the solid. As a result of its increased content of crystal defects, such a material is in a thermodynamically metastable state.

2.2 Microstructure of Cold Worked Metals

From decades transmission electron microscopic techniques have been successfully applied for determining the structures of cold worked materials. Microbeam X-Ray diffraction is also used for studying the dislocation arrangements in heavily deformed material. However thin film electron microscopy enables much more detailed studies to be made than the X-Ray method and for this reason it is now used almost exclusively.

Electron microscopic observations were made on plastically deformed polycrystalline metal and it was found that dislocations introduced into these metals by plastic deformation are arranged in cellular structure.The cell boundaries appear to consist of complex dislocation arrangements together with a large number of small loops. The misorientations across the cell walls are found to be of the order of a degree. The size of a cell may be 1-2 μm and the thickness of its wall, a few tenths of a micrometer. With increasing deformation, the total dislocation density and misorientations across cell boundaries increases and dislocations are redistributed and form dislocation arrays, which divide a grain into volumes that are relatively, free of

dislocations, i.e. a cell structure is formed. At this stage , it is very difficult to identify the grain boundaries.

Weissmann et. Al[1,29,30]. showed that for a weakly deformed (5% cold rolled) specimen the microstructures consists of long, kinked dislocations lines which, upon interaction with other dislocations, form dislocation tangles. Increasing cold-working to10% reduction by rolling, gives rise to a more pronounced dislocation entanglement and a distinct cell structure emerges. At about 30% cold reduction, the formation of cell structure is well advanced, with most of the dislocations entangles arranged in cell walls and relatively few dislocations with in the cells. The cell walls become more sharply delineated with increasing deformation. It is interesting to note that in some metals the cell interior remains relatively free of dislocations even for 90% deformation, although there exists interspersed regions of high dislocation density in which the cell structure is poorly developed. Frequently, without external annealing slip dislocations in heavily cold-rolled specimens are found to align themselves into distinct low angle boundaries, and this is regarded as a manifestation of dynamical recovery.

An important feature in the formation of a cell structure is that the size of cells is only slightly dependent on the original grain size and decreases to a certain limit with increasing deformation. Another feature typical of a cell structure is that the crystal lattice has quite strong distortions at cell boundaries, which depend on the misorientation angle θ.

In addition of usual dislocation substructure, a great number of microtwins and stacking faults are also being observed in some materials. The frequency of occurrence of microtwins and stacking faults is found to be different in different materials though they may have the same cellular structure.

2.3 Stored energy produced by cold rolling

A small fraction of the energy(usually from 1% to 10%) expended in plastic deformation of the metal gets stored in the metal in the following forms:

a) Elastic strain energy

b) Energy of dislocations
c) Energy of point defects
d) Energy associated with stacking faults and twins
e) Energy associated with the disordering

This stored energy causes increase in internal energy of the material. Investigations shows that this increase in internal energy is mainly due to lattice defects and elastic energy contribution is usually very small. The amount of stored energy depends on the purity and composition of metal, deformation method, temperature and grain size.

From the dislocation density and distribution data, one can estimate the stored energy due to dislocations. Annealed metals normally have dislocation densities between 10^6 to 10^8 lines/cm^2 and severely cold-worked metals have usually between 10^{10} to 10^{12} lines/cm^2. The distribution of dislocations depends on metal, its purity and history of deformation.

The stored energy due to vacancies and interstitial atoms is small and can be estimated by measured resistivity changes.

Stacking faults account for the appreciable portion of the stored energy and its distribution also depends on the temperature of deformation. Deformation twins on a fine scale comparable to stacking faults may also contribute significantly to stored energy.

During cold work the movement of dislocations can cause disordering, or shearing of precipitates and cluster of solute atoms which again causes increase in internal energy of the material.

The data, from the work of Gordon[2], show that the stored energy increases with increasing deformation, but at a decreasing rate, so that the fraction of the total energy stored decreases with increasing deformation. The amount of stored energy can be greatly increased by increasing the severity of the deformation, lowering the deformation temperature, and by changing the pure metal to an alloy.

2.4 Release of Stored Energy during Annealing

A plastically deformed material due to its increased content of physical defects is in a thermodynamically metastable state. On increasing the temperature the material can lower its free energy by the removal and rearrangement of lattice defects. A systematic classification of the multitude of the phenomena that may occur on annealing the cold-worked material (below the melting point) can be done in terms of five fundamental structural process which are essentially the following:

(a) Reaction of point defects and point defect agglomerates ; in particular the anihilation of these defects.

(b) The anihilation of defects of opposite signs and the shrinking of dislocation loops.

(c) The rearrangement of dislocations to form energetically more favorable configurations.

(d) The absorption of point defects and dislocations by grain boundaries migrating through the metal.

(e) The reduction in total grain boundary area.

In general, the processes (a) and (b) are termed as 'recovery' and processes (d) and (e) as 'recrystallisation'. In general, the term recovery is supposed to constitute all those annealing phenomena which occur before the appearance of new strain-free-recrystallised grains. 'Recrystallisation' is supposed to involve nucleation and growth of these strain-free grains and the gradual consumption of the cold-worked matrix by the movement of large angle boundaries. Here it is important to note that it is very difficult to draw a distinction between recovery and recrystallisation , and in practice the two processes are usually found to overlap one another.

It is assumed so far that the unstable state is formed prior to annealing. If, however , the unstable state is formed during annealing, e.g. by plastic deformation at sufficiently high temperatures, then one is dealing with case of 'dynamic recovery' or 'dynamic recrystallisation'.

As has been mentioned, the stored energy of cold work provides the driving force for both recovery and recrystallisation. For a given set of materials and deformation conditions, the stored energy is fixed and finite in magnitude. Hence the

apportionment of the stored energy release between the two processes will depend on the relative ease or difficulty of their occurrence.

Two different types of stored energy release during recovery are usually observed. Sharp peaks of energy release are found in case of purer materials and in few impure materials. In almost all impure materials , however , the energy is released over an extended range of temperature and may be either a flat-plateau constant-rate type or gradually increasing rate type. In contrast with recovery, the energy releases during recrystallisation are always of distinct peak type. Illustrations are shown in fig (2) and fig (3). Fig (2) clearly indicates that in the less pure metal ,both peaks due to recovery and recrystallisation appear to be superimposed on a plateau whereas two distinct energy releases can be observed in the purer material. Another point to be noted in this figure is that the second peak (due to recrystallisation) occurs at a much lower temperature (450°C) in the purer material than in the less pure material where it appears at a temperature of about 650°C.

A significant difference in the behaviour of stored energy release for two grades of Copper of 99.67% and 99.988% purity is shown in fig(3). Both the materials were deformed to the same extent and it was found that for the purer material the fraction of stored energy release during recovery ,and also the recrystallisation temperature, was less than the more impure metal .

Alloying can also significantly change the energy release characteristics of deformed material on heating. Fig(4) shows the power difference (ΔP) as a function of temperature obtained at a heating rate of 6°C/min. for 99.98% copper reduced to 45% and for arsenical copper(35%As) reduced to 40%. It is clearly seen that for the pure copper one sharp peak occurs at 300°C whereas for arsenical copper a smaller peak occurs at 440°C. This latter peak is superimposed on a low energy release plateau which begins to appear at 70°C.

Both the total stored energy and the manner in which stored energy is released depends on the grain size.It was found that for the fine grain sized material the energy is released more rapidly than for the coarse grain sized material. It has also been

material than in the coarse grained. For higher strains, however, the total stored energy is same for both grain sizes but the recrystallisation temperature is always found to be lower in the fine grained material.

The magnitude of stored energy released is also dependent on the temperature of plastic deformation. It was found that on increasing the temperature of plastic deformation the released energy gets lessened.

2.5 Recovery

During recovery the material tends to relax, and its internal energy reduces. This decrease in internal energy is achieved by migration of vacancies and dislocations leading to redistribution and annihilation of point defects and dislocations. In this process new grain boundaries do not form and so microstructurally no distinguishable changes are observed.

2.5.1 Property changes during recovery

During recovery material tends to recover its physical and mechanical properties that are changed during cold work but these properties show some changes from the cold-worked values. Normally the restoration of a mechanical property such as hardness or yield strength to its fully annealed value is only about one-fifth completed during recovery.

Physical properties like density and electrical resistivity are also found to undergo detectable change from their cold-worked values during subsequent annealing. The introduction of lattice defects like vacancies and dislocations produce a slight decrease in the density of material during cold –working. During annealing when a gradual loss of these defects take place ,the density again approaches its annealed value during recovery and continues to do so during further annealing leading to recrystallisation.

Electrical resistivity changes from the cold-worked values are frequently employed to follow the progress of both recovery and recrystallisation. It is found that resistivity shows a slight decrease from its cold-worked value during the recovery anneal and rather a sharper decrease as the annealing temperature is increased and

recrystallisation starts. The progress of the recovery process on annealing a cold-worked metal can also be studied by following the changes of X-Ray line broadening. Two factors, particle size and residual stress determine the extent to which X-Ray line is broadened, and the two contributions may be separated using Fourier Analysis Techniques. Using this analysis it has been shown that during the recovery of cold-worked metal, the particle size increases and residual stress decreases.

2.5.2 The kinetics of recovery

It has been found that, in general, the rate of recovery of a property from the cold-worked value depends on instantaneous value of that property. If R is fraction of a property recovered at any time , then we can write

$$\frac{d(1-R)}{dt} \quad \alpha \quad (1-R) \qquad \ldots\ldots\ldots\ldots\ldots\ldots\ldots\ldots 1$$

which on integration gives

$$\ln(1-R) = kt \qquad \ldots\ldots\ldots\ldots\ldots\ldots\ldots\ldots 2$$

This indicates that rate of recovery decays exponentially with time.

Another rate law can be described by hyperbolic law as,

$$1-R = b - a \ln t \qquad \ldots\ldots\ldots\ldots\ldots\ldots\ldots\ldots 3$$

where a and b are both constants dependent on recovery temperature.

Another expression describing the kinetics of recovery process is given by

$$Lnt = \ln A + \frac{Q}{RT} \qquad \ldots\ldots\ldots\ldots\ldots\ldots\ldots\ldots 4$$

Where t is the time required for some particular fraction to be recovered at temperature T, A is a constant and Q is the activation energy for recovery.

.

2.5.3 Recovery mechanisms

Electron microscopic evidence shows that a cold worked metal has cell structure. The cell walls consists of dislocation tangles, and some additional dislocations are found to exist in the cell interiors. As annealing starts, the tangled dislocations in the cell

walls rearrange themselves while some dislocations from within the cells may get attracted to cell walls. During the whole process of recovery dislocation annihilation probably occurs since the dislocation density in the cell interiors is found to decrease gradually on continued annealing. The cell walls become more clearly defined and eventually form sub-grains of about the same size as the initial cells. The sub-grain size does not change much until quite late in the recovery process when it starts increasing slightly. Thus, in general, three processes – dislocation annihilation, subgrain formation and sub-grain growth – may take place during the recovery of most of the metals.

(a) Dislocation annihilation

Keh[3] found the direct experimental evidence, that the dislocation density decreases during the initial stages of recovery. But presumably this does not involve the movements of dislocations over long distances. According to Li[4], dislocation annihilation takes place in the cell boundaries.

It has also been found that elongated dislocation loops, if formed during plastic deformation, will, during recovery, gradually becomes circular and finally vanish. Similarly, stacking faults also, can be annealed out during the recovery stage.

(b) *Polygonisation and sub-grain formation*

Polygonisation is a process which leads to rearrangement of dislocations, with a resulting lowering of lattice strain energy. It can also be understood as the process of formation and coarsening of sub-grains during heating of cold worked metals and alloys. Sub-grains are formed by redistribution of individual dislocations and/or by 'flattening' of spatial dislocation pile-ups due to dislocation slip and climb, with the formation of low-angle dislocation sub-boundaries. Coarsening of sub-grains is realized by their coalescence or by migration of sub-boundaries.

The phenomenon of polygonisation was first proposed by Orowan[5] .The first clear picture of polygonisation was proposed by Cahn[6,10] who reported the results of a study on the effects of annealing bent single crystals of aluminium, zinc, and sodium chloride. These crystals were bent about an axis parallel to their active slip planes. Cahn studied both the deformed and annealed and deformed states in these crystals by taking transmission Laue patterns with the X-Ray beam normal to the active slip

bent crystals became discontinous after anneal. This effect implies that a plastically bent crystal disintegrates on annealing into a number of structurally perfect blocks which are discretely tilted through small angles relative to one another, with misorientation of the crystal remaining unchanged. In that case, each spot is a trace of an interference beam 'reflected' from an individual block.

This has been explained as due to a process – polygonisation – which leads to a rearrangement of dislocations, with a resultant lowering of the lattice strain energy. The mechanism has been shown schematically in Figure5. The random arrangement of excess parallel edge dislocations produced during deformation can clearly be seen, on heating, to align themselves, into walls to small angle, polygonisation or sub-grain boundaries by a process of annihilation and rearrangement. That the dislocation walls so produced were normal to the main slip planes active during bending was verified by Cahn[25] by producing etch pits after the anneal. The process of polygonisation is believed to start with the glide and climb of individual dislocations, thereby forming small segments of boundary perhaps five to ten dislocations high. By further glide and climb these short range boundary segments then combine to give larger boundaries, still of low angle, which may now be termed long range. At higher temperature the spacings between these boundaries are found to increase and this lies led to the suggestion by Dunn and Daniel[7,8] and later Gilman[9] that two neighbouring boundaries may coalesce. This is thought to take place by the so called Y-junction mechanism which produces a single boundary (Figure6). Although misorientation across the single boundary will be the sum of both the original boundaries, the total energy of the system is lowered by this mechanism. The same suggestion was made by Bryshko et.al[11]. during their work on steady state creep at elevated temperature.

(c) *Sub-grain growth*

For the explanation of the sub-grain growth phenomenon during recovery, two mechanisms : sub-boundary migration and sub-grain coalescence , have been proposed. During this process, a slight increase in average particle size occurs prior to recrystallisation temperature.

Growth by sub-grain boundary migration may be thought of similar in terms to primary grain growth, where grains larger than a critical size are supposed to grow at

the expense of those which are small than the critical size. The rate of growth of a particular sub-grain is given as

$$\frac{dR}{dt} = M\left(\Delta G - \frac{2\sigma}{R}\right) \quad \text{.....5}$$

where R is the radius of the growing sub-grain

M is the interface mobility

Δ G is the free energy per unit volume for growth

and σ is the specific surface energy of the interface.

At equilibrium, $\frac{dR}{dt} = 0$ 6

$$R = \frac{2\sigma}{\Delta G} \quad \text{.....7}$$

It follows that growth will occur if

$$R > \frac{2\sigma}{\Delta G} \quad \text{.....8}$$

Sub-grain growth by way of subgrain boundary migration has been objected to on the grounds that low angle boundaries are relatively immobile.

The coalescence model of sub-grain growth proposed by Hu[12,13,15] overcomes the problem of boundary mobility to a large extent. According to this the increase in size of subgrains during recovery is due to a coalescence process whereby adjoining subgrains having slightly different orientation merge into the same orientation giving rise to a bigger subgrain.The entire process of coalescence is shown schematically in fig(7). The whole process probably requires some co-operative climb of dislocations along the disappearing sub-grain boundary and also some atom movements by vacancy diffusion around the sub-grains. The kinetics and thermodynamics of the coalescence process had also been observed in detail by Li[17].

The energy of a sub-grain boundary, E, is related to the misorientation across it, θ, by the Read-Shockley[18] equation

$$E = E_o \theta (A - \ln \theta) \ldots\ldots\ldots\ldots\ldots\ldots\ldots\ldots\ldots\ldots 9$$

Where, E_o and A are both constants. An E versus θ plot is shown in Figure8 . This curve reaches a maximum when $\theta = e^{A-1}$. Hence,

$$E_{max} = \theta_{max} E_o (A - \ln \theta_{max}) \ldots\ldots\ldots\ldots 10$$
$$= \theta_{max} E_o$$

So, the equation () can now be also written as,

$$\frac{E}{E_{max}} = \frac{\theta}{\theta_{max}} \left(1 - \ln \frac{\theta}{\theta_{max}} \right) \ldots\ldots 11$$

Gjasten and Rhines[19] pointed out that this equation is misleading since it ensures a good fit even at high values of θ. By measuring absolute values fir the boundary energies in Copper , they were able to show that Read-Shockley equation can be applied to tilt and twist boundaries for angles up to 6° and 3° respectively.

In any case, the equation (11) predicts that by lowering the misorientation across a sub-boundary the overall energy of the system is decreased. The two neighbouring sub-groups of small misfit, could rotate naturally in a direction which enables low angle boundaries to decrease their angles of misfit. In fact, the mechanism of sub – grain growth on the basis of coalescence model can be treated either in terms of co-operative vacancy diffusion or co-operative climb and also the rate of rotation determined as a function of $\theta \setminus \theta_{max}$. It has been estimated that the time required to eliminate the common boundary between two adjoining sub-grains of slightly different orientation is given by

$$t = \frac{L^2 kT}{3DE_o b^3 j} \ldots\ldots\ldots\ldots\ldots\ldots\ldots\ldots 12$$

where L is the sub -grain size, D is the diffusion coefficient, and j is the jog density. This equation shows reasonable agreement between the predicted and measured rates of sub-grain growth in a material.

2.6 Recrystallization

Recrystallization is a process which involves the nucleation and growth of new strain-free grains which may be widely different in orientation from the surrounding matrix. Recrystallization is a multi-stage process and can be identified as made up of two consequent processes.

Primary recrystallisation

The process occurs in a cold deformed matrix through the appearance and motion of high-angle boundaries It can occur either immediately after polygonization or at the same time with polygonization occuring in the neighbouring portions. This stage reduces most readily the number of crystal structure defects introduced by prior deformation and accordingly the stored volume energy of deformation, up to full restoration of the structure and properties the material has had before the deformation.

Secondary Recrystallisation

If a material in which primary recrystallization is completed is heated further at the same or a higher temperature, it will pass through the stage of grain growth and/or *secondary recrystallization.* In this process, grains which have grown from primary recrystallization nuclei will grow further at the expense of their neighbours by migration of their high-angle boundaries. The size of grains and their distribution in size can vary upto the formation of single crystals (a rare but principally possible case), with there crystallographic orientation being also changed (recrystallization texture). These stages of recrystallization are also associated with reduction of the free energy of the system, though not so intensive as in primary recrystallization.

The difference between grain growth and secondary recrystallization consists in that the former process occurs uniformly whereas the latter does not since there are some grains which, for certain reasons, can grow at an appreciably higher speed than others and thus serve as secondary 'nuclei'.

2.6.1 Nucleation of Recrystallised Grains

Through the advent of transmission electron microscopy, it becomes possible to observe a nucleus before it starts growing, since the structure and orientation of small regions can be examined in detail.

2.6 Recrystallization

Recrystallization is a process which involves the nucleation and growth of new strain-free grains which may be widely different in orientation from the surrounding matrix. Recrystallization is a multi-stage process and can be identified as made up of two consequent processes.

Primary recrystallisation

The process occurs in a cold deformed matrix through the appearance and motion of high-angle boundaries It can occur either immediately after polygonization or at the same time with polygonization occuring in the neighbouring portions. This stage reduces most readily the number of crystal structure defects introduced by prior deformation and accordingly the stored volume energy of deformation, up to full restoration of the structure and properties the material has had before the deformation.

Secondary Recrystallisation

If a material in which primary recrystallization is completed is heated further at the same or a higher temperature, it will pass through the stage of grain growth and/or *secondary recrystallization.* In this process, grains which have grown from primary recrystallization nuclei will grow further at the expense of their neighbours by migration of their high-angle boundaries. The size of grains and their distribution in size can vary upto the formation of single crystals (a rare but principally possible case), with there crystallographic orientation being also changed (recrystallization texture). These stages of recrystallization are also associated with reduction of the free energy of the system, though not so intensive as in primary recrystallization.

The difference between grain growth and secondary recrystallization consists in that the former process occurs uniformly whereas the latter does not since there are some grains which, for certain reasons, can grow at an appreciably higher speed than others and thus serve as secondary 'nuclei'.

2.6.1 Nucleation of Recrystallised Grains

Through the advent of transmission electron microscopy, it becomes possible to observe a nucleus before it starts growing, since the structure and orientation of small regions can be examined in detail.

2.6.1.1 Models of Nucleation

The three principal models of nucleation are : Classical Nucleation Model , Sub-grain growth Model and Strain Induced Boundary Migration Model.

(a) *Classical nucleation model*

The classical Volmer-Becker theory of nucleation, as ordinarily applied to the formation of solid nuclei in supercooled liquids has been extended by Burke and Turnbull[20] to the nucleation problem during primary recrystallisation. This model is based on the assumption that the nucleus which is stable and capable of growth is formed as a result of thermal fluctuations in the sense of the classical nucleation theory of phase transition. A critical nucleus size is determined by the condition that for the nucleus to be just stable, the free energy will not change due to an infinitesimal increase in size, because the reduction in volume free energy will just balance the increase in interfacial energy. In this model the volume free energy change is defined as the difference in strain energy per unit volume between the cold- worked state and the fully recrystallised condition. Similarily, the interface between the recrystallising nucleus and the surrounding deformed matrix can be envisioned approximately as a small angle tilt boundary. New grains should want to form only very small misfit angles with the matrix, since this would lead to lower values of the interfacial energy. Thus plus point of this model is that it can account for existence of of an incubation period. It also predicts the preferential nucleation of recrystallized grains in the most severely deformed regions. This theory has the disadvantage that it predicts that new grains should always be close in orientation with respect to the adjacent cold-worked matrix. Another drawback of this theory is that no effect of purity is allowed for, yet purity very often seems to be of paramount importance in recrystallization.

(b) *Sub-grain growth model*

Originally this model was based on the idea that the cells produced in the cold-worked materials gradually become strain free during annealing by classical polygonisation. Further growth or coarsening of these polygonised cells or sub-grains was supposed to lead to the formation of a recrystallised grains. Now this model has evolved into something which can best be explained by a sketch (Fig9a).The essence of this model

gradient , and by implication of substantial local misorientation, turns into a small strain-free cell by a process of dislocation climb and rearrangement. The structure becomes akin to a cell structure created by creep, and it is known by X-Ray analysis that the boundaries of such cells have dislocations structures similar to sub-boundaries formed by classical polygonisation(of macroscopically bent single crystals).

Once a dislocation-free subgrain has formed, it can grow into its neighborhood. Any subgrain population is characterised by two distinct parameters – the distribution of sizes of the sub-grains and the distribution of the misorientations of subgrains relative to their immediate neighbours. A subgrain can grow at the expense of its immediate neighbours for two distinct reasons: (I) It is substantially larger than its neighbours, so that the triple point angles where it periphery abuts on other sub-boundaries depart from 120° equilibrium (Fig9b) . The subgrain grows because of the attempt to get these triple points back to its equilibrium. This argument is exactly like the accepted interpretation of the coarsening of the large grains in secondary recrystallisation. The argument only applies strictly if all the sub-boundaries in Fig.9b have the same energy, i.e. all misorientations between nearest neighbours are of the same type and magnitude.

Cahn[14,25] has suggested that when a sub-grain starts growing its boundaries sweep up most of the dislocations which they come in contact with. Thus, the periphery of a growing sub-grain acquires an even higher dislocation density. As the sub-boundary angle increases there varies a point at which the individual dislocations on a boundary begin to loose their identity and it is at this stage that the boundary changes its character from a sweeper up of dislocations to a destroyer of dislocations. With such a state of affairs the growth of the enlarging sub-grain may be expected to accelerate. However early works on recrystallisation has fairly established that larger new grains do not readily grow into matrix regions of orientations only a few degrees different from their own. Thus the growth of enlarged sub-grains can be ensured only if long range lattice curvatures exist in cold-worked metal. This whole exercise leads to the point that which is difficult to rationalize, namely, that small angle boundaries consisting of separate identifiable dislocations migrate freely while boundaries of rather larger angles do not , unless the misorientations across them exceeds about 10-15°. Cahn[14] used the terms 'sub-boundary' and 'boundary' to distinguish between the

two categories. However it has not been analyzed perfectly that at what stage the transition from sub-boundary to boundary takes place. Fig(10) shows schematically what has been observed to happen within a sharply misoriented deformation band in cold-rolled Si-Fe. Here relatively large sub-grains have been found to act as preformed nuclei which grow into neighboring sub-grains having sharply different orientations. When this nuclei become large enough to reach the highly misoriented matrix region, the attain large angle boundaries and are then favored for further growth. Evidences of sub-grain growth by boundary migration, ultimately, giving rise to recrystallised grains have also been observed.

The stored energy in cold-worked metal is inefficient for homogenous nucleation of new grains in recrystallisation. Several models for inhomogeneous nucleation were examined taking in consideration of the geometry of the nucleation of the new grains at old grain boundaries shows these sites to be undesirable due to large contact angle. Others have considered the possibility of a low angle grain boundary between the deformed grain and the nucleus , but in this case the lack of mobility of the low angle grain boundaries results in polygonisation rather than recrystallisation. Only boundaries that have misorientations greater than 20° are the potential nuclei. Further, a subgrain of the same size as its neighbour will be unstable, that the subgrain must have a size advantage over its neighbour and at least one high angle boundary to function as a nucleus.

Another sub-grain growth model of nucleation has been termed as 'sub-grain coalescence' model – the mechanism of which has already been described (Fig.11). This model says that a recrystallisation nucleus results from a consequence of sub-grain coalescence process.

(c) *Strain induced boundary migration*

This is basically a model of growth since it assumes that the unstable cold-worked state already has large angle boundaries of macroscopic and microscopic dimensions and that during recrystallisation these boundaries simply bow out leaving strain-free material behind. Here it is observed that recrystallization does not involve any nucleation but only growth of strain-free regions brought about by grain-boundary migration. This process which has been termed as strain-induced boundary migration,

consists of the irregular movement of an existing boundary with an irregular jagged front, which is shown schematically in Figure12 .According to this model there is no incubation period, since no nucleus of new orientation has to be formed. Frequently it is observed that the victim grain is the one which is more severely work-hardened, the stored energy of this grain provides the driving force for the entire process. The grain with the larger cell-size will have the lower energy, so that recrystallization occurs by the movement of a portion of the boundary into the high energy grain having a smaller cell-size. According to Doherty[33], nucleation at a grain boundary by strain-induced boundary migration requires a heterogeneity of sub-grain size which was achieved (in Al) by sub-grain coalescence, but this coalescence only occurs where a deformation band was present. In iron reduced 40%, the heterogeneous strain allowed nucleation by a strain-induced boundary migration without the need of free coalescence.

Bailey and Hirsch[21,22] developed a simple model to analyze the energetics of this process. According to their model local regions of an original grain boundary migrate by bowing out into the shape of a spherical cap. Figure13 shows how a length 2L of a grain boundary gradually bulges out to successively larger sizes. They have shown that growth rate of the recrystallizing grain can be written as,

$$\frac{dv}{dt} = A\,b\,f\left[E-\gamma\left(\frac{dA}{dv}\right)\right] \quad \text{.....13}$$

where, v = volume of the recrystallising grain

A = area of the recrystallising grain

E = difference in stored energy per unit volume across the migrating boundary

γ = specific grain boundary energy

b3 = volume occupied by one atom

and

$$f=\left(\frac{\nu K}{RT}\right)\exp\left(-\frac{\Delta F_a}{RT}\right) \quad \text{.....14}$$

where ΔF_a = free energy difference per gram-atom between an atom in the initial state and the new activated state

R = gas constant

T = absolute temperature

K = atomic weight / density

and ν = atomic jump frequency.

It has been shown that the condition for growth to occur can be given by the expression

$$L > \frac{2\gamma}{E} \quad \text{.....15}$$

Bailey and Hirsch[21,22] found this criterion to be approximately satisfied in their own work on cold-rolled deformed silver.

2.6.2 Role of Transition Bands in the Recrystallisation of Metals

It is generally found that in cold-worked metals there are regions of high local deformation and sharp lattice curvature. Such regions which results from inhomogenous deformation of metals , have been termed as 'transition bands'. During annealing , nucleation has frequently been observed to occur within these bands. The conditions under which transition bands may be created during deformation and the mechanism by which recrystallised grains can develop there, are given as following...

(i) For the nucleation of recrystallised grain within the transition band the local curvature should not be too high or too low but rather have an intermediate value.

(ii) Nucleation will be favored if there is structure gradient of increasing dislocation density on either side of the centre of the orientation spread.

(iii) The strains at which the transition band is such as to satisfy the above two condition is determined by the way in which the rate of crystal rotation is related to the orientation.

2.7 Grain boundary migration

Grain boundary migration is known to play an essential role in recrystallization and subsequent grain growth. A grain boundary may be defined as a layer of distorted material which is the result of atomic mismatch between two adjoining crystals of different orientations.

2.7.1 Orientation dependence of boundary migration

Studies on the growth of new grains in strained single crystals have convincingly demonstrated that growth can be orientation dependent. This points to the fact that there is a marked orientation dependence of grain boundary migration. By careful experiments an anisotropy of the migration rate has been confirmed. The highest migration rate in f.cc metals has been obtained when the growing grain is crystallographically related to the matrix by a 30-40° rotation about a common <111> axis. It may be pointed out that this relationship holds in the case of tilt boundaries only; for twist boundaries substantially lower rates are generally found. In principle, the anisotropy of the boundary migration rate can be interpreted as due to the orientation dependence of either the driving force or the boundary mobility. In highly deformed materials which show a complex dislocation structure, the anisotropy of driving force can be ruled out as a possibility and hence an orientation dependence of boundary mobility is quite expected. The first attempt to rationalize the orientation dependence of grain boundary mobility is due to Kronberg and Wilson[23] who proposed a grain boundary model based on lattice coincidences. The lattices of the two grains on the two sides of a special boundary do possess a special kind of sublattice. This sublattice is called 'coincidence lattice' which consists of an array of points common to lattices of both the grains. The presence of high density of coincidence atoms can make the boundaries highly mobile. A more recent model based on the concept of boundary coincidence has been proposed by Bishop and Chalmers[24] in order to characterize the special orientations which show high grain boundary mobility. The structure of a symmetric tilt boundary with a rotation of 28.1° about a <100> axis based on this model is shown in fig(14).

The orientation dependence of grain boundary migration seems to be affected strongly by the presence of impurities. Theoretical treatments of the effect of impurities on

grain boundary mobility have been presented by Cahn[25]. The theory is based on a common assumption that there is an interaction between the impurity atoms and the grain boundary and that during migration the solute atoms have to travel along with the boundary. If the driving force is large enough to overcome the dragging effect of the impurities then the boundary might breakaway from the impurity atmosphere and this according to all theories will increase the mobility considerably.

According to Ray[26] ,recrystallization was found to be easier in foils made from the transverse and longitudinal sections than from ones parallel to the rolling plane. This is due to the fact that the cells produced by deformation are pancaked shaped with the cell boundaries lying nearly parallel to the rolling plane. Foils which were taken parallel to this plane may not contain a sufficient number of cells through the thickness to allow formation of a recrystallization nucleus with a high-angle boundary. In such foils growth may also be inhibited.

During initial stages of annealing of pure Cu, in the rolling plane section, the small grains having the orientation (110) [1$\bar{1}$2] were found to nucleate in situ. In the later stages, however, cube-oriented grains appear to engulf small grains of the orientations. In contrast to rolling plane sections in transverse section foils of pure Cu (110) [1$\bar{1}$2] oriented grains are found to grow to large sizes.

The kinetics of secondary recrystallization is affected by

(i) the value and the behaviour of pinning force and

(ii) the magnitude of the driving force for grain growth.

The former depends on the volume fraction, the dispersion and the nature of the fine precipitates. The later is influenced by initial grain size distribution and the curvature of the moving boundaries. The two dimensional growth slows down the secondary recrystallization when the initial average grain size exceeds one-tenth of the sheet thickness.

2.8 Continuous Grain Growth

Continuous grain coarsening is a recrystallization process which proceeds without nucleation. Textures formed during this process are thus exclusively due to the orientation dependence of the grain boundary velocity which is the product of the

driving force and grain boundary mobility. The mobility of a boundary depends among others, on the orientation difference Δg_o of the continuous grains. The driving force in the grain coarsening is constituted by the deviation from equilibrium between the forces exerted by the grain boundaries a and b respectively as shown in Figure 5. These forces also depend on the orientation difference of the contiguous grains, i.e., go and g_{io} for a-boundaries and g_{io} and g_{jo} for the b-boundaries. In order to reduce the deviation from the equilibrium state, the system lowers its free energy by enlarging the grains , thereby reducing the surface free energy. So this is essentially a process, where a grain of a favoured orientation consumes other grains of unfavorable orientations. The interface boundary as shown in Figure moves from region 2 to region 1.

Assumption : The grains are spherical

Now dn moles of material is transferred from 1 to 2 as a result of which size of 2 is increased. Chemical free energy is same for both regions.

Δg : free energy change per mole

Total change of free energy = change in surface area x surface energy

so, $\Delta g\, dn = dA\, \sigma$

Let V_o be the molar volume. Then the change in volume of region 2 due to transfer of dn moles = $V_o\, dn = dV$

or $dn = dV / Vo = 4\pi R^2\, dR / V_o$

Now $V = 4\pi R^3 / 3$ and $A = 4\pi R^2$

Therefore, $\Delta g\, 4\pi R^2\, dR / V_o = \sigma\, 8\pi R\, dR$

Hence, $\Delta g = 2\, \sigma\, V_o / R = 4\, \sigma\, V_o / D$

For a given system V_o and σ are constant. So $\Delta g \alpha 1/D$

During the grain coarsening the rate of increase of size = dD / dt

Now growth rate $G = - V_o\, n\, A\, \nu \exp (- \Delta G / kT)\, \Delta g / kT$

Where ΔG = energy barrier and ν = vibration frequency of atoms. For a given temperature $G \alpha \Delta g$, others being constant. So $G \alpha \Delta g \alpha 1/D$ or $G = dD / dt = k / D$ which gives $D\, dD = k\, dt$, integrating the relation we have $D^2 = kt$. Now general relation is $D = k\, t^n$, $n = 0.5$ for ideal spherical shaped grains. In real situation, the value of n is observed to be less than 0.5. Usually values $n < 0.5$ were observed which were generally ascribed to the drag caused by dissolved or precipitated foreign atoms.

For an individual grain boundary it is not definite which way it should move so that the average grain size may increase. It will instead move towards its individual mean centre of curvature. This is determined by the condition that in equilibrium the three boundaries forming a grain edge should intersect at angles of 120°. Figure15 shows in the two dimensional example that this condition gives small grains (having few sides) convex boundaries and large grains (having many sides) concave boundaries, so that larger grains will tend to grow at the expense of smaller ones. Once again, grain boundary curvature serves as the means to spread the localized driving forces over the boundary area.

2.9 Preferred Orientation or Texture

2.9.1 Introduction

When a polycrystalline material is plastically deformed the lattice orientations in individual grains are found to rotate and the material thereby assumes a preferred orientation . The nature of the preferred orientation or the 'texture' which the material acquires is characteristic of the material itself and also depends on the variables connected with the deformation process. When the deformed material is recrystallised, grain rotation again takes place giving rise to a new preferred orientation.

2.9.2 Representation and Description of Textures

The most complete description of texture in a polycrystalline material can be given by stating the crystallographic orientation of each and every crystallite belonging to it. This is virtually impossible for fine-grained polycrystalline materials where the number of crystallites is high and it is therefore customary to use a statistical description instead. X-Ray diffraction methods are now widely used to yield a collective determination of orientation over a large number of crystals through scanning and integrating mechanisms. The diffracted intensity data obtained from X-Ray techniques are corrected for background intensity and absorption and then normalized relative to the intensity of a random specimen. These data are then represented by the conventional pole figures or by means of mathematical functions.

Pole figures :

Rolling plane of the material and rolling direction (crystallographic planes and direction) are needed for the determination of texture. For example, a sheet is rolled on such a way that its rolling plane is (hkl) and direction is [uvw], then its texture is represented as {hkl}<uvw>, as shown in figure16 . This is displayed by a *pole figure* which is nothing but the stereographic projection on the (hkl) plane, taking (uvw) pole as the north pole. The experimental procedure of the pole figure construction is briefly shown in Figure17 . The material is first subjected to X-ray diffraction, and the intensity vs. angle data is recorded. Then these data is transformed from a linear scale to a polar plot (pole figure). Several contours shown on the pole figure account for the different orientations of different densities.

Orientation Distribution Function :

Mathematical techniques for the representation of preferred orientations have also been proposed which involves formulation of 'orientation distribution function (ODF)' from a set of data of several individual pole figures.

It is easily understood that a frame of three mutually perpendicular axes can be superimposed on another frame of three mutually perpendicular axes. The same principle is followed here, the specimen frame as shown in Figure18a is superimposed on the crystallographic frame by means of three successive rotations (Figure 18b).

(a) A first rotation Φ_1 around N.D. transforms T.D. and R.D. into the new directions $T.D._1$ and respectively. Φ_1 has to have such a value that $R.D._1$ will be perpendicular to the plane formed by N.D. and [001].

(b) A second rotation Φ around the new direction $R.D._1$ with Φ having such a value that N.D. is transformed into [001] and T.D. into $T.D._2$.

(c) The third rotation Φ_2 with Φ_2 having such a value that $R.D._1$ is transformed into [100] and $T.D._2$ into [010].

So, Φ_1,Φ,Φ_2; the set of these three angles completely represent the orientation of a particular texture. Immediately for every set of {hkl}<uvw> values there is exactly one set of Φ_1,Φ,Φ_2 values. Now depending on this concept, a three dimensional space has been evaluated where three mutually perpendicular axes represent the values of Φ_1,Φ,Φ_2; from 0° to 90°. This is known as orientation space (Figure18c), and is widely used for universal texture notation.

The ODF technique is not more correct process than the pole figure technique is, but of course, the resolution is much higher in this system, and also it allows the quantitative measurement of the strength of a particular texture component in volume fraction.

2.9.3 Rolling Texture

A random polycrystalline aggregate will develop preferred orientations, or textures, upon sufficient plastic deformation. The nature of the deformation texture depends essentially on the crystal structure of the metal and the characteristics of the flow. The resulting texture may be affected by many other factors, such as the initial texture, the chemical composition, the previous thermal or mechanical treatment, the temperature, rate, or physical constraints during deformation. Deformation textures have their origins in the crystallographic nature of the common deformation processes of slip and twinning. Where large strains are involved, slip is usually the major factor but twinning can also be highly significant in texture development because of the massive re-orientations that are involved. During the slip process the crystal lattice rotates as a result of the shape change and the geometrical constraints of its surroundings. The restricted number of slip systems available produces rotations towards a limited number of end-points and so a deformation texture is produced. It is clear that the resulting texture will depend on the nature of the imposed stress (or strain) system, the extent of deformation, and the operative deformation modes which are themselves defined by the crystal structure and atomic bonding.

Temperature also plays an important role for determining the rolling texture. The slip systems are activated in larger extent at high temperature, slip deformation is more probable than twinning. Exactly, the reverse effect is expected at lower temperatures. Pure copper which on rolling at room temperature gives very sharp Cu type texture exhibits totally Bs type texture when it is rolled at liquid nitrogen temperature.

2.9.4 Annealing Texture

There are three general possibilities for the formation of annealing texture. In the first, inspite of softening , the deformation texture is retained or only sharpened. This can be attributed to both subgrain formation and enlargement and recrystallisation. The second possibility consists of change in the texture produced either by primary

recrystallisation , normal grain growth, secondary or tertiary recrystallisation. The final possibility is that a random orientation is set up on annealing but this occurs much less often than is commonly supposed and is usually associated with a very coarse grain which hinders the texture formation.

Since primary recrystallisation involves nucleation of a new set of strain free grains and their subsequent growth, it is clear that the orientations present in the fully recrystallised material require both the presence of nuclei in these orientations and the ability of the recrystallised grains of the orientations in question to grow during the annealing process. In the search of the origin of the recrystallisation textures, one of the principle questions arise ;whether the orientations absent from the recrystallisation textures are suppressed because of the unavailability of the nuclei in these orientations or because of the inability of such nuclei to grow to an appreciable volume in competition with nuclei of other orientations. These two ideas form the basis of two theories to explain the development of primary recrystallisation texture. In the 'oriented nucleation' theory the nucleation process is supposed to be of primary importance in determining the range of available nuclei which can contribute to the recrystallisation texture. It was observed that application of oriented nucleation mechanism to polycrystalline metals faces some difficulties.Such a mechanism depends on a definite orientation relationship between nuclei and matrix , and since the nucleation orientation must be related to the orientation of the microscopic matrix region immediately surrounding it ,the range of nucleus orientations is bound to be at least as large as that of matrix orientations. Thus on the basis of this theory , a complex deformation texture,should on annealing, yield an extraordinarily large number of nucleus orientations and consequently an extremely complicated recrystallisation texture. However , it has been found that under suitable conditions only very sharp single component is actually formed on recrystallisation.

To overcome this difficulty the 'oriented growth' theory was proposed. According to this theory, nuclei are formed in random orientations and selective growth decides which of them give rise to the primary recrystallisation texture , i.e. recrystallisation texture is supposed to be the result of growth selection due to the orientation dependence of the rate of grain boundary mobility. Again, in the case of grain growth , texture is determined by the grains , which, as a result of favorable orientational

relationships, grow most rapidly at the expense of the matrix. However it was found that the orientation dependence of the grain boundary mobility, which forms th basis of oriented growth theory , is not sharp enough to account for the well defined recrystallisation texture obtained on annealing highly deformed polycrystalline metals.

A new turning point was reached with the advent of electron microscopy which yielded important data concerning the nucleation stage. It was showed that , as well as or even instead of growth selection as a consequence of orientation dependent growth rate , the orientation of the nuclei is of great importance. It must therefore be decided in each individual case whether and to what extent oriented nucleation and oriented growth operate together.

On annealing a deformed material, the rolling texture completely or partially changes to a new texture, which is the recrystallization or annealing texture. It is also observed, that there is one-to-one correspondence between the rolling texture and annealing texture. So it can be inferred that the ultimate annealing texture of the material is dependent on the following factors:

(a) Deformation mode
(b) Degree of deformation
(c) Temperature at which the rolling is carried out
(d) Stacking fault energy
(e) Critical resolved shear stress for slip and twinning.

2.9.5 Recryslallisation and Cube Texture

When the cold worked metal is annealed, the Cu type texture essentially changes to cube texture {100}<001>. This is a familiar phenomenon for the pure f.c.c. metals like Cu, Ni etc. except Al. The reverse effect is observed in case of Bs type rolling texture. On recrystallization it does not yield Cu type texture. In a series of Ni-Co alloys, it has already been observed that the compositions having higher magnitude of SFE (0, 10, 20, 30 % Co) yield cube texture. Composition of low SFE (Ni-60 Co) does not yield cube texture, rather the Bs texture transforms to {332}<113> type texture. The intermediate composition Ni-40Co exhibits some amount of

recrystallized cube texture along with some amount of twin of cube texture {122}<212>.

The formation of cube texture (shown in Figure19) is not a desirable one so far as the material property is concerned. The formation of cube texture is a very fast process and just after the starting of recrystallization, the complete material immediately becomes highly anisotropic. But the reason for the dominating characteristic of cube texture and its actual origin is still not known.

2.10 Rolling Texture and Annealing Texture of Ni-Co alloy

For higher stacking fault energy, the stacking fault width is very low, and the stacking faults are easily constricted. In that situation, the cross-slip becomes easier and the material undergoes slip deformation rather than twinning. When the deformation is governed by slip mode, the deformation texture is generally copper type {112}<111>. Example, pure copper, pure nickel or nickel with low amount of cobalt, Ni-Fe alloy etc. The (111) pole figure for 95% cold rolled pure copper is shown in Figure20a.

Along with the copper components of texture other components like Bs component {110}<112>, S component {123}<634>, Goss component {110}<001> etc, are present in very small percentage. The materials with lower SFE predominantly exhibit Bs type of texture. For lower SFE, the stacking fault width is much greater, which makes it difficult to create any constriction within the stacking fault region and the cross-slip becomes difficult. As a result of it, the critical resolved shear stress (CRSS) for twin becomes lower than that of slip and the plastic deformation is essentially governed by the twinning process. Figure20b exhibits the typical Bs type texture of a Ni-Co alloy with a lower SFE.

In Ni-Co alloy system, the SFE significantly decreases on increasing the Co percentage (fig.21). Accordingly it is observed that the Cu component of rolling texture gradually decreases from pure nickel to Ni-30% Co (Figure22a , 22b). Ni-40 Co alloy shows a transition from Cu type to Bs type rolling texture, and Ni-60 Co alloy predominantly exhibits Bs type texture. This is also observed that Cu type texture decreases with increasing amount of deformation. In case of Ni-40 Co alloy,

the intensity of Cu type texture remarkably decreased from 40% cold rolling to 95% cold rolling.

In the ODFs of f.c.c. metals and alloys, three fibre textures have been generally recognized. These are

(a) an α-fibre which extends from the Goss orientation {011}<100> through the Bs orientation {011}<211> to {011}<011>;

(b) a τ-fibre which extends from {001}<110> through the Cu position {112}<111> and going up to the Goss orientation {011}<100>;

(c) a β-fibre which runs from the Cu position {112}<111>, through the S orientation {123}<634> and meets the α –fibre at the Bs position, shown in Figure 23.

An analysis of the ODF results for the Ni-Co alloys shows significant difference in the rolling texture of these alloys as a function of Co-content. The detailed analyses of the ODF results of pure Ni and Ni-Co alloys, done by Ray[32], shows that Ni-Co alloys with up to 30% cobalt, which show copper-type textures, exhibit only an inhomogeneous α-fibre or α-tube, but a strong and reasonably homogeneous β-tube. In the Ni-40% Co alloy the α-tube also is found to be reasonably strongly developed and this becomes more intense in the Ni-60% Co alloy. The intensity of the Goss position also improves in these two alloys. For convenience, an auxiliary Bs/Goss component, {011}<511>, is introduced between the Bs and the Goss positions. Increase in Co-content leads to a systematic decrease in the *f(g)* value of the Cu orientation. In fact, the intensity of the Cu orientation is very weak in the Ni-40% Co alloy and it is practically non-existent in the Ni-60% Co alloy. Furthermore, the twin Cu position shows a slight maximum for both the Ni-40% Co and Ni-60% Co alloys, but the positions of these maxima are found to be somewhat shifted towards the {332}<113> position. The positions of the texture components along the β-tube vary substantially depending on the Co-content of the alloys. In general, the locations of the texture components shift to lower Φ_1 and higher Φ values with increasing Co-content.

In Ni-40% Co alloy, there are a host of orientations which do not contribute to the major texture components as such but constitute a large "random " background. The alloy in the transition range, Ni-40% Co, is likely to be the one where both slip and twinning will be taking place, probably with equal ease.

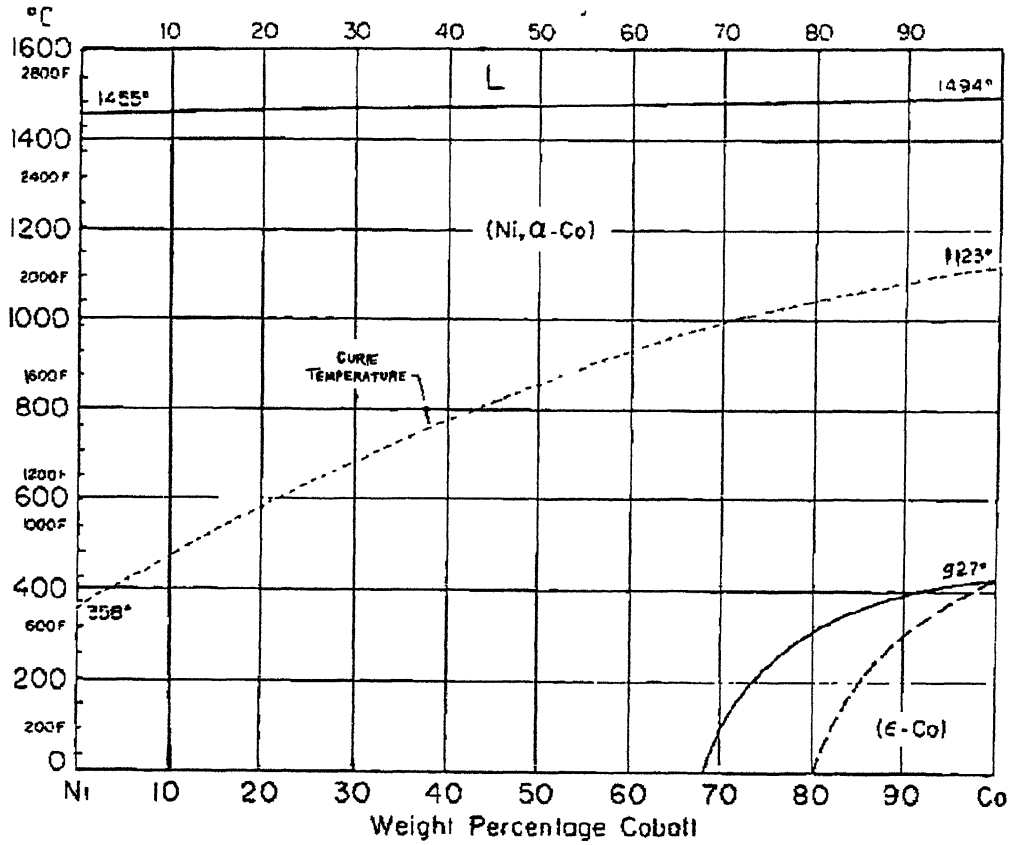

Fig. 1 Phase diagram of binary Nickel – Cobalt system

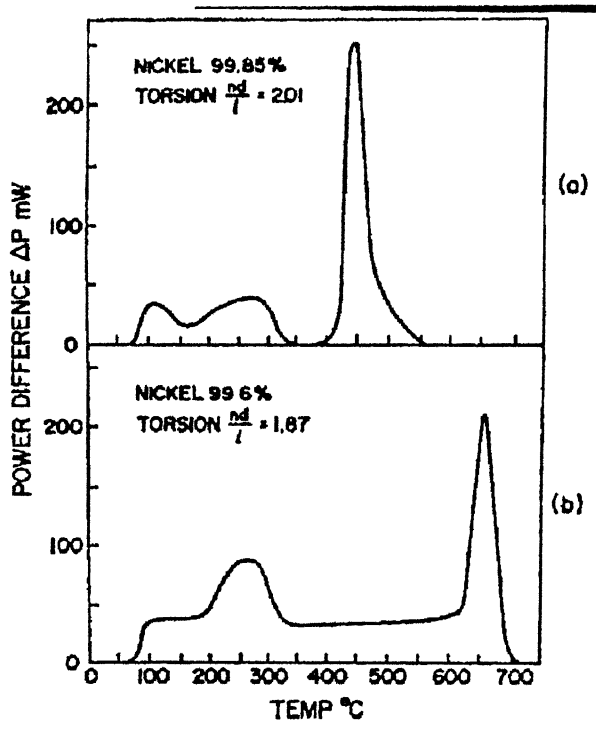

Fig. 2 Power difference as a function of temperature for samples of nickel of two purities deformed in torsion
a)99.85% Ni deformed to nd/l = 2.01
b)99.6% Ni deformed to nd/l = 1.87

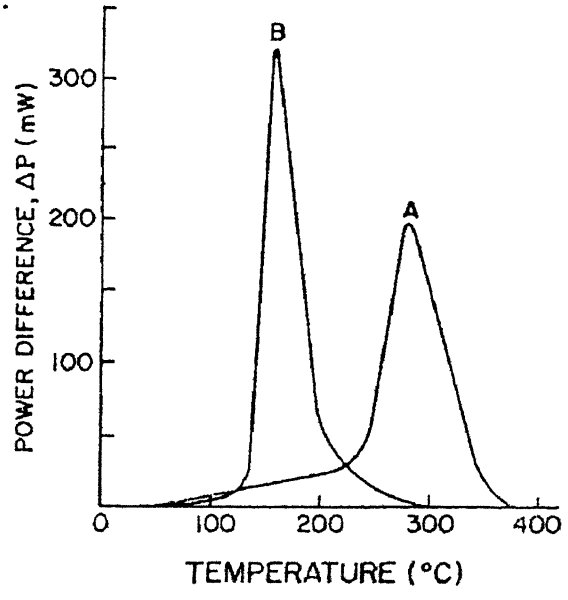

Fig3. Power Difference as a function of temperature for 99.967% Cu (curveA) and 99.988% (curve B) deformed to fracture in torsion and heated 6C/min

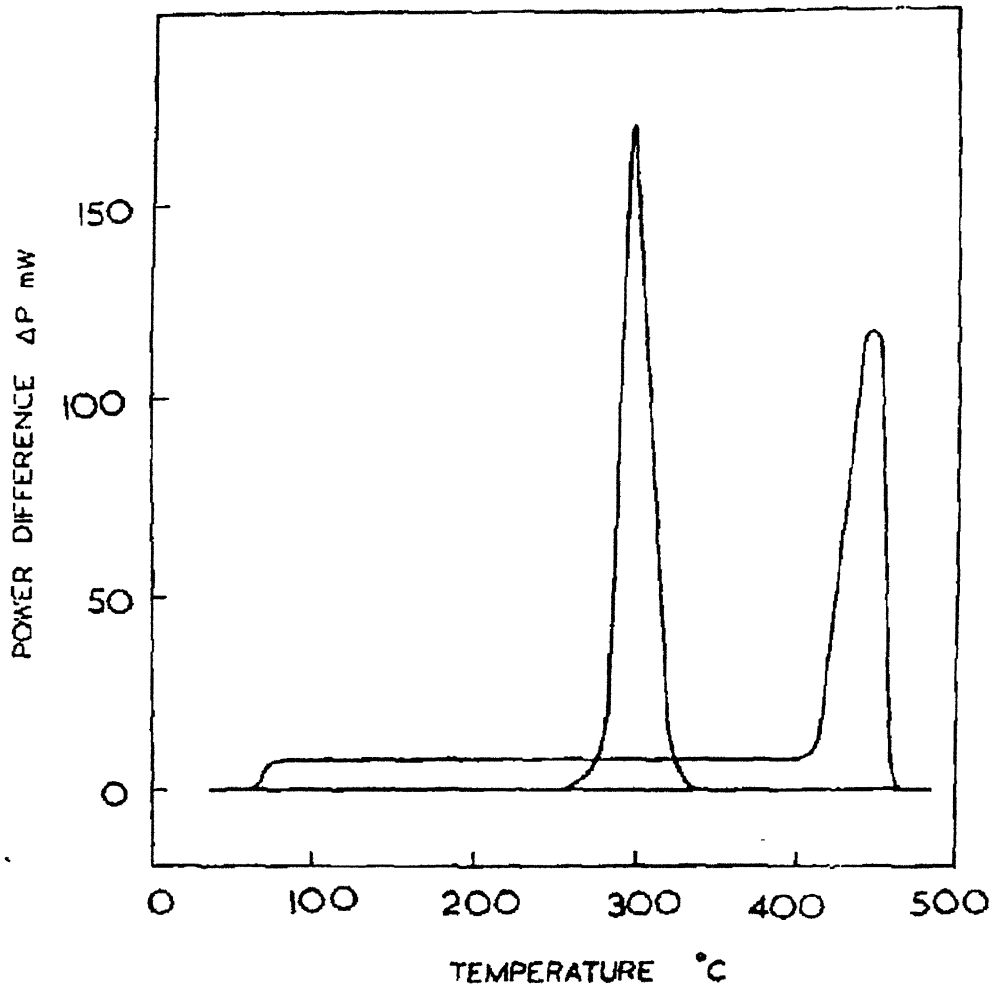

Fig 4 Power difference as a function of temperature obtained at a heating Rate of 6° C/min for nominally 99.98% Cu deformed to 45% Elongation and for arsenical copper deformed to 40% elongation.

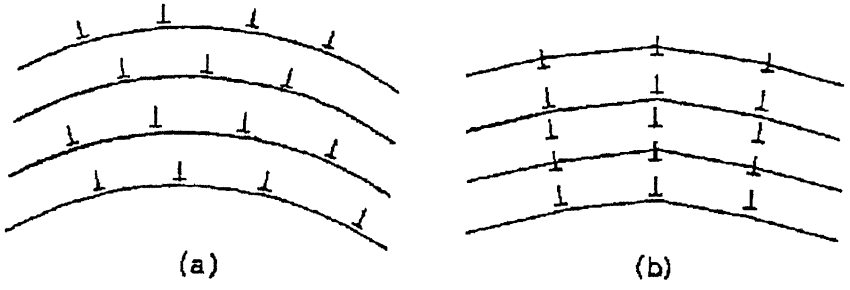

Fig5. (a) Random arrangement of excess parallel edge dislocations
(b) Allignment into dislocation walls

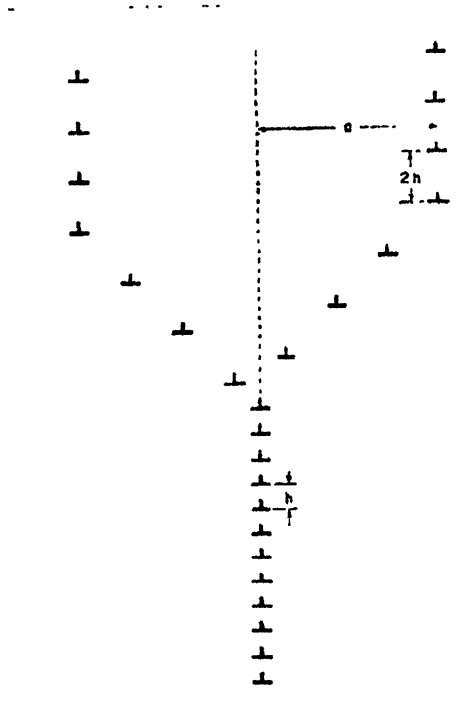

Fig. 6 Dislocation structure of a Y-junction

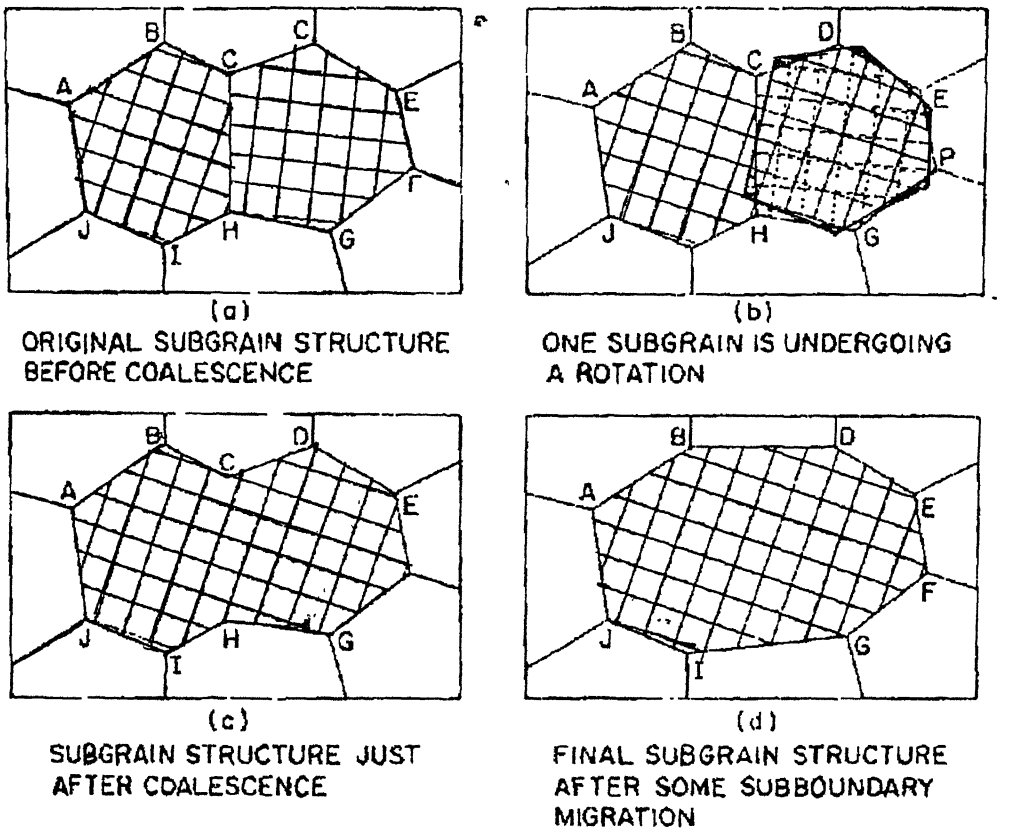

Fig 7. Schematic representation of subgrain coalescence by subgrain rotation

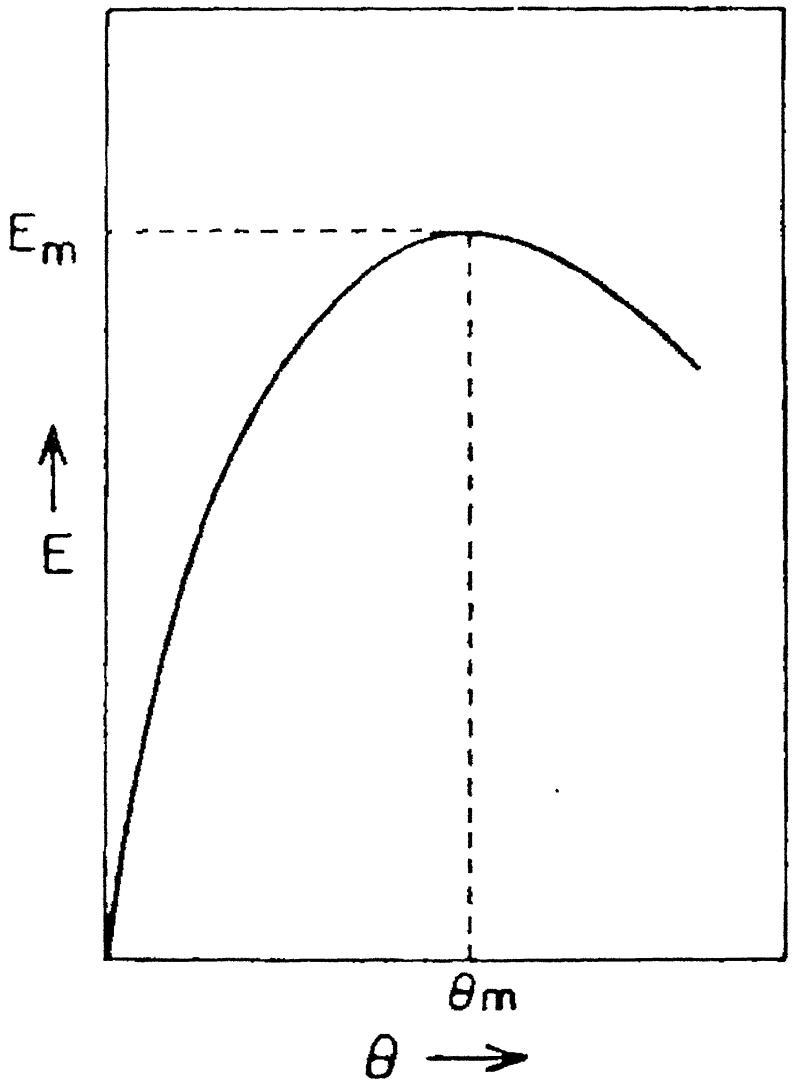

Fig. 8 Plot of E versus θ

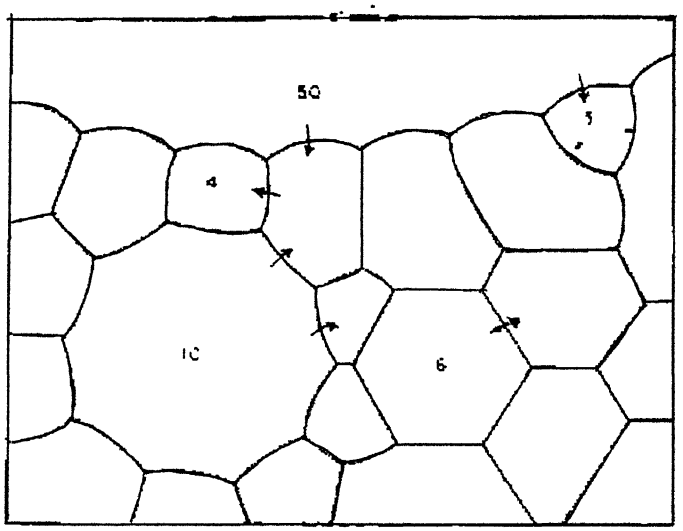

Fig. 9 (a) Nucleation by subgrain growth (schematic). Subgrain boundaries thickly populated by dislocations (dot) have a high misorientation angle,and are the most likely to migrate.
(b) Effect of relative size of a grain on the curvature of grain boundaries. arrows show direction of boundary migration, provided all boundary energies are equal.

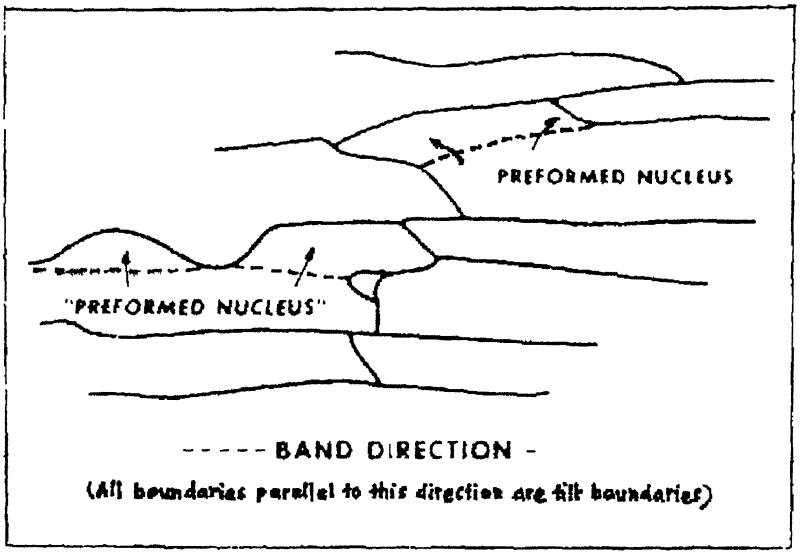

Fig. 10 Nucleation by subgrain growth in a deformation band in rolled Fe-Si alloy

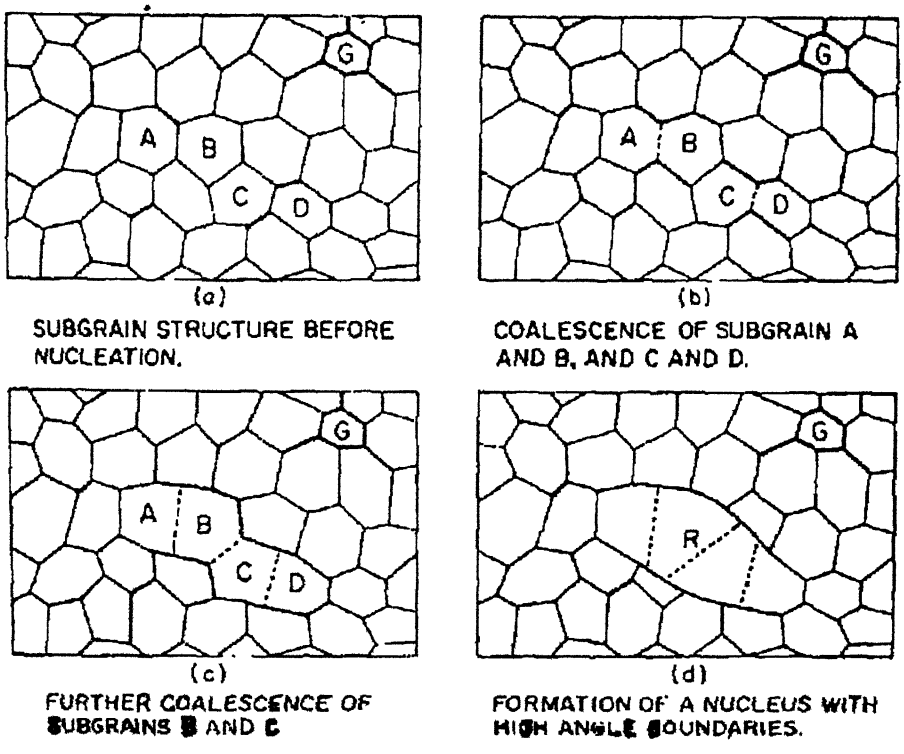

Fig. 11 Schematic representation of the formation of a recrystallised grain by the coalescence of sub-grains

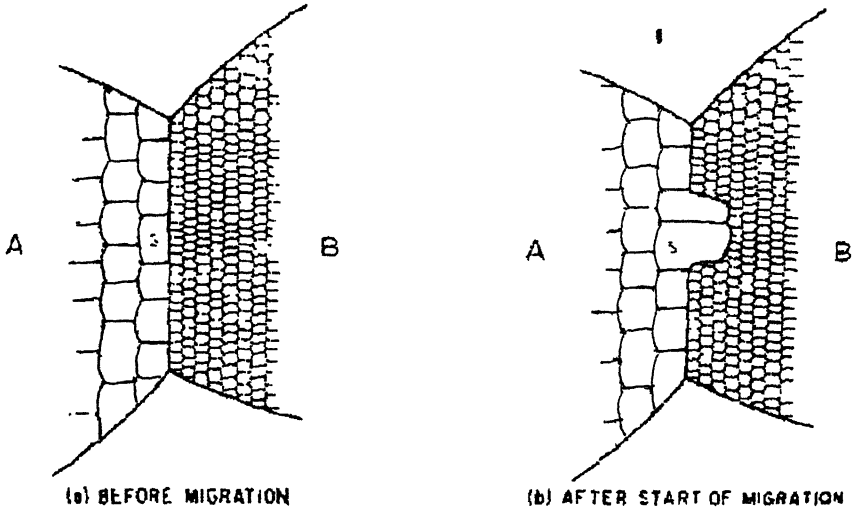

Fig. 12 Model for strain induced boundary migration.

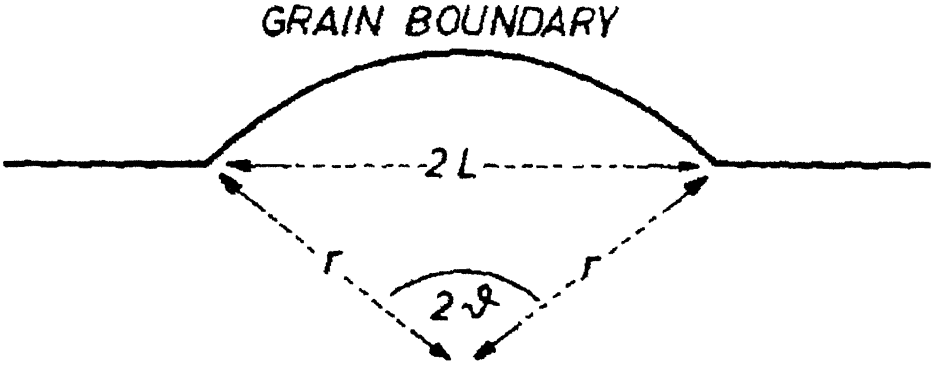

Fig. 13 Nucleation by strain induced boundary migration

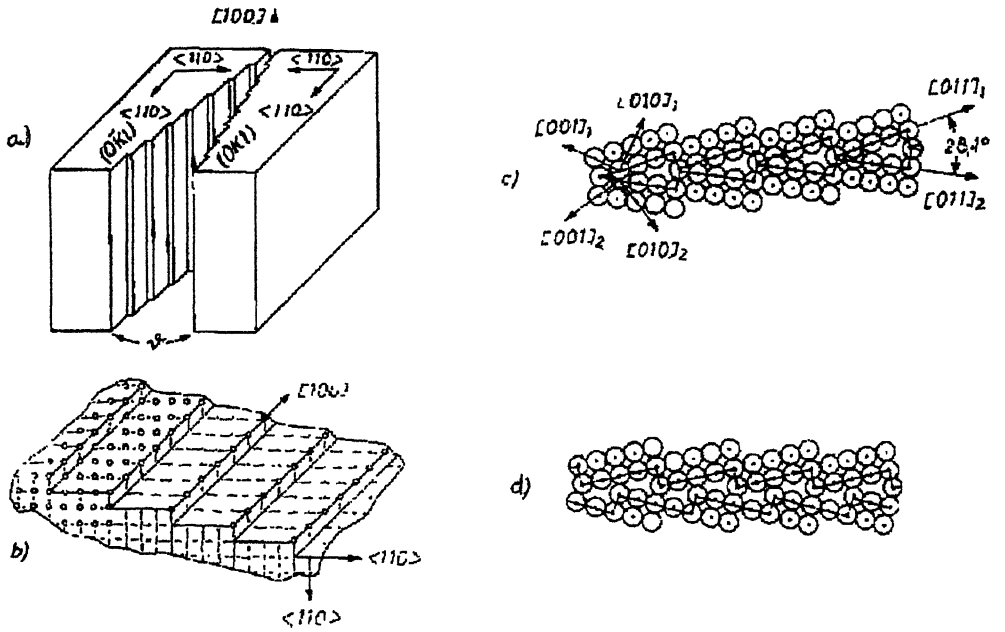

Fig. 14 Geometric model of symmetric <100> tilt boundary with ideal boundary coincidence in fcc lattice :

(a)Formation of the boundary by two adjoining lattices with a misorientation angle θ

(b) Visualisation of atomic steps in a partition surface between the two lattice regions.

(c) Arrangement of atoms in the grain boundary (as seen along the common <100> direction) showing exact coincidence of the atoms lying in the boundary plane

(d) Arrangement of the atoms after having removed one of the 'overlapping' atoms adjoining the coincidence atoms in ©

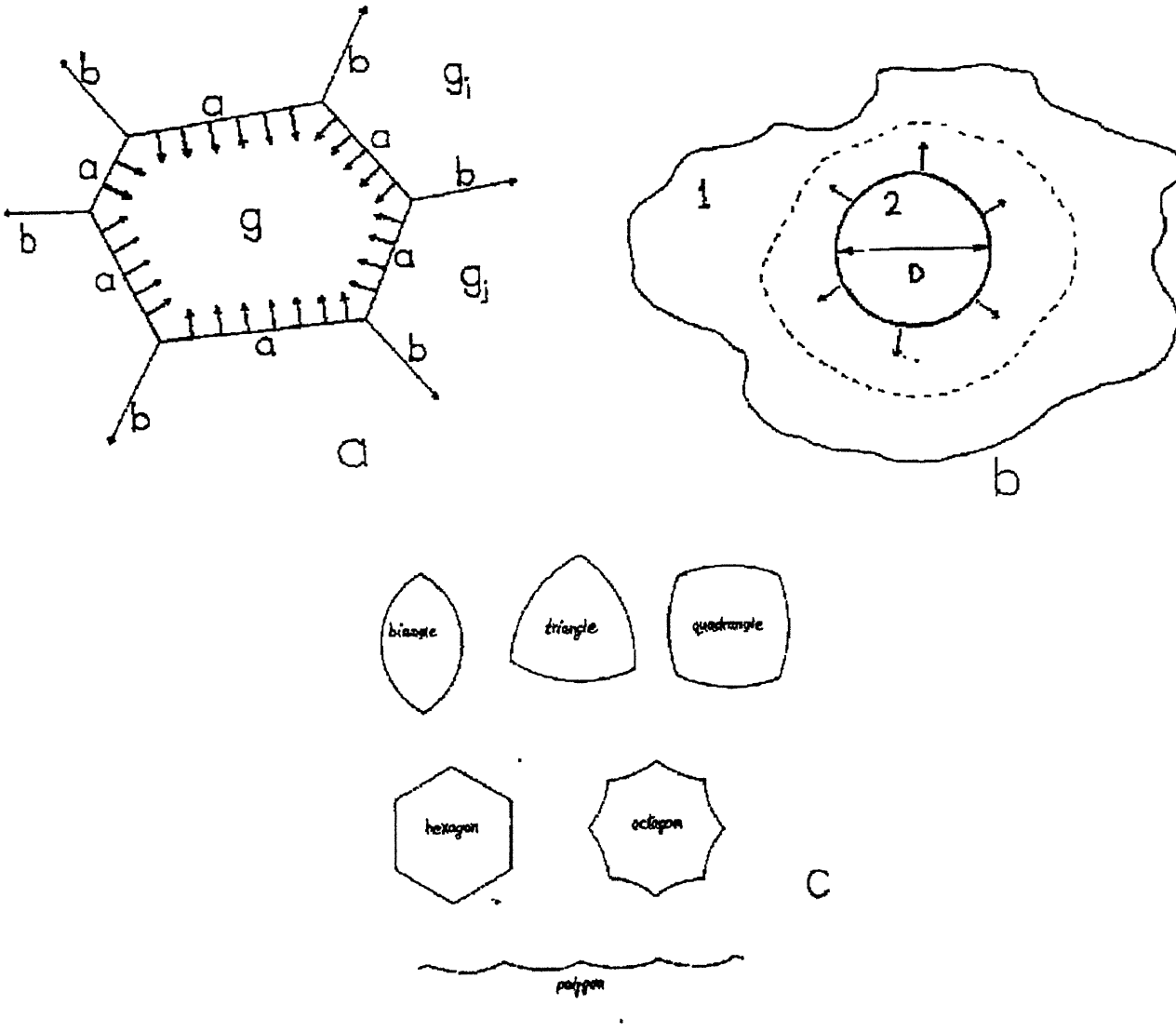

Fig. 15

(a)A grain of the orientation g is surrounded by grains of the orientations G_i and g_j. The energy of the a-boundaries tends to contract the grain whereas the b-boundaries tend to expand it

(b)Growth of region 2 by the movement of interface boundary from region 2 to region 1

(c) Curvature of grain boundaries in n-sided two dimensional grains.

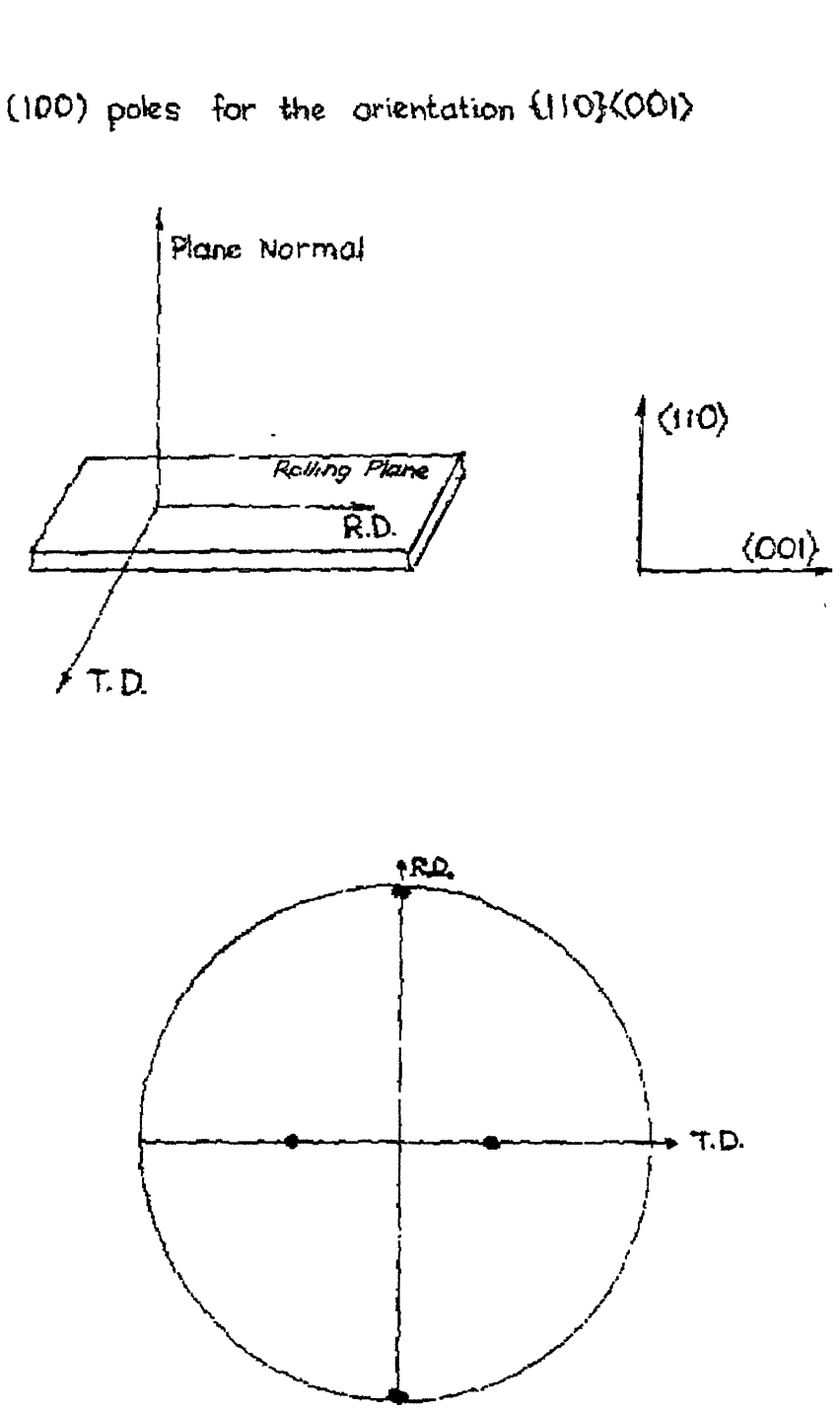

Fig. 16 The rolling plane and rolling direction in a metal sheet subjected to rolling

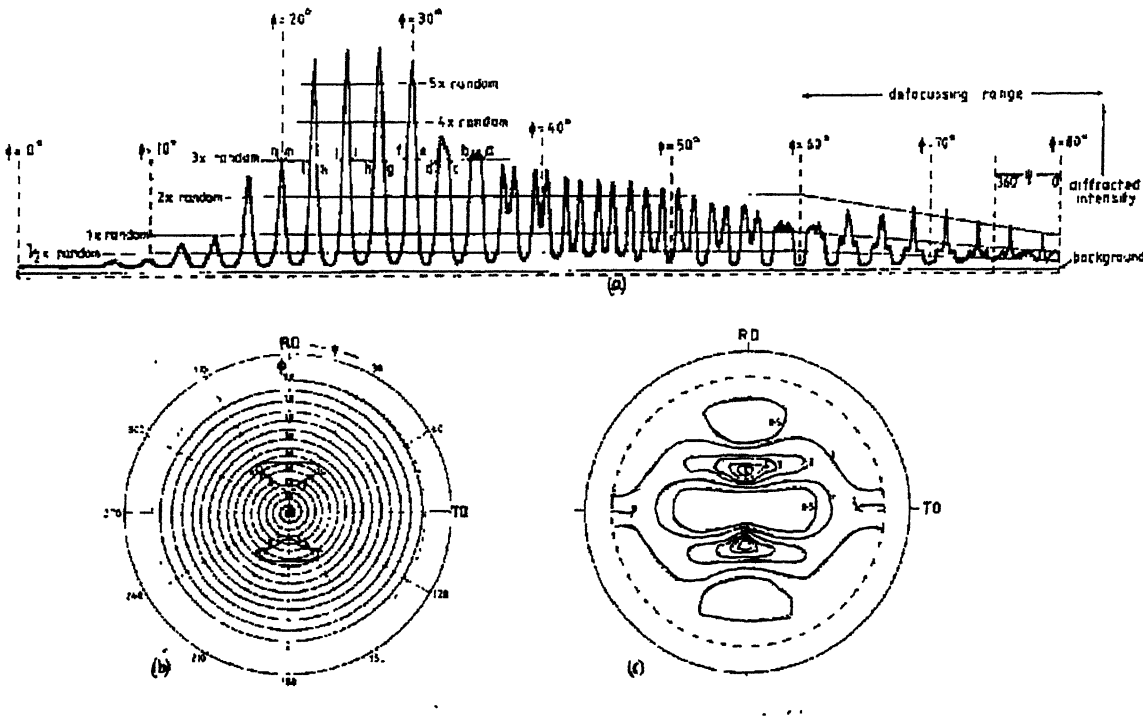

Fig. 17
Schematic representation of the construction of pole figure
(a)Chart recording for the (111) reflection of cold rolled aluminium
(b) Partly plotted pole figure showing the 3 x random contour
(c)Final (111) pole figure

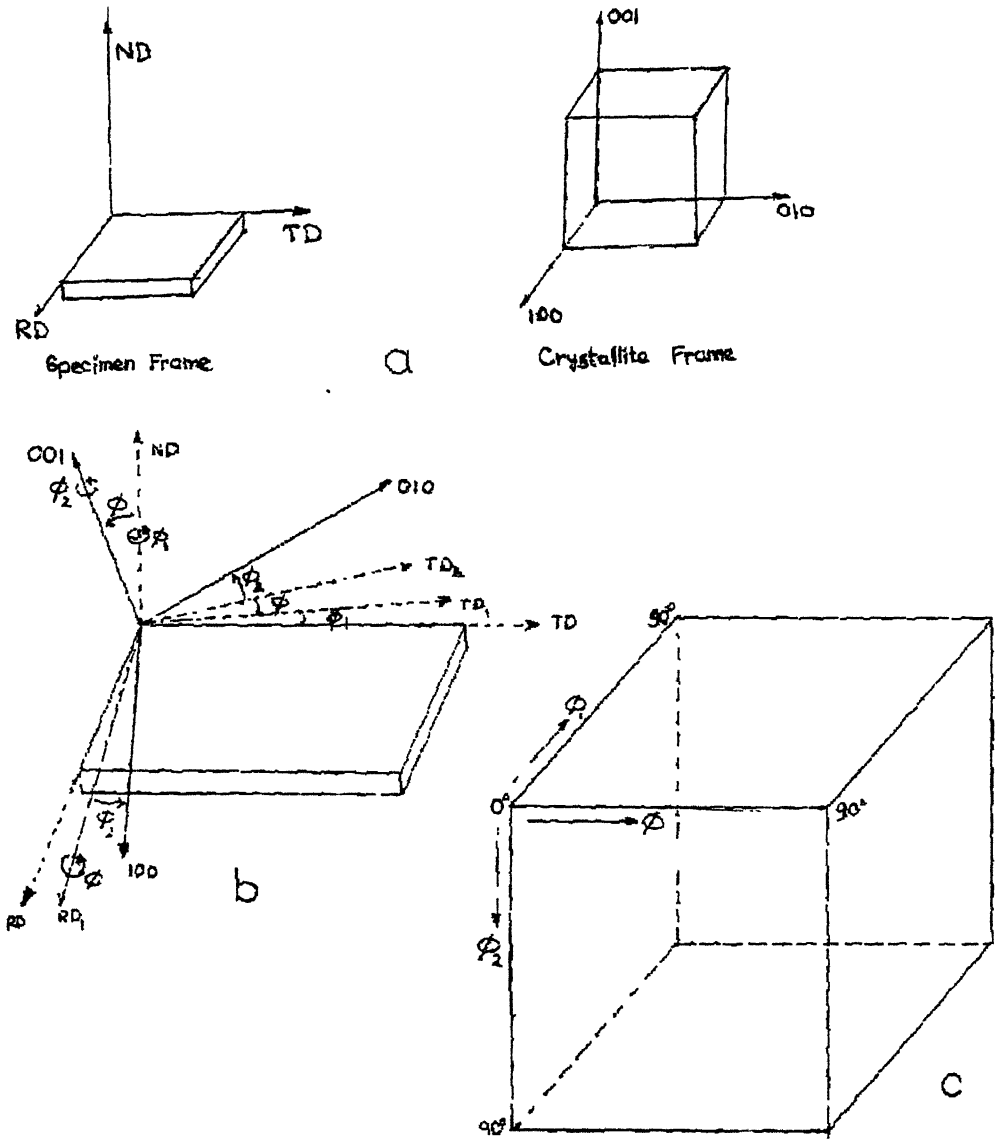

Fig. 18

(a) Specimen frame and crystallite frame

(b) The three rotations for superimposing crystallite frame on reference frame

(c) Orientation space.

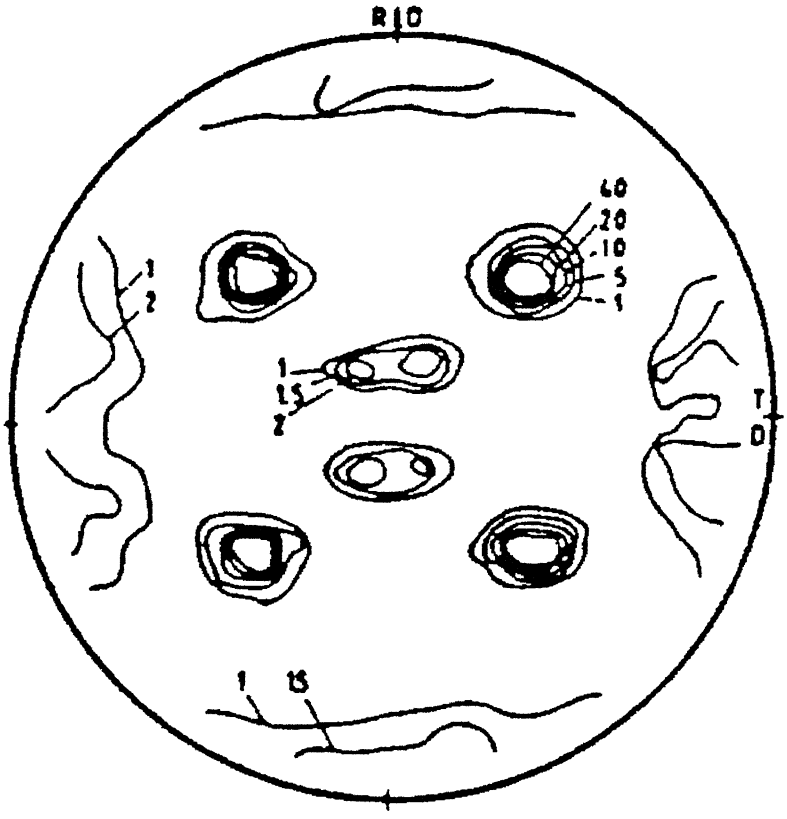

Fig. 19 Typical Cube Texture in Nickel, {111} poles shown in {100}<001> texture.

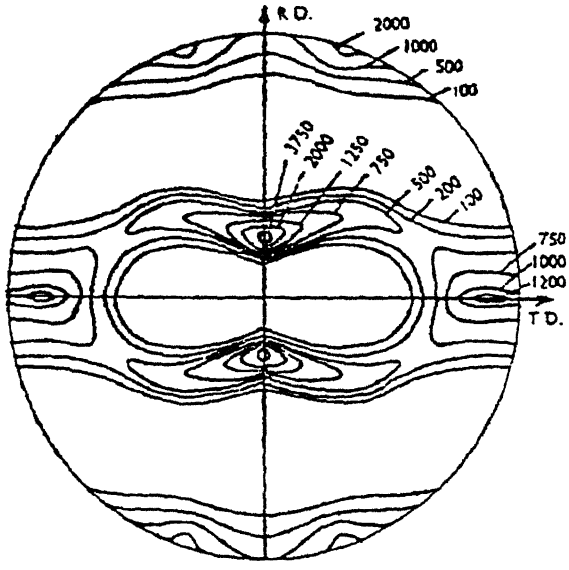

Fig. 20(a) (111) Pole figure for 95% cold rolled pure Copper

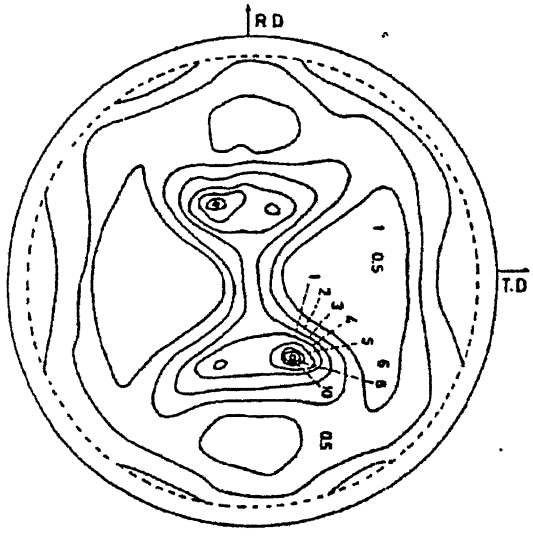

Fig.20(b) Ni-60Co, Typical Bs type deformation Structure

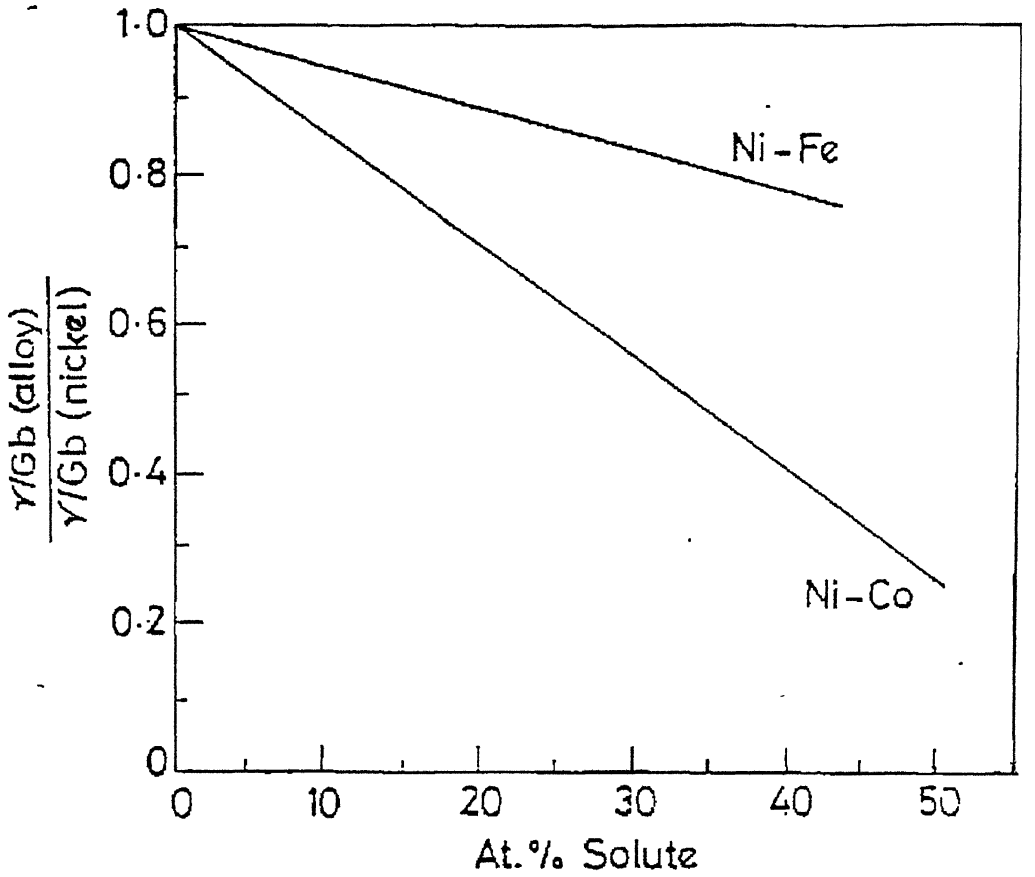

Fig. 21 Effect of composition on Stacking Fault Energy.

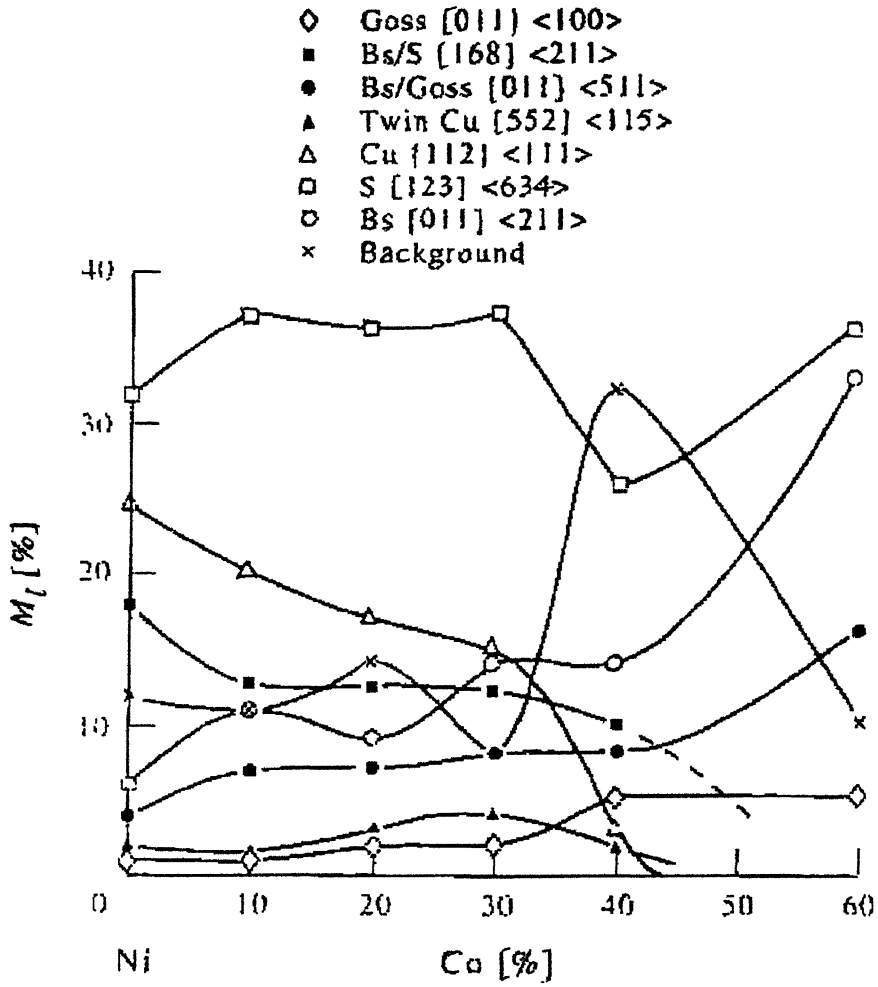

Fig.22a Plot showing the variation of volume fraction of different texture components with %Co in Ni-Co alloys

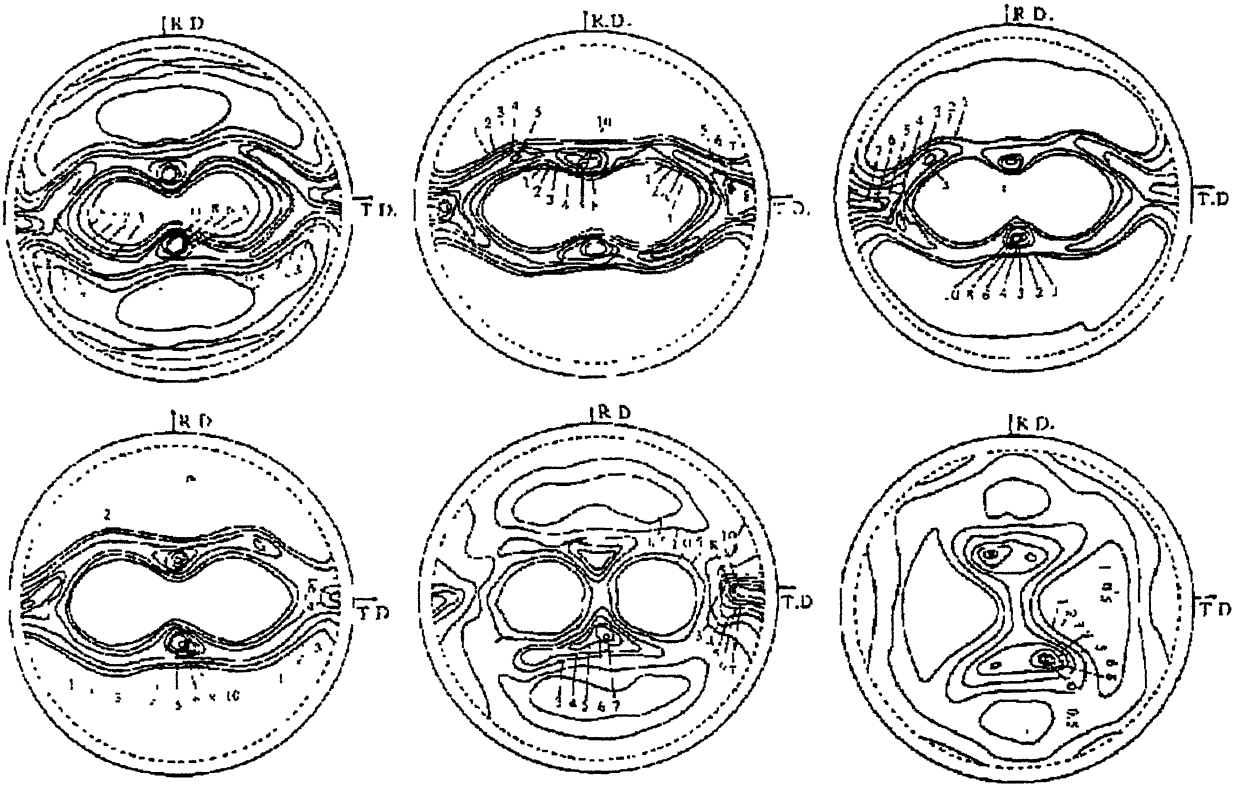

Fig. 22(b) Rolling textures of different Ni-Co alloys (I)Pure Ni (ii) Ni-10%Co (iii)Ni-20%Co (iv) Ni-30%Co (v) Ni-40%Co (vi) Ni-60%Co

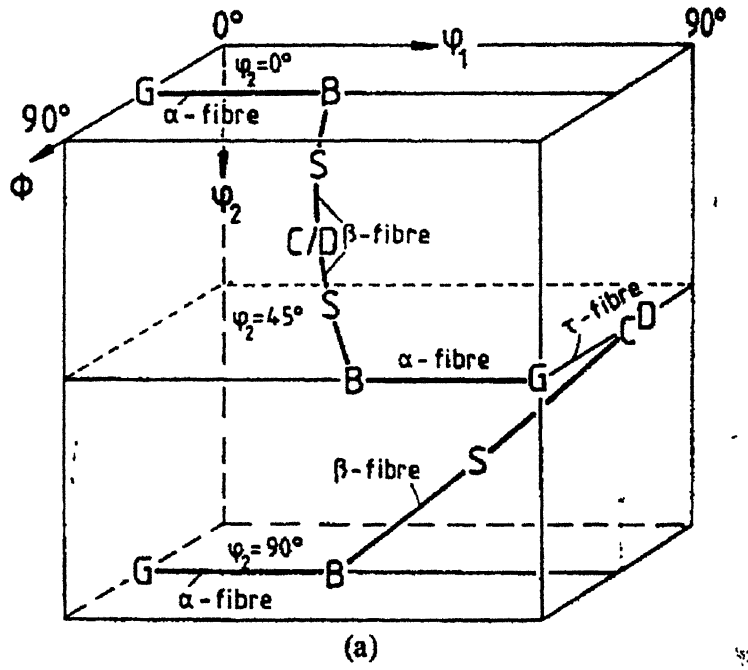

Fig.23 Position of the α, β and τ texture fibres in the Euler space.

Chapter 3

EXPERIMENTAL PROCEDURE

3.1 Initial Material:

The Ni-Co binary system has been selected for the experiments. The three nominal compositions taken as follows :

(i) Ni-30Co alloy

(ii) Ni-40Co alloy

(iii) Ni-60Co alloy

The chemical composition of all the alloys are given below :

Table2. Chemical Composition of the Alloys

Designation	Weight percentage of Alloying Elements						
	C	Si	Mn	P	S	Ni	Co
Ni-30Co	0.006	0.03	0.03	0.004	0.003	68.85	30.90
Ni-40Co	0.006	0.03	0.03	0.003	0.004	58.70	41.05
Ni-60C0	0.006	0.06	0.03	0.003	0.004	39.20	60.50

All the alloys were induction melted and cast under an argon atmosphere using virgin metals of purity greater than 99.99%. The ingots were cylindrical in shape having a height of about 20mm. For each alloy 12mm thick samples were cut down from the cast blocks.

3.2 Material Preparation

The following four treatments were given to each alloy:

(i) The 12mm thick slabs were cold rolled 50% followed by homogenization annealing in vaccum at 820C for three hours. This treatment has been given the name '50pct.820C-3h(I)'.

(ii) After the treatment (i) , the ~6mm thick strips were again cold rolled to 50% followed by homogenisation annealing in vaccum at 820C for three hours. This treatment has been given the name ' 50pct.820C-3h(ii)'.

(iii) After the treatment (ii), the ~3mm thick strips were annealed at 820° C for another 7 hours. This treatment has been given the name ' Annealed-820° C-10h'.

(iv) After the treatment (ii), the ~3mm thick strips were annealed at 850^0 C for 3 hours. This treatment has been given the name 'Annealed-850^0 C-3h'.

3.2 .1 Cold Rolling

The cut samples were cold rolled in 2-high laboratory rolling mill where paraffin oil was used as lubricant. The directions of the strips were reversed end to end after each pass. In between any two successive passes, the strips were dipped into cold water bath to minimise any unwanted rise in the temperature. The change in thickness after each passes were noted.

3.2.2 Annealing

After cold rolling the samples were annealed. Annealing was carried out in a Laboratory Tube type furnace. The samples were suspended with the help of wires inside the furnace in an Argon atmosphere. Gas was continuously passed through the furnace, and finally the samples were quenched in normal water.

3.3 Optical Microscopy

After the heat treatments, small pieces of all the materials were mounted using cold setting resin for optical microscopy. The mounting was done in such a manner that the longitudinal sections of the rolled and annealed sheets could be examined .

After mounting , the samples were subjected to conventional metallographic polishing and then etching. The etching reagent was prepared by mixing 65% (by volume) conc. HNO_3 With 18% (by volume) glacial acetic acid. Sometimes, a few drops of hydroflouric acid was added for better and instant effect. To get the best effect, always freshly prepared etching reagent was used.

The etched samples were examined under an optical microscope and a number of photographs of each sample was taken.

3.4 Grain Size and Volume Fraction Measurement :

The Image Analysis Method was used to measure the grain size and volume fraction. In this method , the image analysis software takes grains as bright objects by drawing the outline of each grain. Now in each object several diameter lines are drawn , (the software itself gives the length of the line) and mean of all these measurements are taken. This way mean diameter of each grain is calculated.

As area fraction will be equal to volume fraction, so the same image analysis method is used to calculate it. As previously mentioned, the grains are identified as bright objects by the software. The area of each grain is measured by the software itself. Now, in the grain diameter measurement, we had already identified the ranges of grain diameter of the small and big grains, we can selectively choose the area of big and small grains. Now the area of small and big grains are summed up separately and area fraction of small and big grains can be calculated. Now as previously mentioned, this area fraction is equal to volume fraction.

Fig.24 Microstructure of Ni-30Co alloy for the heat treatment 50pct.820° C-3h(i)

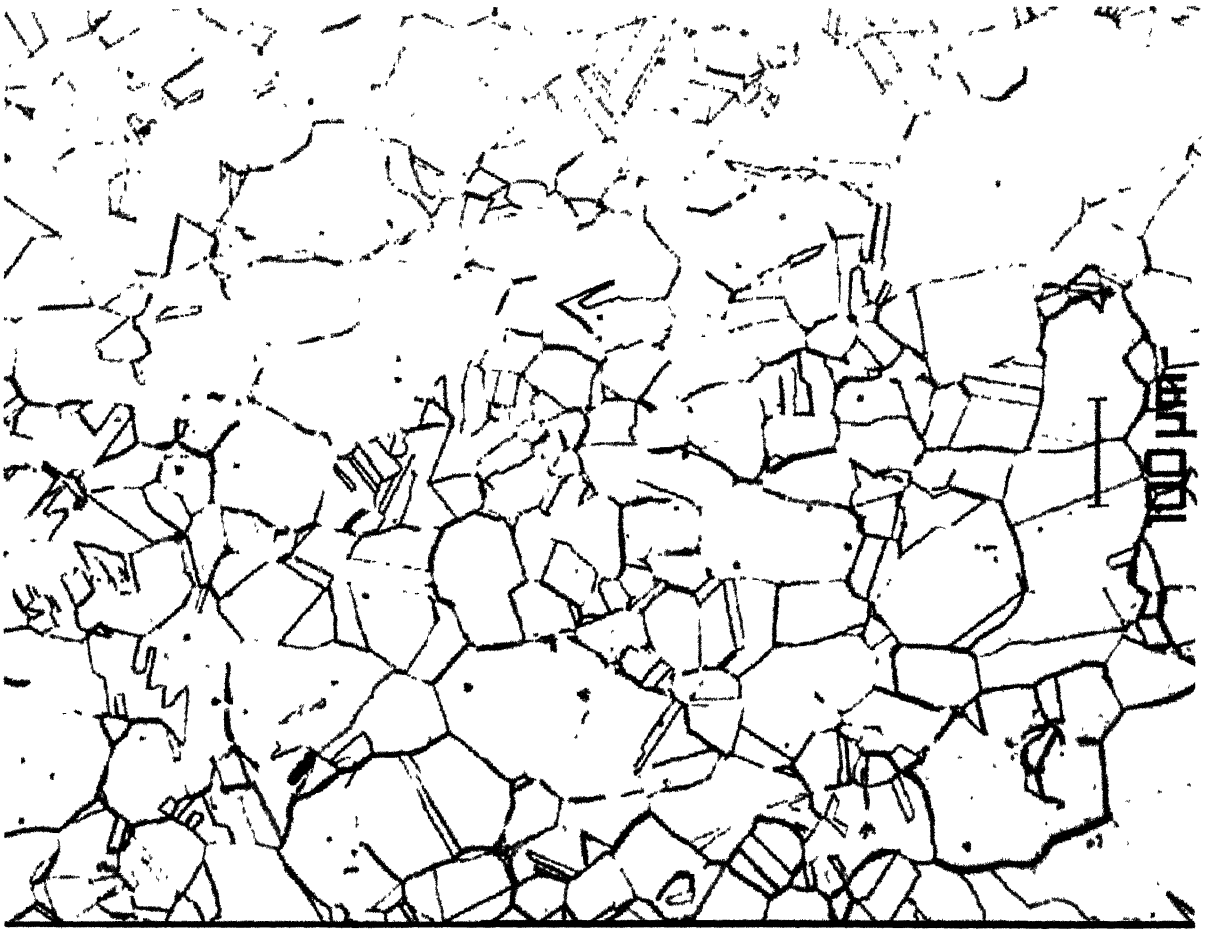

Fig.25 Microstructure of Ni-40Co alloy for the heat treatment 50pct.820° C-3h(i)

Fig.26 Microstructure of Ni-60Co alloy for the heat treatment 50pct.820°C-3h(I)

Fig.27 Microstructure of Ni-30Co alloy for the heat treatment 50pct.820°C-3h(ii)

Fig.28 Microstructure of Ni-40Co alloy for the heat treatment 50pct.820°C-3h(ii)

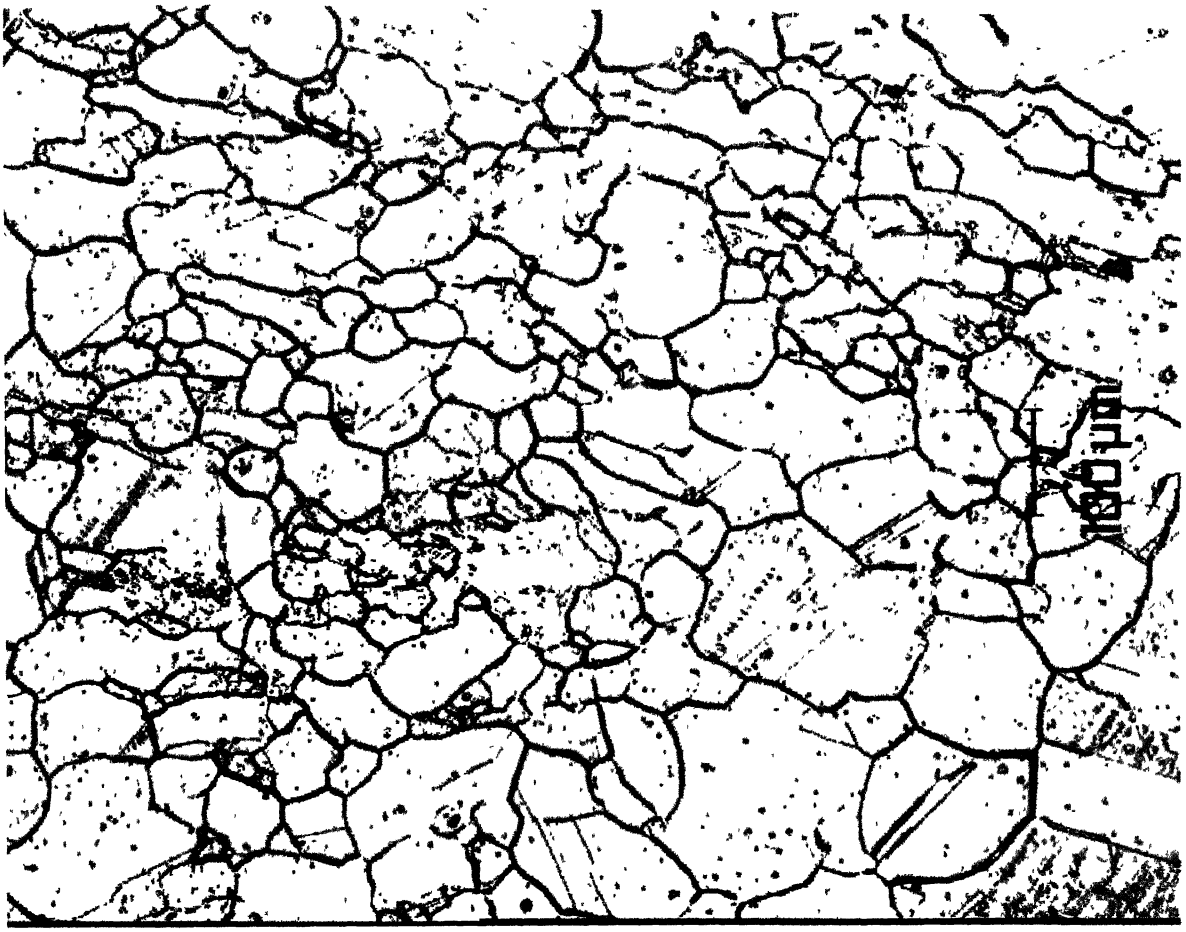

Fig.29 Microstructure of Ni-60Co alloy for the heat treatment 50pct.820°C-3h(ii)

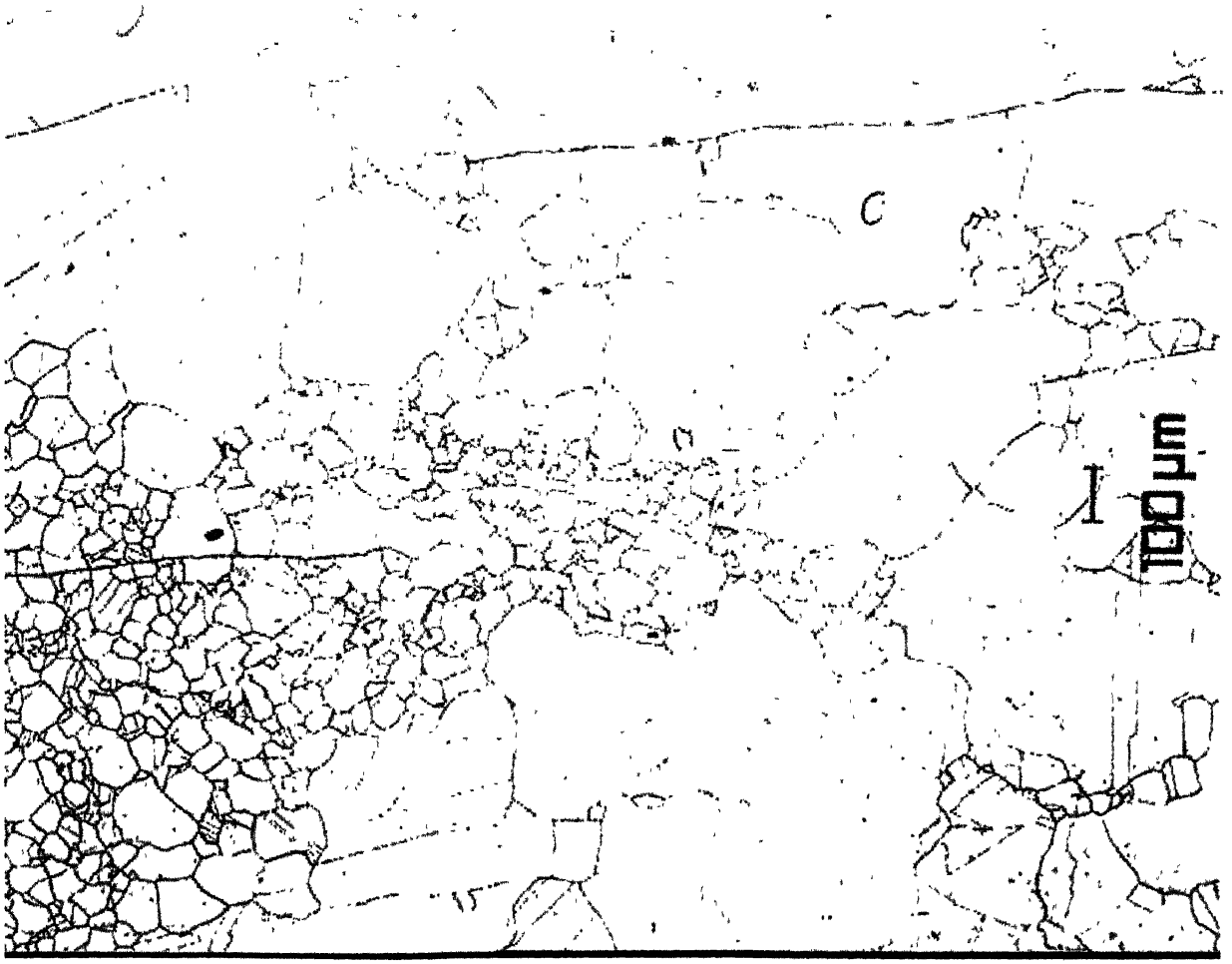

Fig.30 Microstructure of Ni-30Co alloy for the heat treatment Annealed-820°C-10h

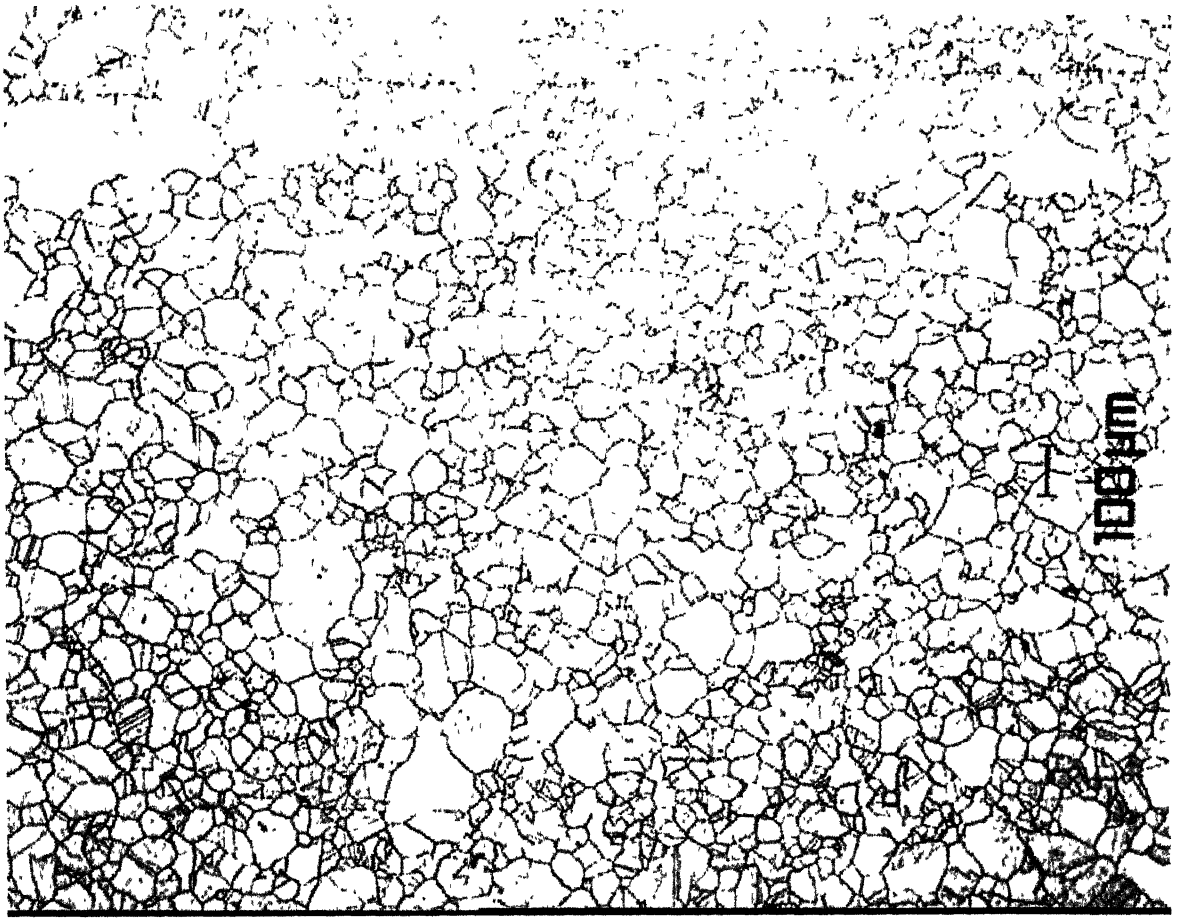

Fig.31 Microstructure of Ni-40Co alloy for the heat treatment Annealed-820°C-10h

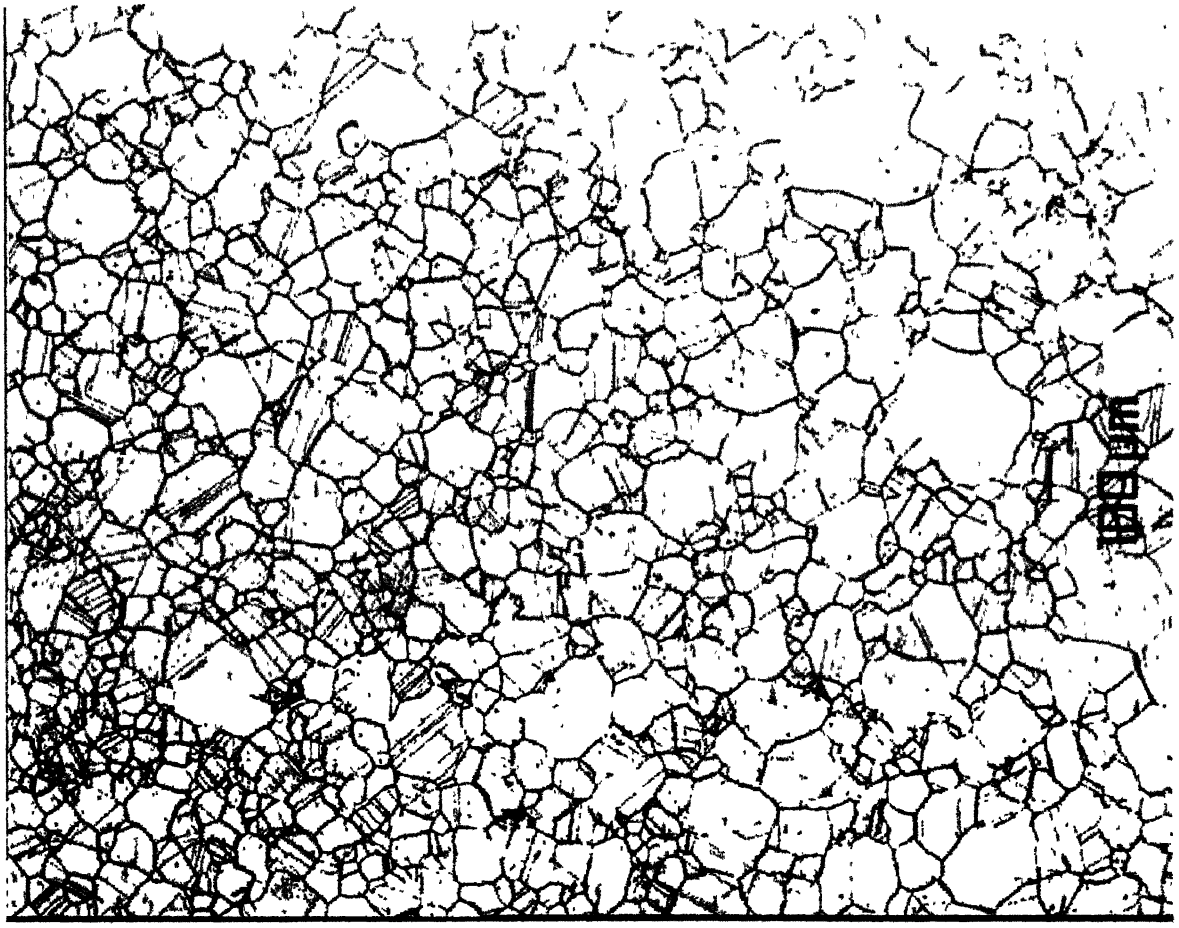

Fig.32 Microstructure of Ni-60Co alloy for the heat treatment Annealed-820°C-10h

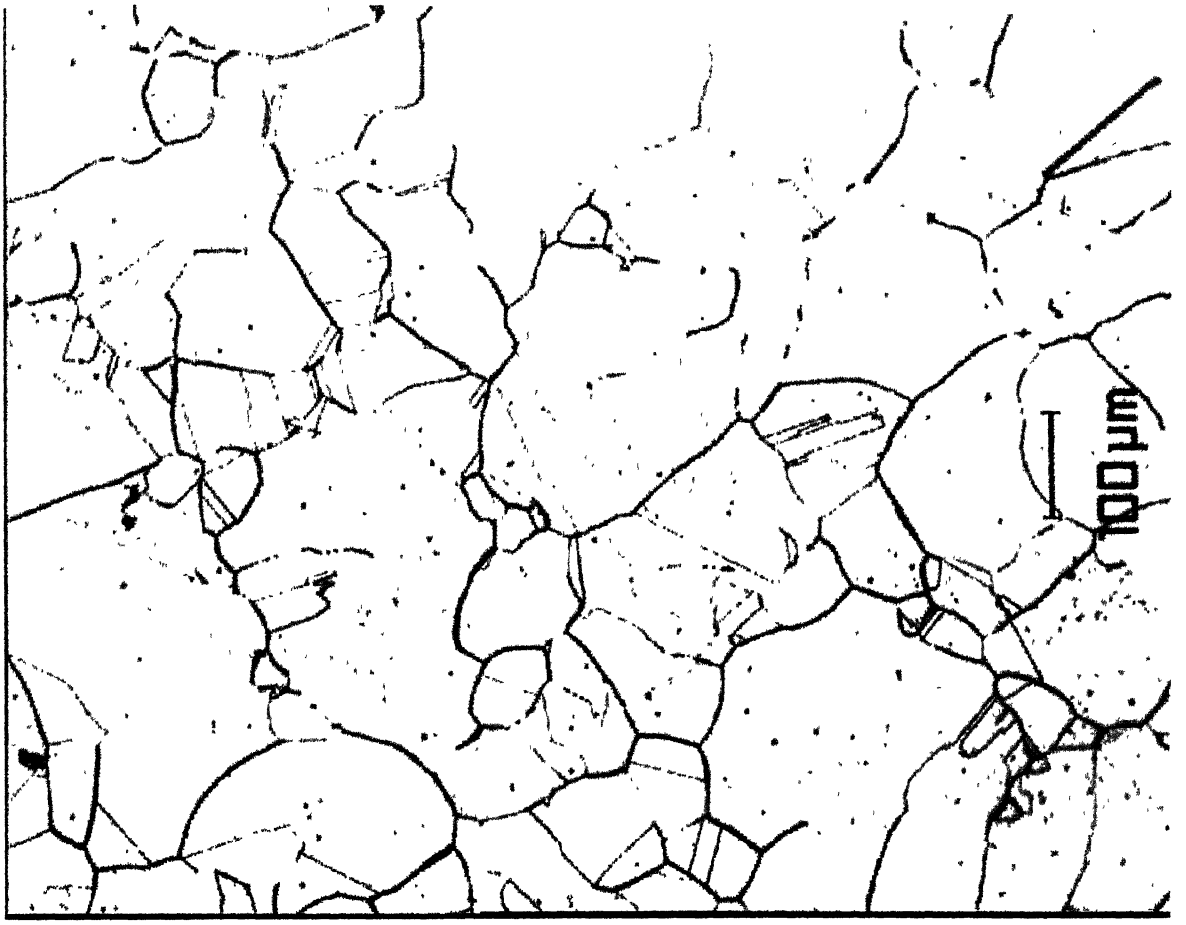

Fig.33 Microstructure of Ni-30Co alloy for the heat treatment Annealed-850°C-3h

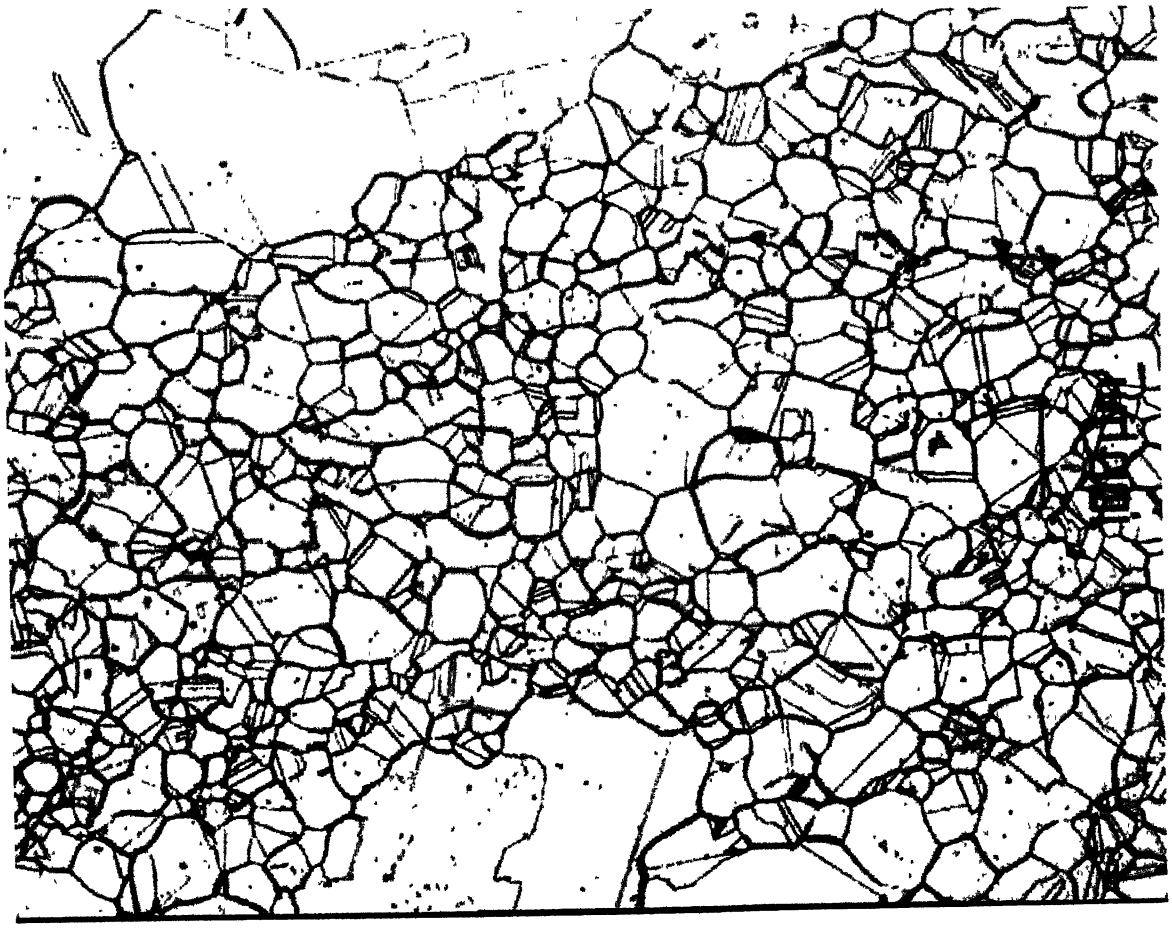

Fig.34 Microstructure of Ni-40Co alloy for the heat treatment Annealed-850°C-3h

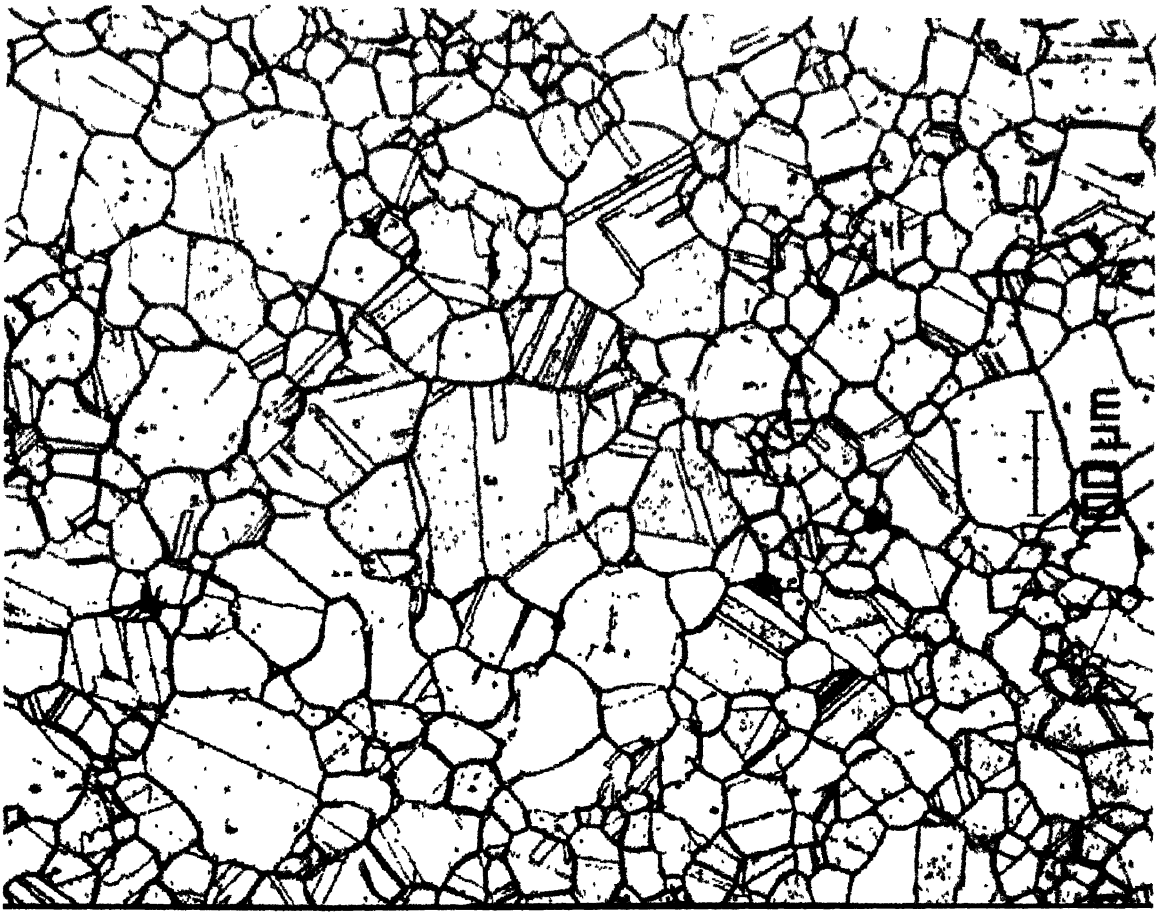

Fig.35 Microstructure of Ni-60Co alloy for the heat treatment Annealed-850°C-3h

Chapter 4

RESULTS

4.1 Optical Microstructures

Representative optical micrographs of the twelve heat treated samples from the three alloys are presented from figures 24 to 35. It is at once clear from these micrographs that in each case, the microstructure shows two distinct features, namely, colonies of relatively small sized grains which are embedded in a matrix of relatively coarse sized grains. Since this pattern has been found to be rather uniformly true for all the different heat treatments, as well as for different alloys, it was decided to carry out quantitative grain size measurements from (i) the small grains forming colonies, (ii) the big grains in the matrix and also from (iii) the mixed grains constituting the total microstructure. From these measurements histograms of frequency of grain size distribution versus their sizes are calculated.

4.2 Histograms of Grain Sizes

4.2.1 Ni –30Co Alloy

For Big Grains :

From fig.36(a), it can be seen that for the heat treatment ,50pct.820C-3h(i) , the big grain size distribution starts from 60microns and maximum grain size is found to be ~210micron. The distribution is found to be uniformly decreasing. The maximum numbers of grains are found at 60microns.

From fig.36(b), it can be seen that for the heat treatment , 50pct.820C-3h(ii) , the big grain size distribution starts from 60microns and maximum grain size is found to be ~250micron. The distribution is found to be uniformly decreasing with a slight increase at ~200micron. The maximum numbers of grains are found at 60microns.

From fig.36(c), it can be seen that for the heat treatment , Annealed-820C-10h , the big grain size distribution starts from 60microns and maximum grain size is found to be ~240micron. The distribution is found to be uniformly decreasing but the rate of decrease is small. The maximum numbers of grains are found at 60microns.

From fig.36(d), it can be seen that for the heat treatment , Annealed-850C-3h , the big grain size distribution starts from 80microns and maximum grain size is found to be ~240micron. The distribution is found to be uniformly decreasing. The maximum numbers of grains are found at 80microns.

For Small Grains :

From fig.37(a), it can be seen that for the heat treatment,50pct.820C-3h(i) , the small grain size distribution starts from 5microns and maximum grain size is found to be ~60micron. The distribution has a maximum at 15micron.

From fig.37(b), it can be seen that for the heat treatment, 50pct.820C-3h(ii) , the small grain size distribution starts from 5microns and maximum grain size is found to be ~60micron. The distribution is found to be sharply decreasing. The maximum numbers of grains are found at 5microns.

From fig.37(c), it can be seen that for the heat treatment, Annealed-820C-10h , the small grain size distribution starts from 5micron and maximum grain size is found to be ~80micron. The distribution is found to be uniformly decreasing. The maximum numbers of grains are found at 5micron .

From fig.37(d), it can be seen that for the heat treatment, Annealed-850C-3h , the small grain size distribution starts from 5microns and maximum grain size is found to be ~80micron. The distribution is found to be uniformly decreasing. The maximum numbers of grains are found at 5microns and 15micron.

For Mixed Grains :

From fig.38(a), it can be seen that for the heat treatment ,50pct.820C-3h(i) , the mixed grain size distribution starts from 5micron and maximum grain size is found to be

~210micron. The distribution is found to be sharply decreasing. The maximum numbers of grains are found at 5micron.

From fig.38(b), it can be seen that for the heat treatment ,50pct.820C-3h(ii) , the mixed grain size distribution starts from 5micron and maximum grain size is found to be ~220micron. The distribution is found to be sharply decreasing. The maximum numbers of grains are found at 5micron.

From fig.38(c), it can be seen that for the heat treatment , Annealed-820C-10h , the mixed grain size distribution starts from 5microns and maximum grain size is found to be ~160micron. The distribution is found to be uniformly decreasing. The maximum numbers of grains are found between 5microns and 25micron.

From fig.38(d), it can be seen that for the heat treatment , Annealed-850C-3h , the mixed grain size distribution starts from 5microns and maximum grain size is found to be ~160micron. The distribution is found to be uniformly decreasing with a slight increase at 80micron The maximum numbers of grains are found between 5micron to 35microns.

4.2.2 Ni –40Co Alloy

For Big Grains :

From fig.39(a), it can be seen that for the heat treatment ,50pct.820C-3h(i) , the big grain size distribution starts from 60microns and maximum grain size is found to be ~190micron. The distribution is found to be non-uniformly decreasing. The maximum numbers of grains are found at 60microns.

From fig.39(b), it can be seen that for the heat treatment , 50pct.820C-3h(ii) , the big grain size distribution starts from 60microns and maximum grain size is found to be ~190micron. The distribution is found to be uniformly decreasing. The maximum numbers of grains are found at 60microns.

From fig.39(c), it can be seen that for the heat treatment , Annealed-820C-10h , the big grain size distribution starts from 60microns and maximum grain size is found to be ~200micron. The distribution is found to be decreasing. The maximum numbers of grains are found at 60microns .

From fig.39(d), it can be seen that for the heat treatment , Annealed-850C-3h , the big grain size distribution starts from 80microns and maximum grain size is found to be ~210micron. The distribution is found to be uniformly decreasing. The maximum numbers of grains are found between 60microns and 95micron.

For Small Grains :

From fig.40(a), it can be seen that for the heat treatment ,50pct.820C-3h(i) , the small grain size distribution starts from 5microns and maximum grain size is found to be ~60micron. The distribution is found to have maxima at 15microns.

From fig.40(b), it can be seen that for the heat treatment , 50pct.820C-3h(ii) , the small grain size distribution starts from 5microns and maximum grain size is found to be ~60micron. The distribution is found to have maxima at 15microns.

From fig.40(c), it can be seen that for the heat treatment , Annealed-820C-10h , the small grain size distribution starts from 5microns and maximum grain size is found to be ~60micron. The distribution is found to be uniformly decreasing. The maximum numbers of grains are found at 5micron .

From fig.40(d), it can be seen that for the heat treatment , Annealed-850C-3h , the small grain size distribution starts from 5microns and maximum grain size is found to be ~60micron. The distribution is found to be uniformly decreasing. The maximum numbers of grains are found at 5micron.

For Mixed Grains :

From fig.41(a), it can be seen that for the heat treatment ,50pct.820C-3h(i) , the mixed grain size distribution starts from 5microns and maximum grain size is found to be ~210micron. The distribution is found to have maximum at 15micron.

From fig.41(b), it can be seen that for the heat treatment ,50pct.820C-3h(ii) , the mixed grain size distribution starts from 5microns and maximum grain size is found to be ~210micron. The distribution is found to have maximum at 15micron.

From fig.41(c), it can be seen that for the heat treatment , Annealed-820C-10h , the mixed grain size distribution starts from 5micron and maximum grain size is found to be

~180micron. The distribution is found to be uniformly decreasing with a slight increase at 110micron. The maximum numbers of grains are found at 15micron.

From fig.41(d), it can be seen that for the heat treatment , Annealed-850C-3h , the mix grain size distribution starts from 5microns and maximum grain size is found to be ~150micron. The distribution is found to have maximum at 15micron and 80micron.

4.2.3 Ni –60Co Alloy

For Big Grains :

From fig.42(a), it can be seen that for the heat treatment ,50pct.820C-3h(i) , the big grain size distribution starts from 60microns and maximum grain size is found to be ~150micron. The distribution is found to be sharply decreasing. The maximum numbers of grains are found at 60microns.

From fig.42(b), it can be seen that for the heat treatment , 50pct.820C-3h(ii) , the big grain size distribution starts from 60microns and maximum grain size is found to be ~200micron. The distribution is found to be sharply decreasing. The maximum numbers of grains are found at 60microns.

From fig.42(c), it can be seen that for the heat treatment , Annealed-820C-10h , the big grain size distribution starts from 60microns and maximum grain size is found to be ~210micron. The distribution is found to be sharply decreasing. The maximum numbers of grains are found at 60microns .

From fig.42(d), it can be seen that for the heat treatment , Annealed-850C-3h , the big grain size distribution starts from 80microns and maximum grain size is found to be ~240micron. The distribution is found to be uniformly decreasing. The maximum numbers of grains are found at 60micron.

For Small Grains :

From fig.43(a), it can be seen that for the heat treatment ,50pct.820C-3h(i) , the small grain size distribution starts from 5microns and maximum grain size is found to be ~60micron. The distribution is found to have maxima at 15microns.

From fig.43(b), it can be seen that for the heat treatment , 50pct.820C-3h(ii) , the small grain size distribution starts from 5microns and maximum grain size is found to be ~60micron. The distribution is found to have maxima at 15microns.

From fig.43(c), it can be seen that for the heat treatment , Annealed-820C-10h , the small grain size distribution starts from 5microns and maximum grain size is found to be ~60micron. The distribution is found to be sharply decreasing. The maximum numbers of grains are found at 5micron .

From fig.43(d), it can be seen that for the heat treatment , Annealed-850C-3h , the small grain size distribution starts from 5microns and maximum grain size is found to be ~60micron..The maximum numbers of grains are found at 5micron.

For Mixed Grains :

From fig.44(a), it can be seen that for the heat treatment ,50pct.820C-3h(i) , the mixed grain size distribution starts from 5microns and maximum grain size is found to be ~210micron. The distribution is found to have maxima at 15micron.

From fig.44(b), it can be seen that for the heat treatment ,50pct.820C-3h(ii) , the mixed grain size distribution starts from 5microns and maximum grain size is found to be ~210micron. The distribution is found to have maxima at 15micron.

From fig.44(c), it can be seen that for the heat treatment , Annealed-820C-10h , the mixed grain size distribution starts from 5microns and maximum grain size is found to be ~160micron. The distribution is found to be uniformly decreasing. The maximum numbers of grains are found at 5micron.

From fig.44(d), it can be seen that for the heat treatment , Annealed-850C-3h , the mixed grain size distribution starts from 5microns and maximum grain size is found to be ~190micron. The distribution is found to have maximum at 5micron and 80micron .

4.3 Graphical Representations of the Histograms as a function of Heat Treatment

The above results are also shown in graphical form from figures 45 – 53. Here the points at the maximum values of the histograms have been joined by straight lines. This type of

diagram allows one to compare the grain size distribution in each alloy as a function of heat treatment.

4.3.1 Ni-30Co Alloy

For Big Grains :

From fig.45 , it was found that between size range 80micron and 100micron ,maximum number of grains are for the heat treatment ,Annealed-850C-3h. For the size range 130micron and 150micron , maximum number of grains are for the heat treatment, Annealed-820C-10h. The curve for the heat treatment, 50pct.820C-3h(ii), in all size ranges lies below all the curves except at 70micron. It was found that, in totality, all the curves have very little differences and between size ranges 160micron and 240micron all the curves try to merge in one another.

For Small Grains :

From fig.46 , it was found that between size ranges 5micron and 35micron the difference in the frequency for the various heat treatments is large but it gradually decreases as the size of grain increases. For the size range 20micron and 40micron the maximum number of grains are for the heat treatment, 50pct.820C-3h(i). Except for size range from 5micron to 15micron, the curve for the heat treatment , Annealed-820C-10h , lies below all the curves.

For Mixed Grains :

From fig.47 , it was found that for all the size ranges the curves for various heat treatments are very close to one another. For the size range from 25micron to 90micron the number of grains for the heat treatment , Annealed-820C-10h , lies below all the curves. For the size range from 75micron to 210micron the curve for the heat treatment, 50pct.820C-1h(i) , lies above all the curves. The curve for the heat treatment,

Annealed-850C-3h , in the size range from 100micron to 175micron, lies below all the curves.

4.3.1 Ni –40Co Alloy

For Big Grains :

From fig.48 , it was found that for the size range from 65micron to 140micron, the curve for the heat treatment, Annealed-820C-10h , lies below all the curves. For the size range from 60micron to 100micron, the curve for the heat treatment , 50pct.820C-3h(ii) , lies above all the curves. For the size range from 60micron to 90micron the differences in the values of the frequencies for various heat treatments are small , but the differences widen up as the grain size increases.

For Small Grains :

From fig.49 , it was observed that for the size ranges from 5micron to 45microns the difference in the frequency values for various heat treatments is large but this difference decreases to some extent as the grain size increases. For the size range from 20micron to 100micron, the curve for the heat treatment, Annealed-820C-10h, lies below all the curves. For the size range from 30micron to 45micron, the curve for the heat treatment, 50pct.820C-3h(ii) , lies above all the curves.

For Mixed Grains :

From fig.50 , it was found that for all the size ranges the frequency values for various heat treatments differ largely from one another. For the size range from 50micron to 200micron, the curve for the heat treatment , 50pct.820C-3h(ii) , lies above all the curves, except at 75micron. For the size range from 35micron-60micron and 150micron-200micron, the curve for the heat treatment , Annealed-820C-10h , lies below all the curves.

4.3.2 Ni-60Co Alloy

For Big Grains :

From fig.51 , it was found that for the size range from 90micron to 130micron the frequency values for various heat treatments differ largely from one another. However, within this range the frequency values for the heat treatments, 50pct.820C-3h(ii) and Annealed-850C-3h, are found to be exactly same. For the size range from 70micron to 130micron, the curve for the heat treatment , 50pct.820C-3h(i) , lies above all the curves, except at 100micron. For the size range from 80micron to 130micron, the curve for the heat treatment , Annealed-820C-10h , lies below all the curves.

For Small Grains :

From fig.52 , it was observed that for the size ranges from 5micron to 50microns the difference in the frequency values for various heat treatments is large but this difference decreases to some extent as the grain size increases and at very large values various values are found to be exactly the same. For the size range from 20micron to 110micron, the curve for the heat treatment , Annealed-820C-10h , lies below all the curves. For the size range from 40micron to 110micron, the curve for the heat treatment , 50pct.820C-3h(i) , lies above all the curves except at 60micron.

For Mixed Grains :

From fig.53 , it was found that for all the size ranges the frequency values for various heat treatments differ largely from one another. For the size range from 50micron to 210micron, the curve for the heat treatment , 50pct.820C-3h(i) , lies above all the curves. For the size range from 60micron to 110micron-200micron, the curve for the heat treatment , Annealed-820C-10h , lies below all the curves. For the size range from 110micron to 190micron, the curve for the heat treatment , Annealed-850C-3h , lies below all the curves.

4.4 Graphical Representations of the Histograms as a function of Alloying

In this section the maximum values of the histograms have been joined by straight lines and comparison of grain size distribution at various heat treatments is done for all the three alloys.

4.4.1 *Big Grains*

For heat treatment , 50pct.820C-3h(i) :

From the fig. 54a , it can be seen that for size range from 60micron to 120micron the difference in the frequency values for the three alloys are very much different from each other but this difference decreases as the grain size increases. For size range from 80micron to 120micron maximum number of grains are for Ni-30Co alloy and minimum number of grains are for Ni-40Co alloy. For size range 120micron to 130micron the maximum number of grains are for Ni-60Co alloy.

For heat treatment , 50pct.820C-3h(ii) :

From the fig.54b , it can be seen that for the size 60micron , the difference in the frequency values for the three alloys are very much different from each other but this difference decreases drastically as the grain size increases and it was found that from size range 110micron to 190micron the values get merged into each other. For size range from 60micron to 110micron maximum number of grains are for Ni-30Co alloy and minimum number of grains are for Ni-40Co alloy.

For heat treatment, Annealed-820C-10h :

From the fig.54c , it can be seen that for the size range from 60micron to 110micron, the difference in the frequency values for the three alloys are different from each other but this difference decreases as the grain size increases and it was found that from size range 160micron to 240micron the values approach each other. For size range from 80micron to 240micron maximum number of grains are for Ni-30Co alloy and minimum number of grains are for Ni-60Co alloy. For the sizes 70micron and 140micron the frequency value for Ni-40Co alloy is found to be lowest.

For heat treatment, Annealed-850C-3h :

From the fig.54d , it can be seen that for the size range from 80micron to 200micron, the difference in the frequency values for the three alloys are different from each other but this difference decreases as the grain size increases and it was found that from size range from 190micron to 240micron the values get merged into each other. For size range from 80micron to 200micron maximum number of grains are for Ni-30Co alloy and minimum number of grains are for Ni-60Co alloy.

4.4.2 Small Grains

For heat treatment , 50pct.820C-3h(i) :

From the fig.55a , it can be seen that for all size ranges, the difference in the frequency values for the three alloys are much different from each other. The frequency values for Ni-30Co alloy and Ni-40Co alloy are very much similar to each other. For size range from 5micron to 100micron maximum number of grains are for Ni-60Co alloy. For the sizes 70micron and 100micron the frequency value for Ni-40Co alloy is found to be lowest.

For heat treatment , 50pct.820C-3h(ii) :

From the fig.55b , it can be seen that for size range from 5micron to 20micron the difference in the frequency values for Ni-60Co alloy is very much different from Ni-30Co alloy and Ni-40Co alloy ,but this difference decreases as the grain size increases. For the size range from 5micron to 40micron maximum number of grains are for Ni-60Co alloy. For size range from 40micron to 60micron and size range from 80micron to 110micron, the minimum number of grains are for Ni-40Co alloy and Ni-30Co alloy.

For heat treatment, Annealed-820C-10h :

From the fig.55c , it can be seen that for size range from 5micron to 20micron the difference in the frequency values for Ni-60Co alloy is very much different from Ni-30Co alloy and Ni-40Co alloy ,but this difference decreases as the grain size

increases. For size range from 5micron to 100micron maximum number of grains are for Ni-60Co alloy except at 25micron , where largest value is for Ni-40Co alloy. For size range 25micron to 90micron the minimum number of grains are for Ni-30Co alloy.

For heat treatment, Annealed-850C-3h :

From the fig.55d , it can be seen that for size range from 5micron to 20micron the difference in the frequency values for Ni-60Co alloy is very much different from Ni-30Co alloy and Ni-40Co alloy ,but this difference decreases as the grain size increases. For size range from 5micron to 50micron maximum number of grains are for Ni-60Co alloy and minimum numbers of grains are for Ni-30Co alloy. For size range 60micron to 90micron the maximum number of grains are for Ni-40Co alloy.

4.4.3 Mixed Grains

For heat treatment , 50pct.820C-3h(i) :

From the fig.56a , it can be seen that for size range from 5micron to 60micron, the difference in the frequency values for the three alloys are very much different from each other, but this difference gradually decreases as the grain size increases . For size range from 25micron to 90micron maximum number of grains are for Ni-60Co and minimum number of grains are for Ni-30Co alloy . For the size range from 100micron to 150micron the frequency value for Ni-40Co alloy is found to be highest.

For heat treatment , 50pct.820C-3h(ii) :

From the fig.56b , it can be seen that for size range from 50micron to 60micron, the difference in the frequency values for the three alloys are very much different from each other (though Ni-30Co alloy and Ni-40Co alloy have very much similar values), but this difference gradually decreases as the grain size increases. other. For size range from 25micron to 110micron maximum number of grains are for Ni-60Co and minimum number of grains are for Ni-30Co alloy . For the size range from 110micron to 200micron the frequency value for Ni-40Co alloy is found to be highest. At size range from

180micron to 210micron the frequency values for Ni-40Co alloy and Ni-60Co alloy are found to be exactly the same.

For heat treatment, Annealed-820C-10h :

From the fig.56c , it can be seen that for size range from 5micron to 60micron the difference in the frequency values for all the three alloys is different from each other, but this difference decreases as the grain size increases. At higher values of grain sizes the frequency values tend to merge into each other. For size range from 5micron to 100micron and size range from 110micron to 210micron , the maximum number of grains are for Ni-60Co alloy and Ni-30Co alloy respectively. For size range 60micron to 90micron and from size range from 110micron to 160micron, the minimum number of grains are for Ni-40Co alloy and Ni-60Co alloy respectively.

For heat treatment, Annealed-850C-3h :

From the fig.56d , it can be seen that for size range from 5micron to 60micron the difference in the frequency values for all the three alloys is different from each other, and this difference decreases at very high grain size values. For size range from 15micron to 75micron , the maximum number of grains are for Ni-60Co alloy . For size range 30micron to 50micron and from size range from 110micron to 160micron, the minimum number of grains are for Ni-30Co alloy and Ni-60Co alloy respectively.

4.5 Volume Fraction of the big and Small Grains

The volume fractions of the big grains and the small grains (in colonies) in the different alloys, as a function of heat treatment, were determined and these are shown in tabular form in Table2.

Table2. Volume Fraction of big and small grains

Alloy	Ni-30Co		Ni-40Co		Ni-60Co	
Heat Treatment	Big	Small	Big	Small	Big	Small
50pct.820C-3h(I)	0.78	0.22	0.61	0.39	0.56	0.44
50pct.820C-3h(ii)	0.79	0.21	0.51	0.49	0.76	0.24
Annealed-820C-10h	0.63	0.37	0.52	0.48	0.54	0.46
Annealed-850C-3h	0.65	0.35	0.53	0.47	0.56	0.44

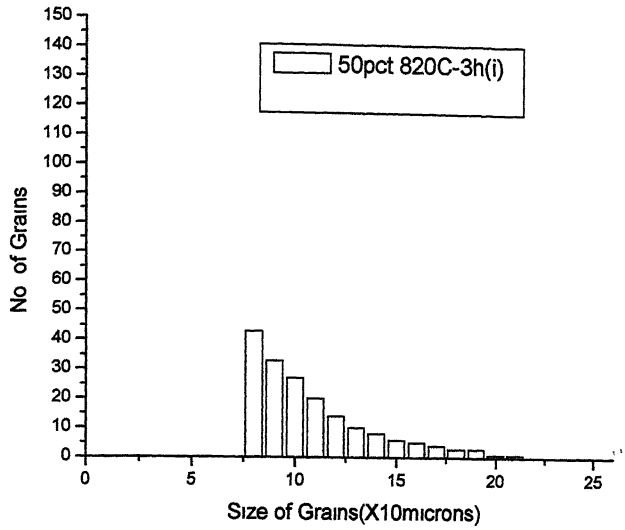

(a)

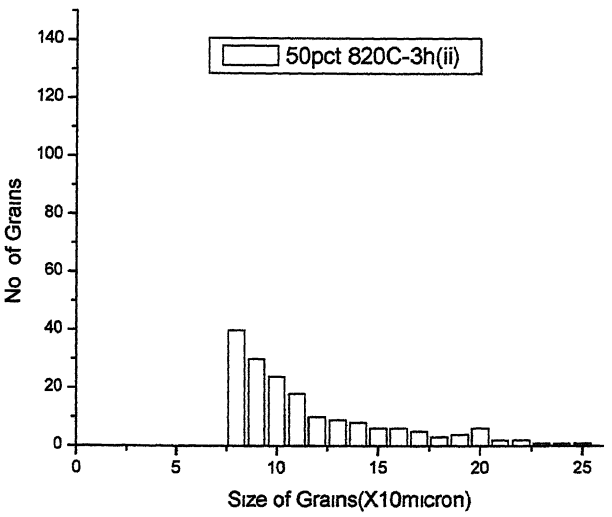

(b)

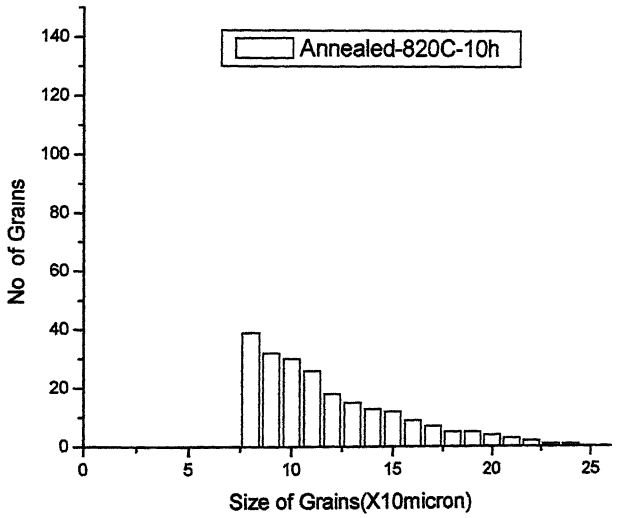

(c)

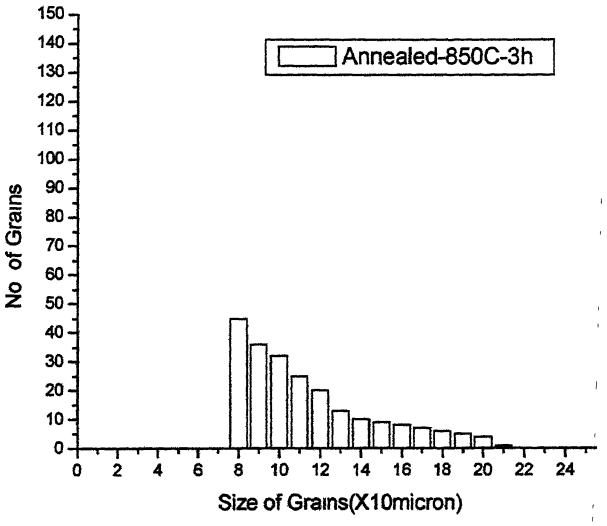

(d)

Fig. 36 Histograms for Big Grains for Ni-30Co Samples for the heat treatments

(a) 50pct.820°C-3h(i)
(b) 50pct.820°C-3h(ii)
(c) Annealed-820°C-10h
(d) Annealed-850°C-3h

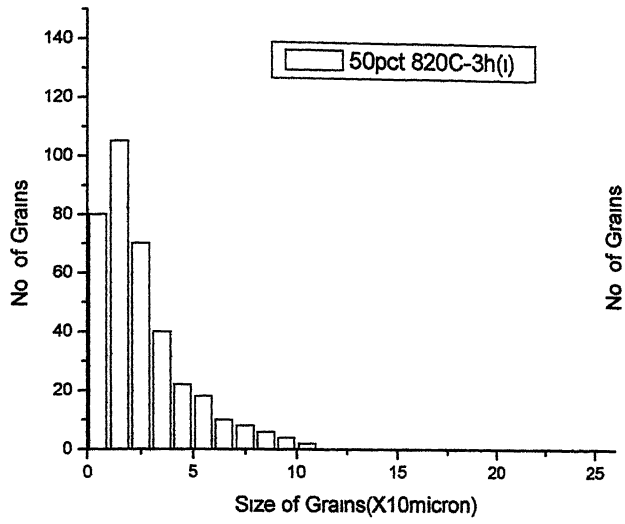

(a)

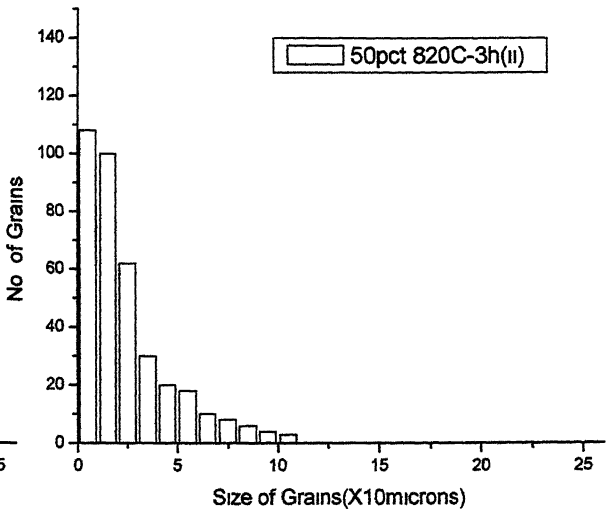

(b)

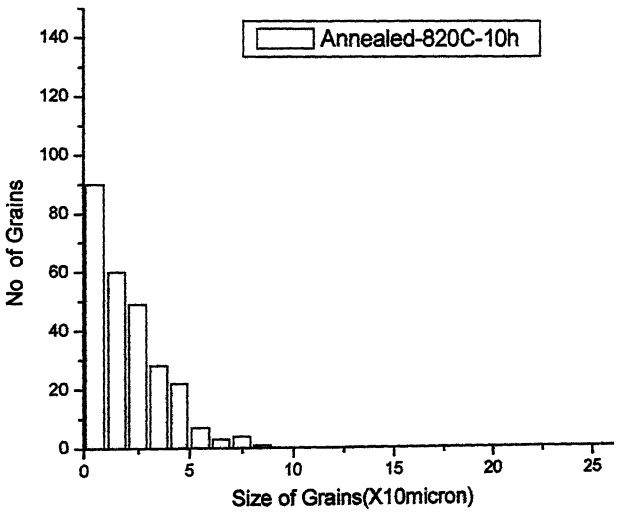

(c)

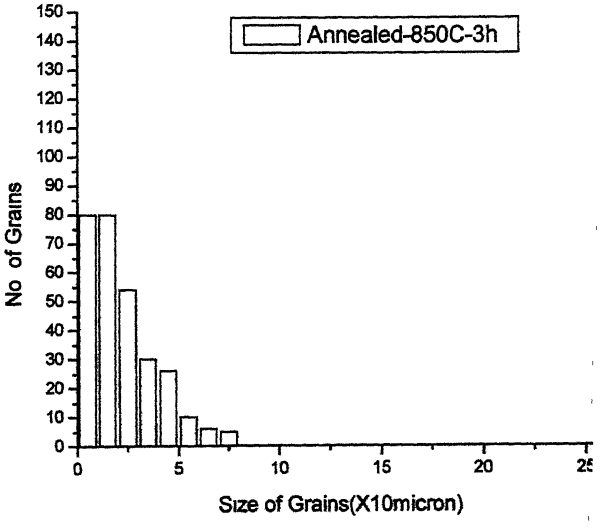

(d)

Fig. 37 Histograms for Small Grains for Ni-30Co Samples for the heat treatments
(a) 50pct.820°C-3h(i)
(b) 50pct.820°C-3h(ii)
(c) Annealed-820°C-10h
(d) Annealed-850°C-3h

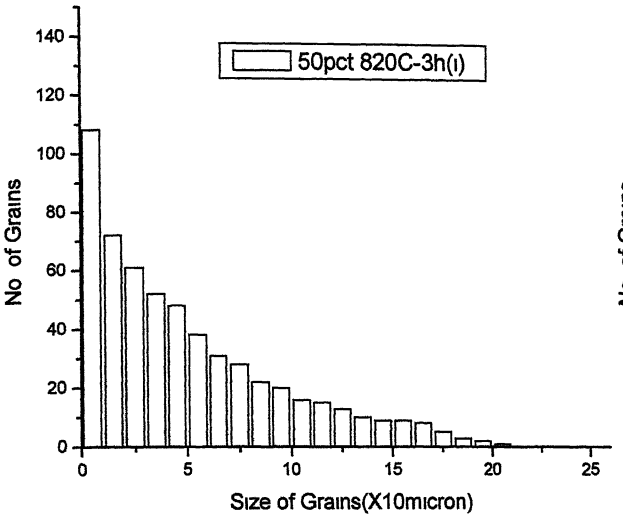

(a)

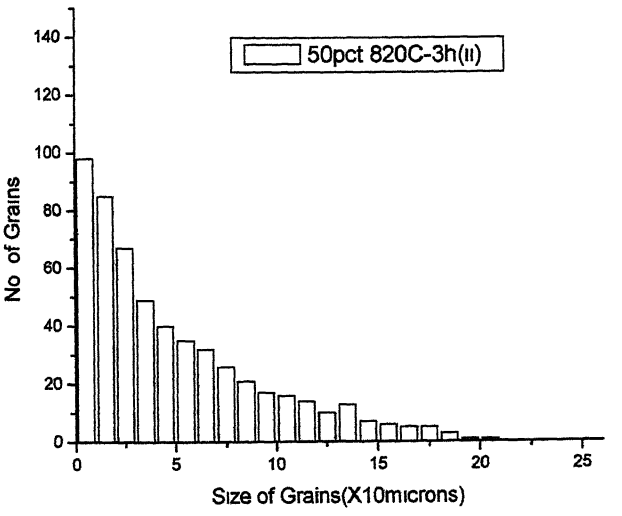

(b)

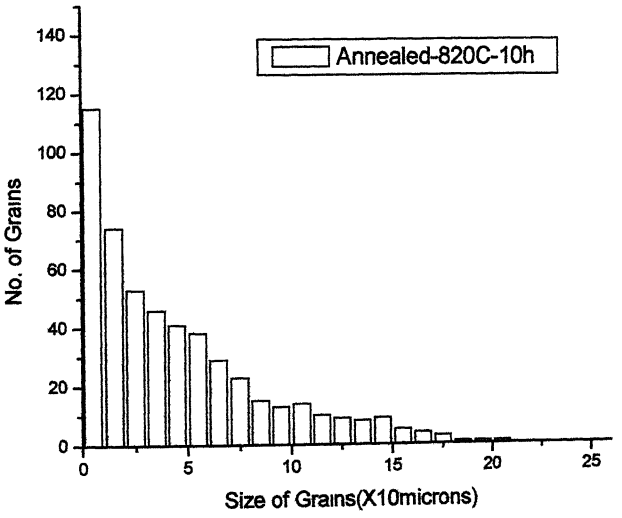

(c)

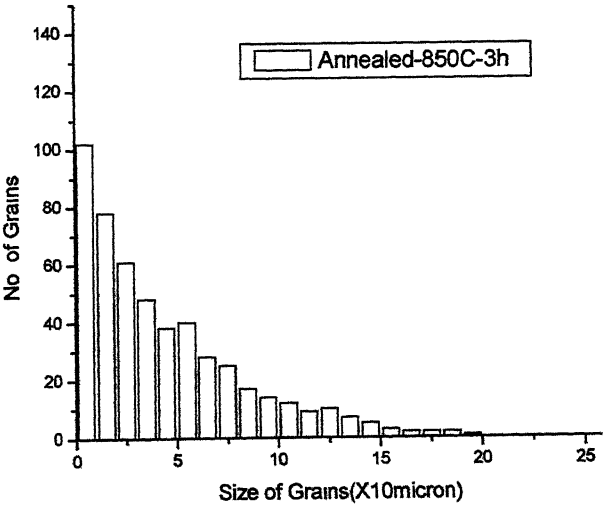

(d)

Fig. 38 Histograms for Mixed Grains for Ni-30Co Samples for the heat treatments
(a) 50pct.820°C-3h(i)
(b) 50pct.820°C-3h(ii)
(c) Annealed-820°C-10h
(d) Annealed-850°C-3h

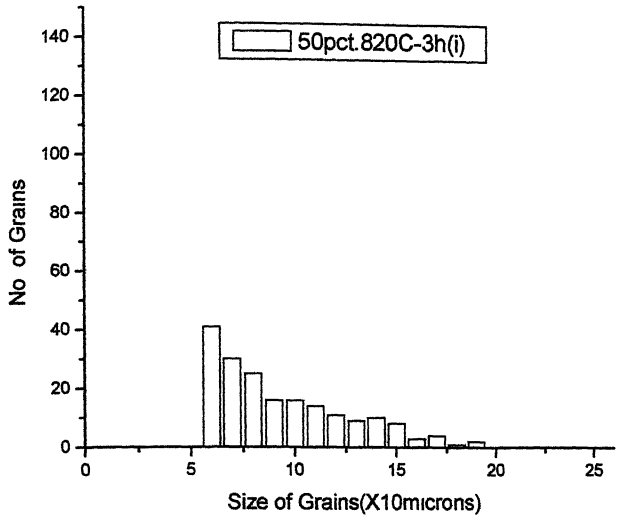

(a)

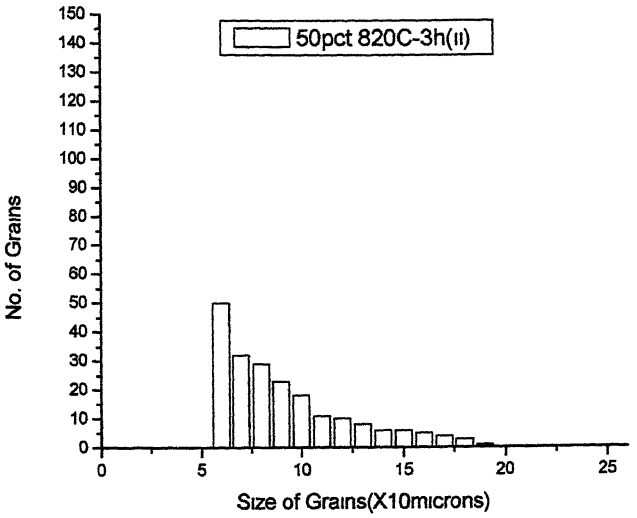

(b)

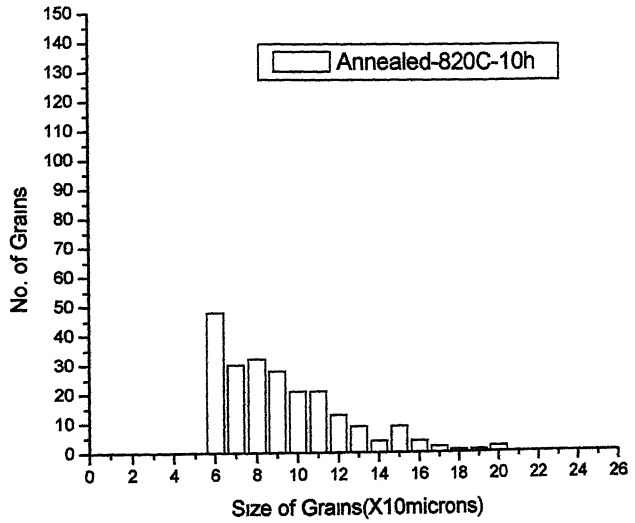

(c)

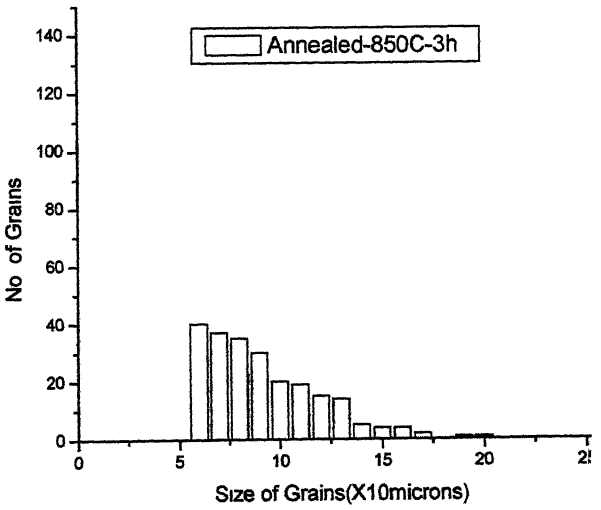

(d)

Fig. 39 Histograms for Big Grains for Ni-40Co Samples for the heat treatments
(a) 50pct.820°C-3h(i)
(b) 50pct.820°C-3h(ii)
(c) Annealed-820°C-10h
(d) Annealed-850°C-3h

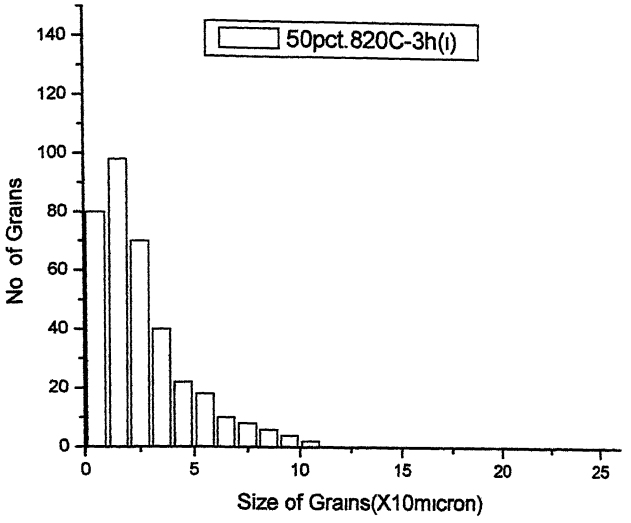

(a)

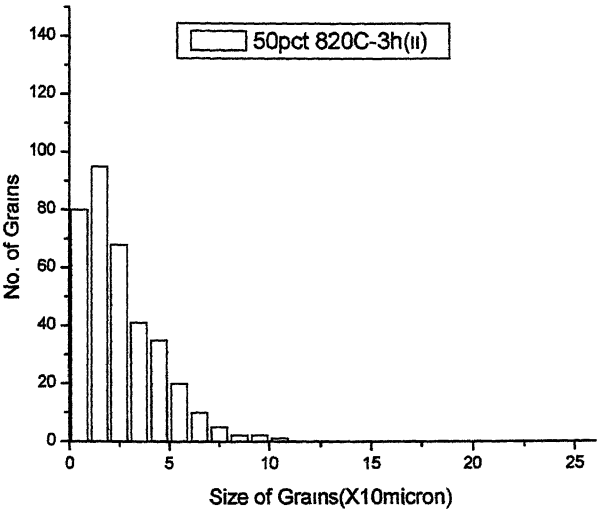

(b)

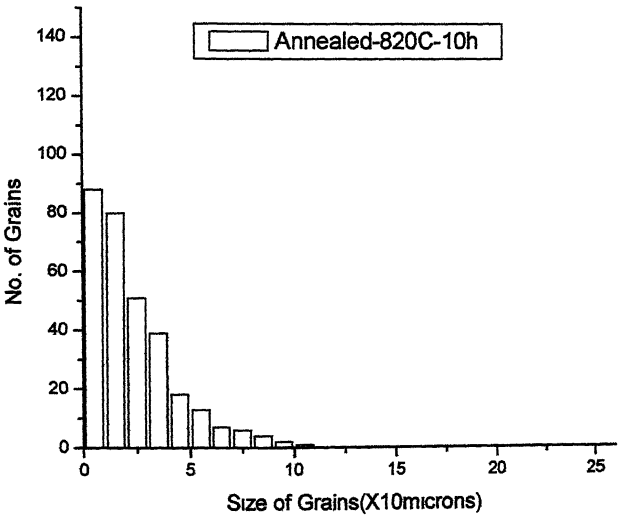

(c)

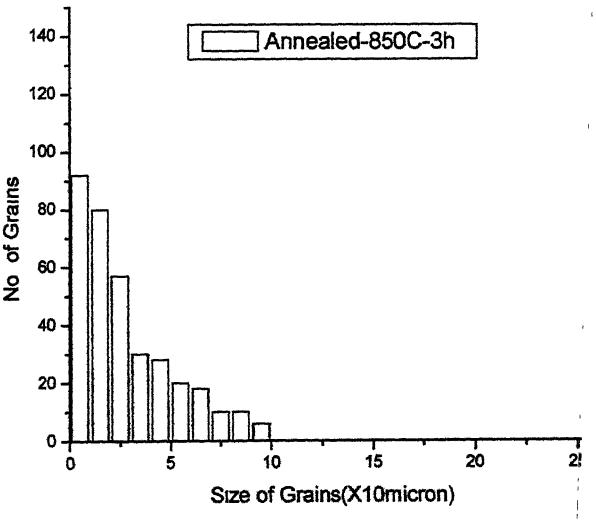

(d)

Fig. 40 Histograms for Small Grains for Ni-40Co Samples for the heat treatments
(a) 50pct.820°C-3h(i)
(b) 50pct.820°C-3h(ii)
(c) Annealed-820°C-10h
(d) Annealed-850°C-3h

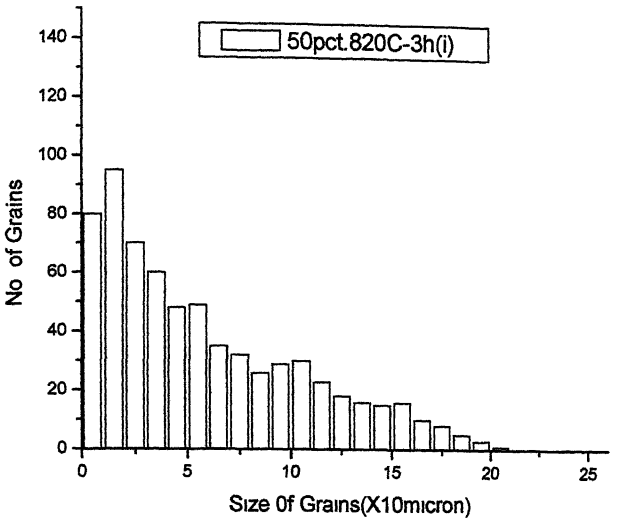

(a)

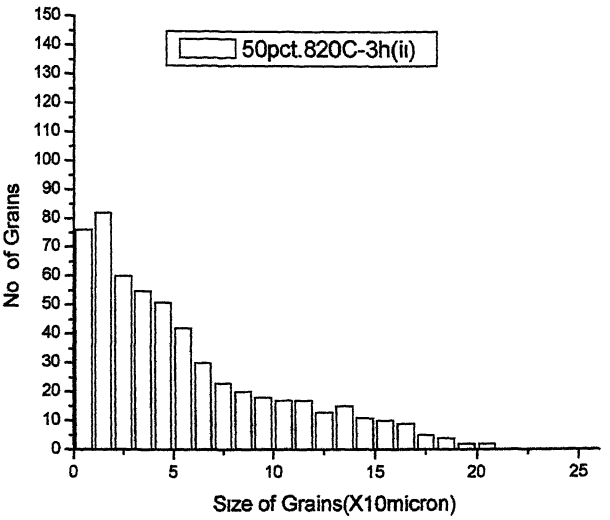

(b)

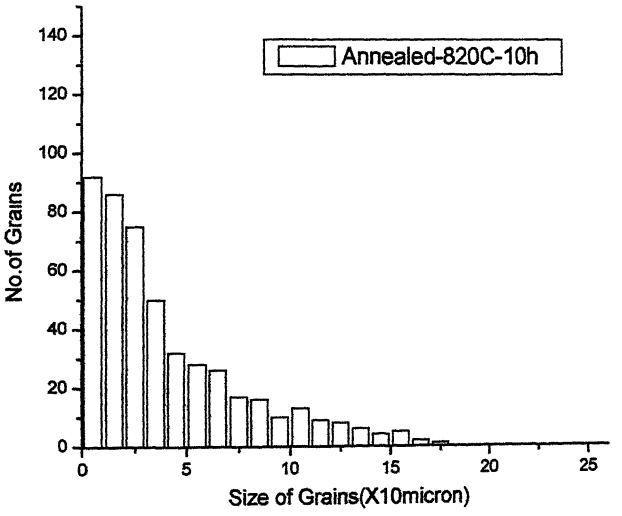

(c)

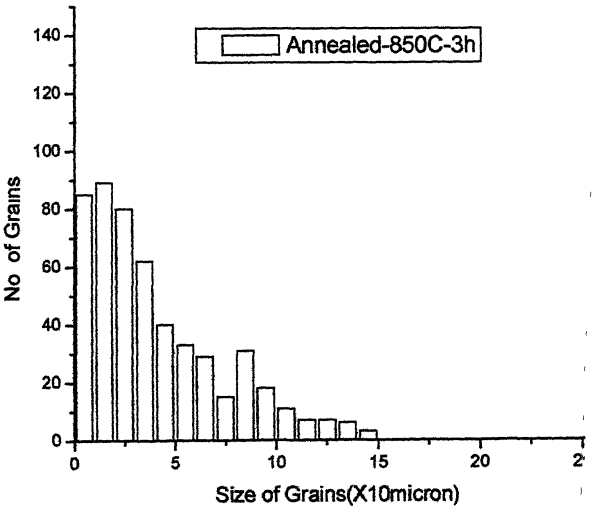

(d)

Fig. 41 Histograms for Mixed Grains for Ni-40Co Samples for the heat treatments

(a) 50pct.820°C-3h(i)
(b) 50pct.820°C-3h(ii)
(c) Annealed-820°C-10h
(d) Annealed-850°C-3h

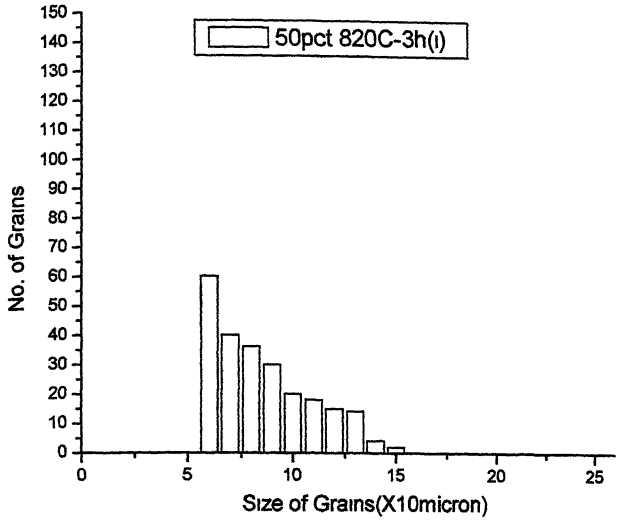

(a)

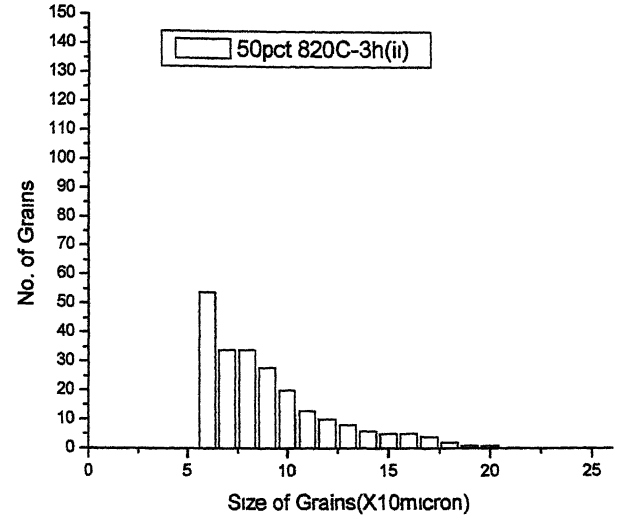

(b)

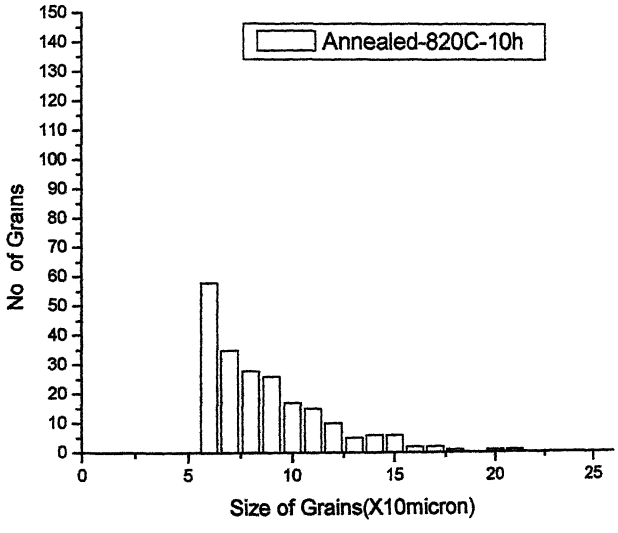

(c)

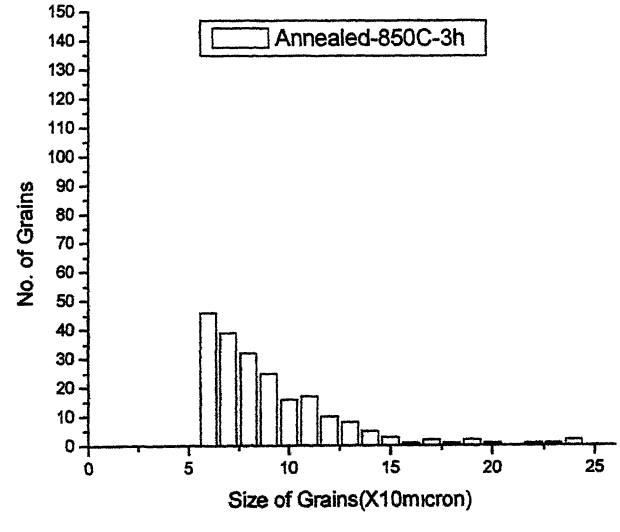

(d)

Fig. 42 Histograms for Big Grains for Ni-60Co Samples for the heat treatments
(a) 50pct.820°C-3h(i)
(b) 50pct.820°C-3h(ii)
(c) Annealed-820°C-10h
(d) Annealed-850°C-3h

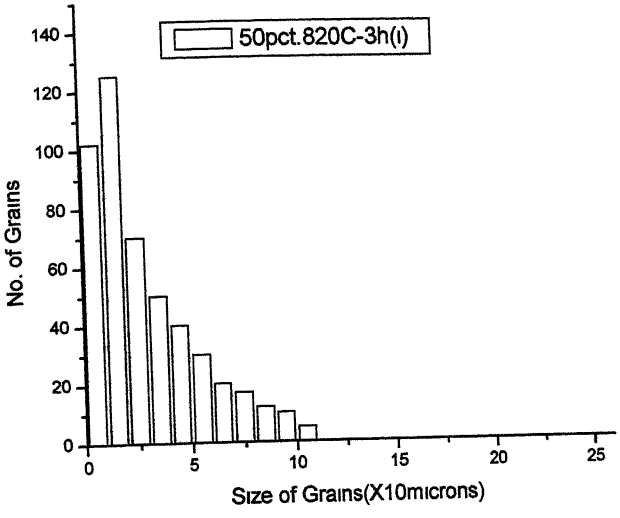

(a)

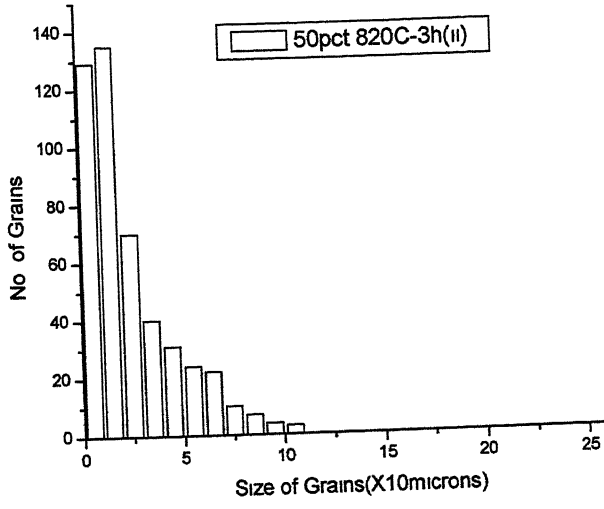

(b)

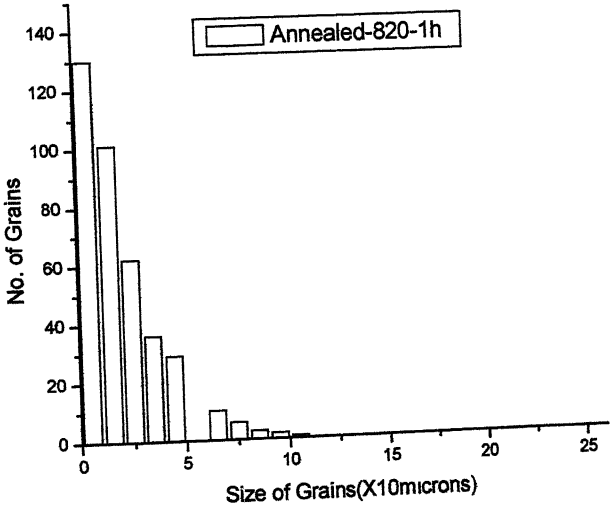

(c)

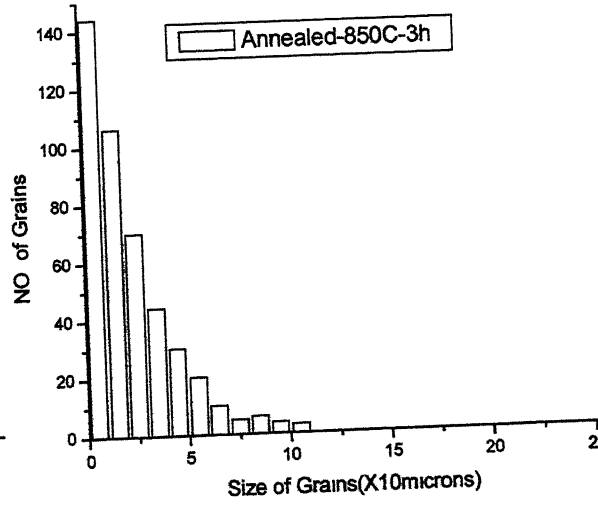

(d)

Fig. 43 Histograms for Small Grains for Ni-60Co Samples for the heat treatments
(a) 50pct.820°C-3h(i)
(b) 50pct.820°C-3h(ii)
(c) Annealed-820°C-10h
(d) Annealed-850°C-3h

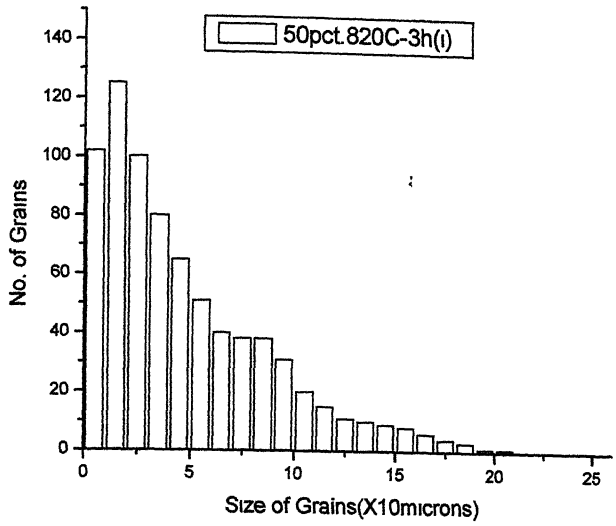

(a)

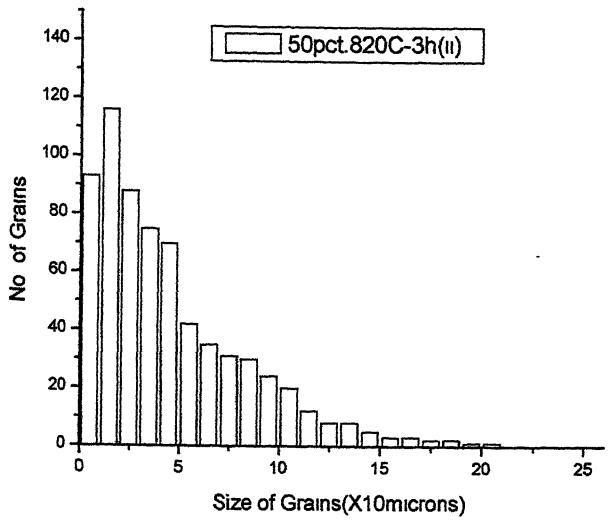

(b)

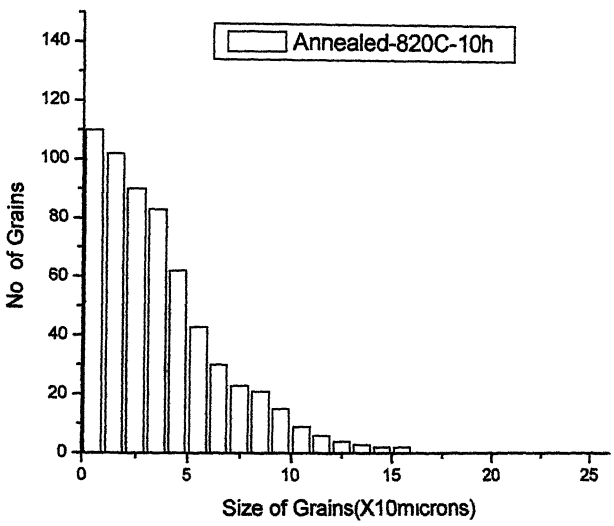

(c)

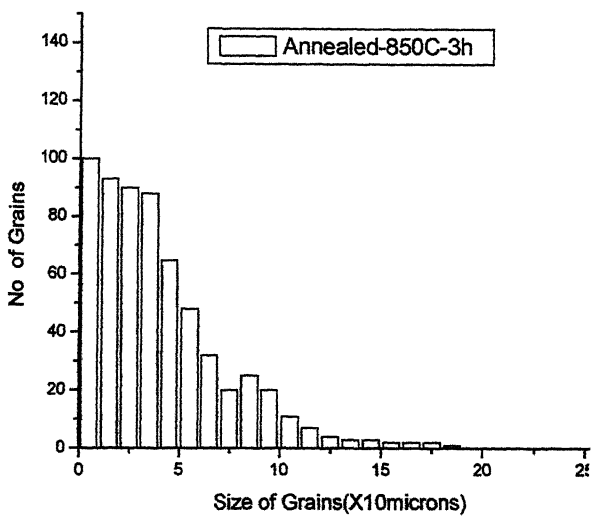

(d)

Fig. 44 Histograms for Mixed Grains for Ni-60Co Samples for the heat treatments

(a) 50pct.820°C-3h(i)
(b) 50pct.820°C-3h(ii)
(c) Annealed-820°C-10h
(d) Annealed-850°C-3h

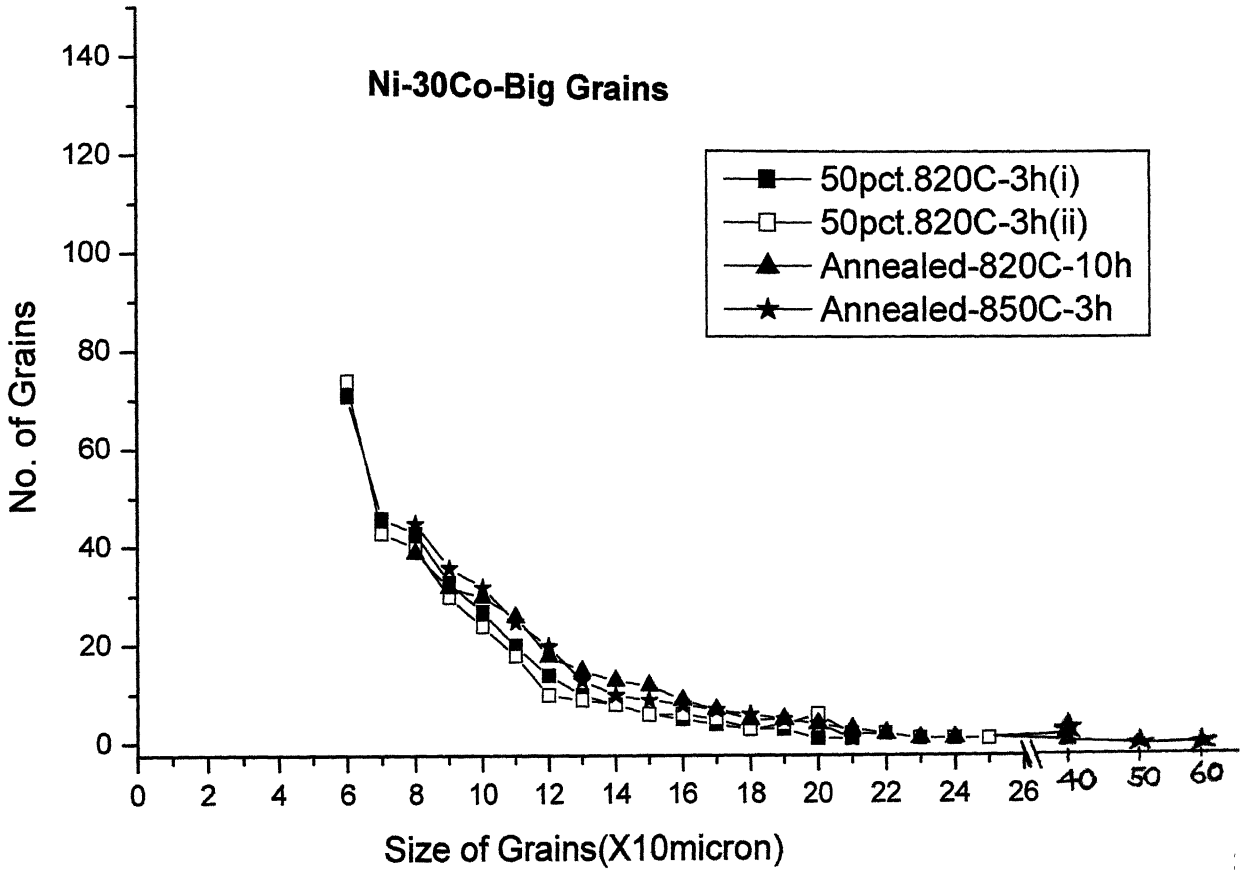

Fig. 45 Plot of Number of Grains vs. Grain Size for big grains for Ni-30Co alloy at different heat treatments

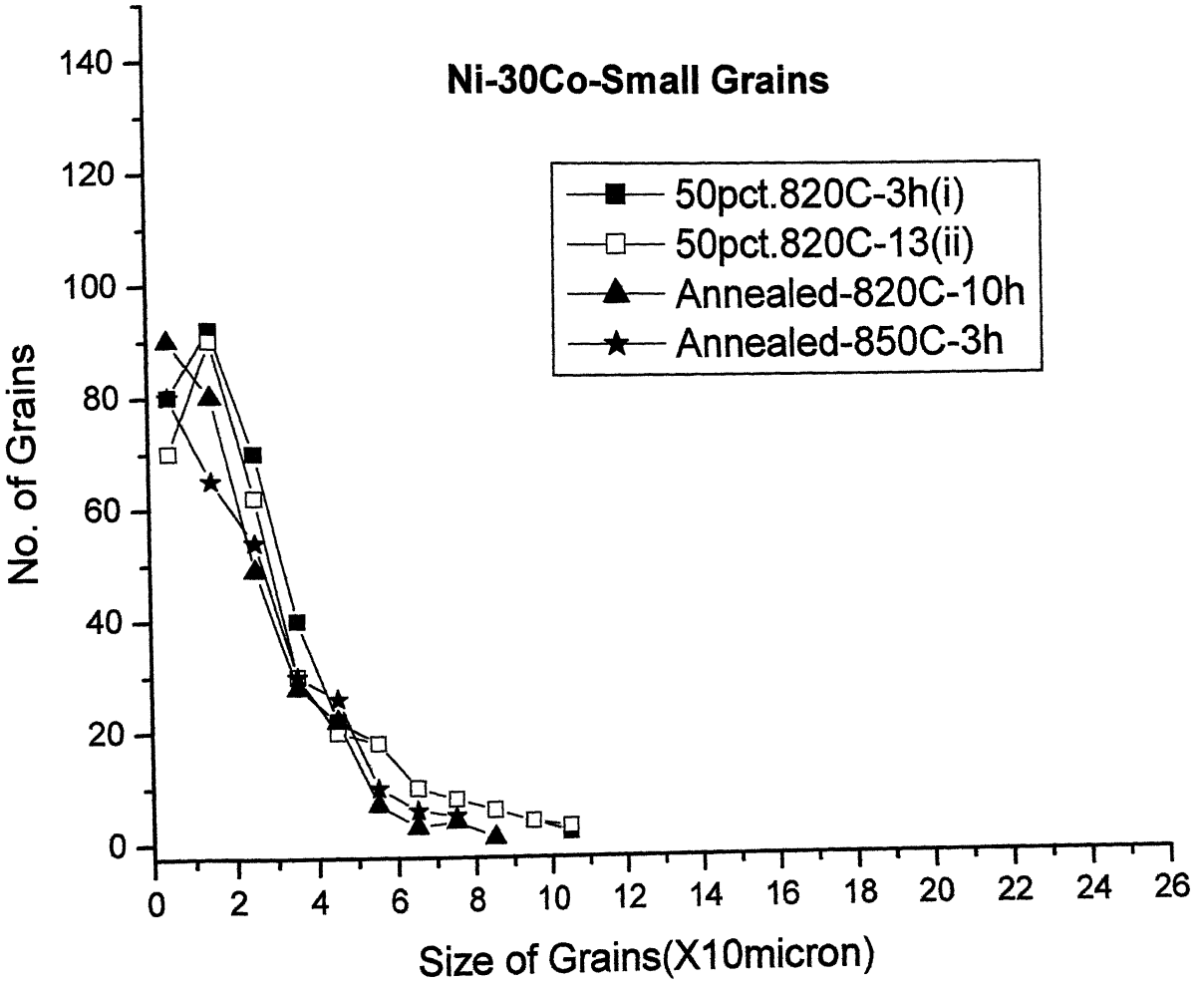

Fig. 46 Plot of Number of Grains vs. Grain Size for small grains for Ni-30Co alloy at different heat treatments

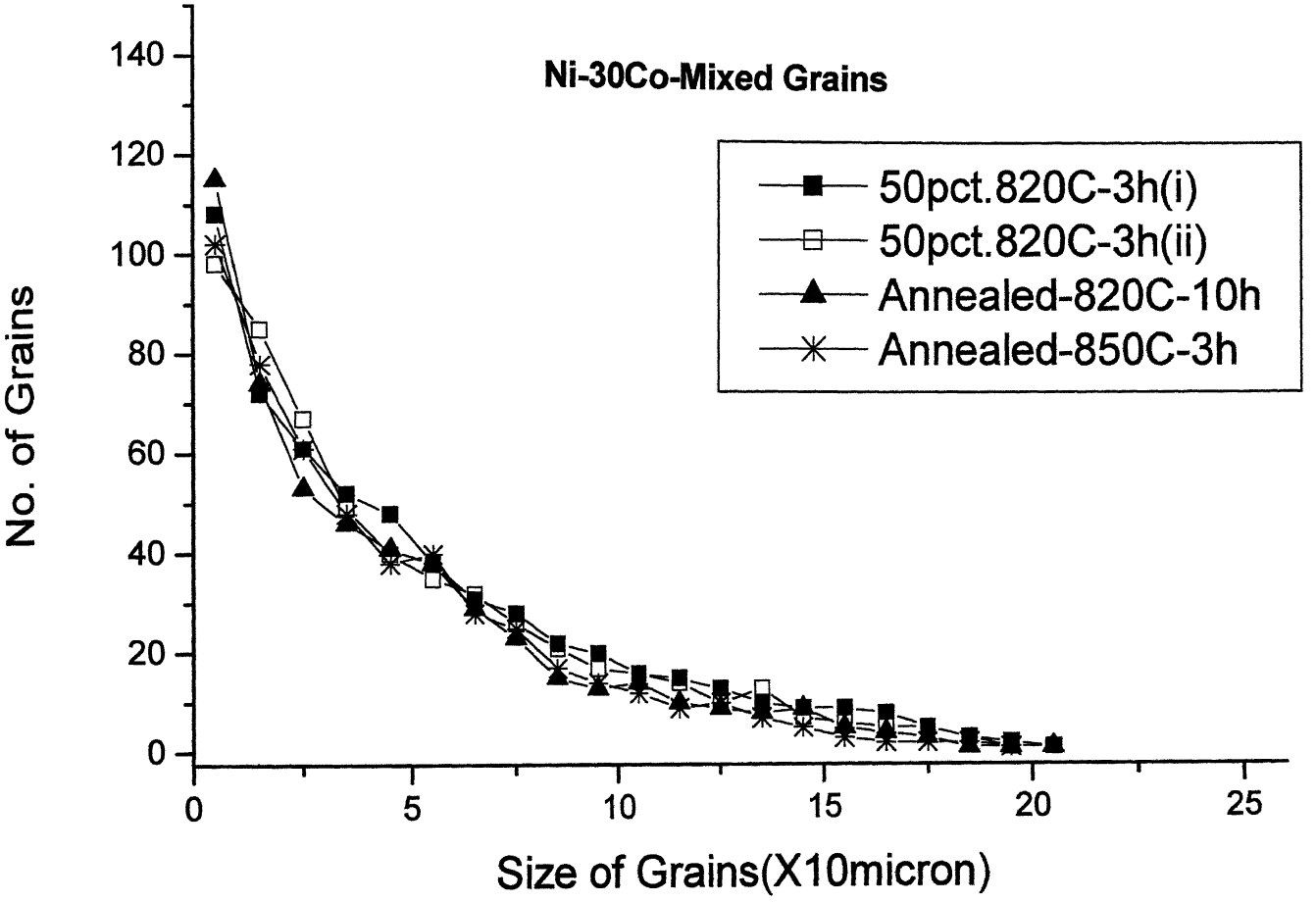

Fig. 47 Plot of Number of Grains vs. Grain Size for mixed grains for Ni-30Co alloy at different heat treatments

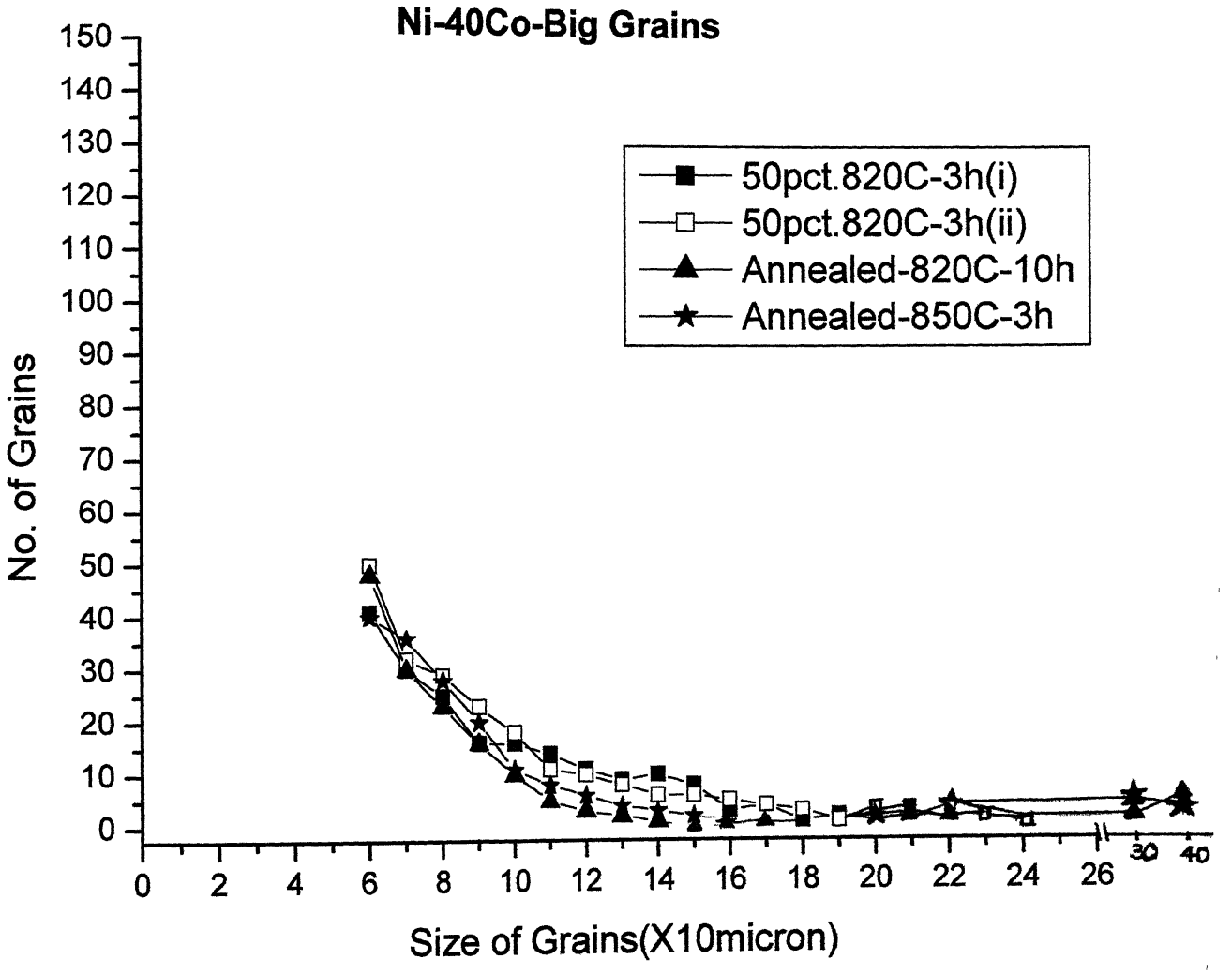

Fig. 48 Plot of Number of Grains vs. Grain Size for big grains for Ni-40Co alloy at different heat treatments

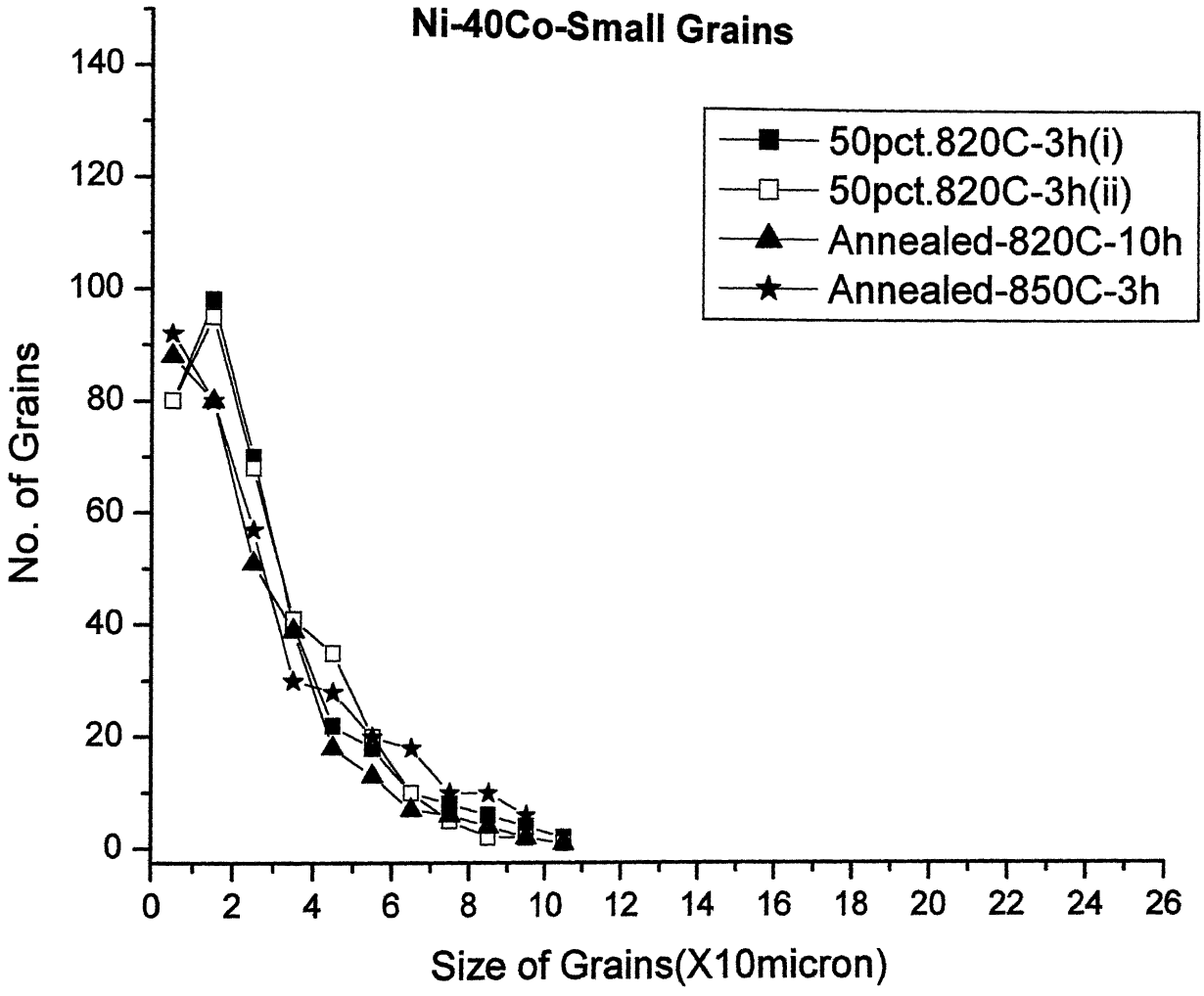

Fig. 49 Plot of Number of Grains vs. Grain Size for small grains for Ni-40Co alloy at different heat treatments

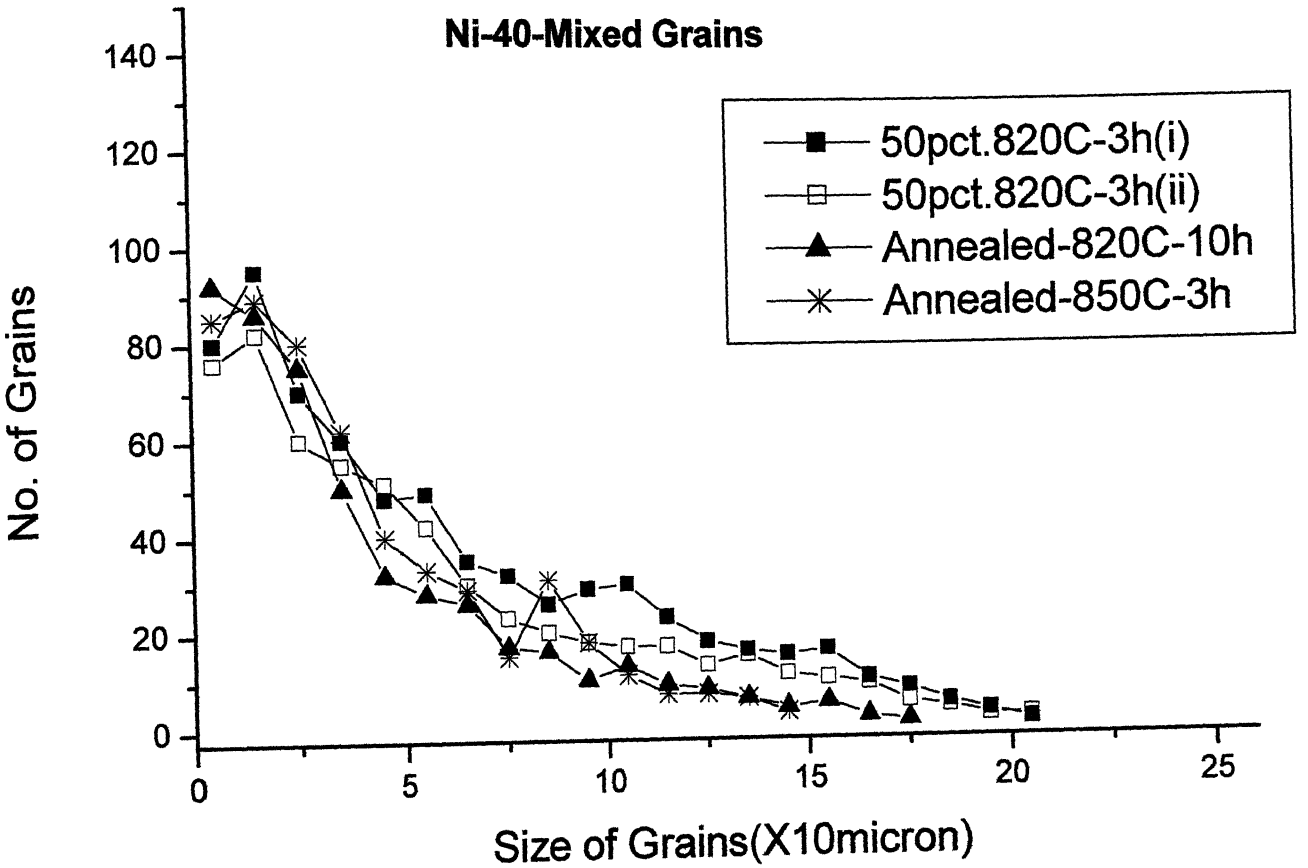

Fig. 50 Plot of Number of Grains vs. Grain Size for mixed grains for Ni-40Co alloy at different heat treatments

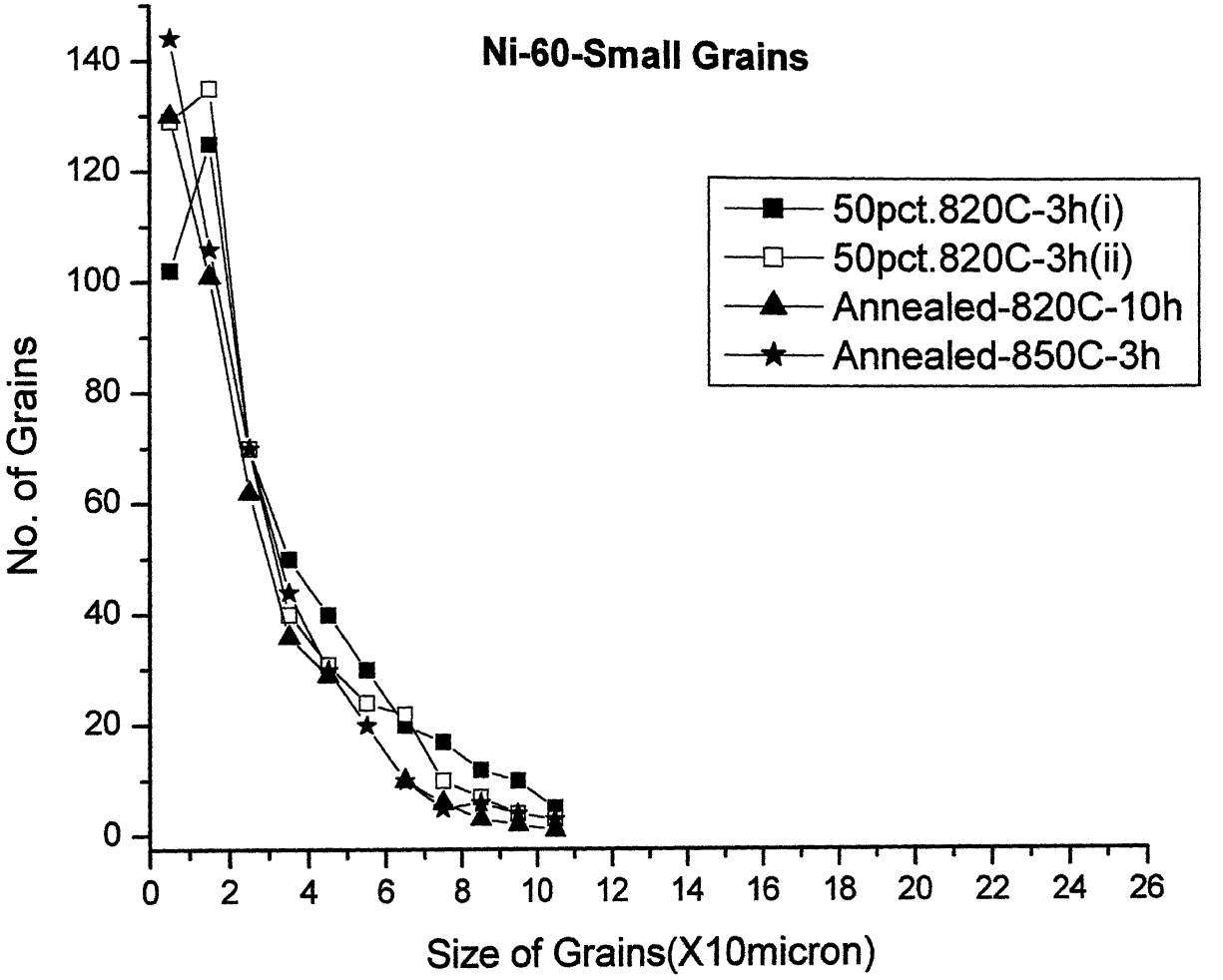

Fig. 52 Plot of Number of Grains vs. Grain Size for small grains for Ni-60Co alloy at different heat treatments

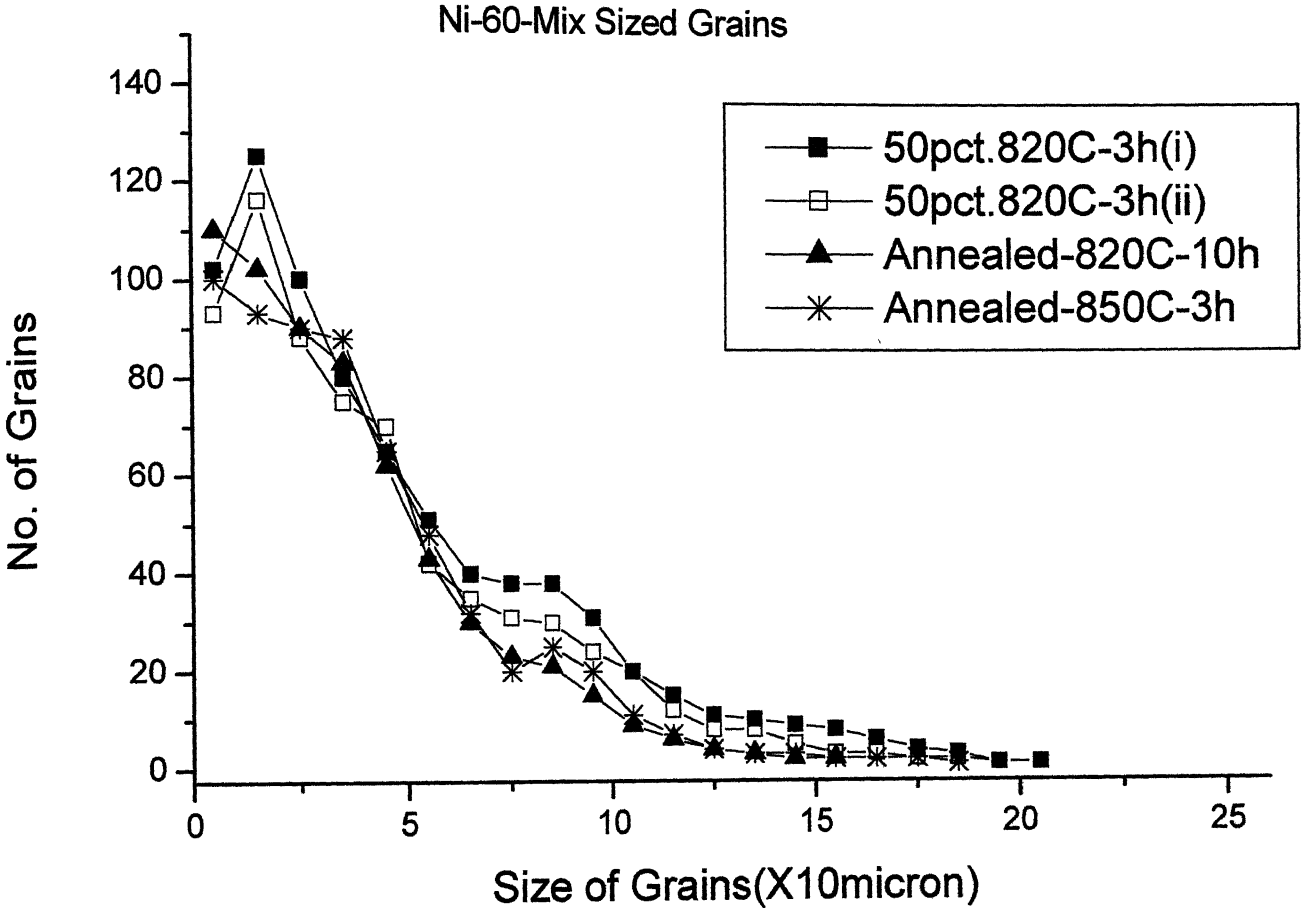

Fig. 53 Plot of Number of Grains vs. Grain Size for mixed grains for Ni-60Co alloy at different heat treatments

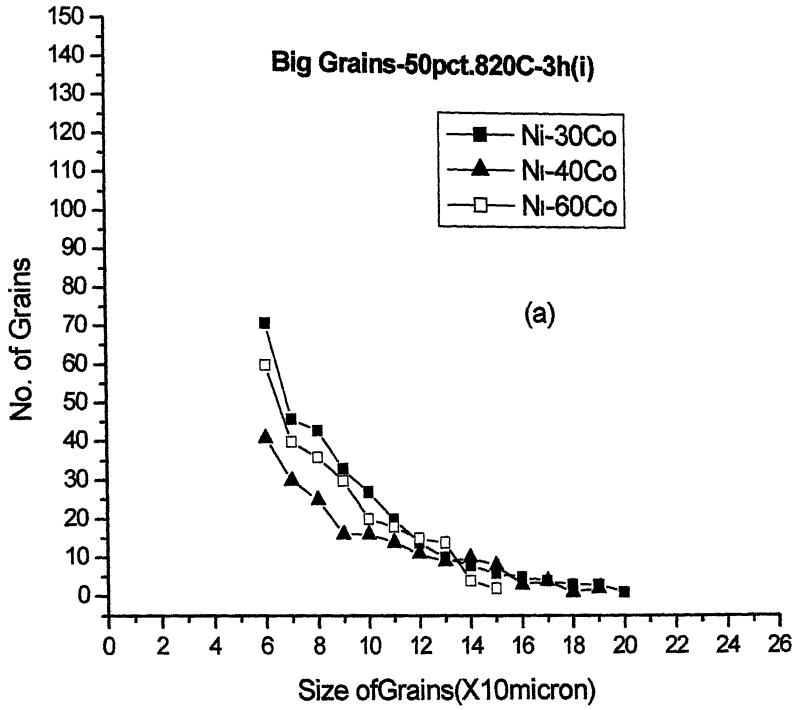

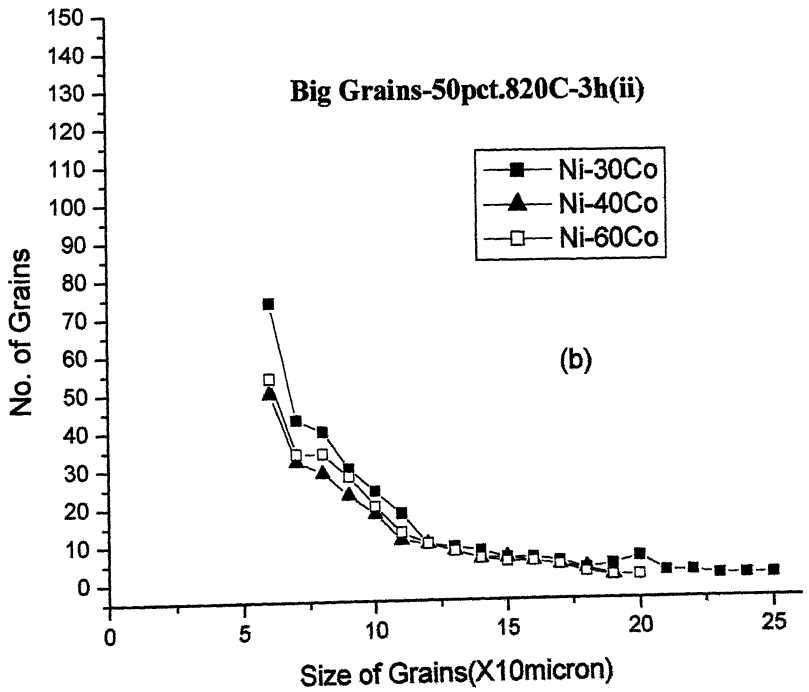

Fig. 54 (a) Plot of Number of grains vs. Size of Grains for the big grains for the heat treatment, 50pct.820°C-3h(i), for the three alloys
(b) Plot of Number of grains vs. Size of Grains for the big grains for the heat treatment ,50pct.820°C-3h(ii), for the three alloys

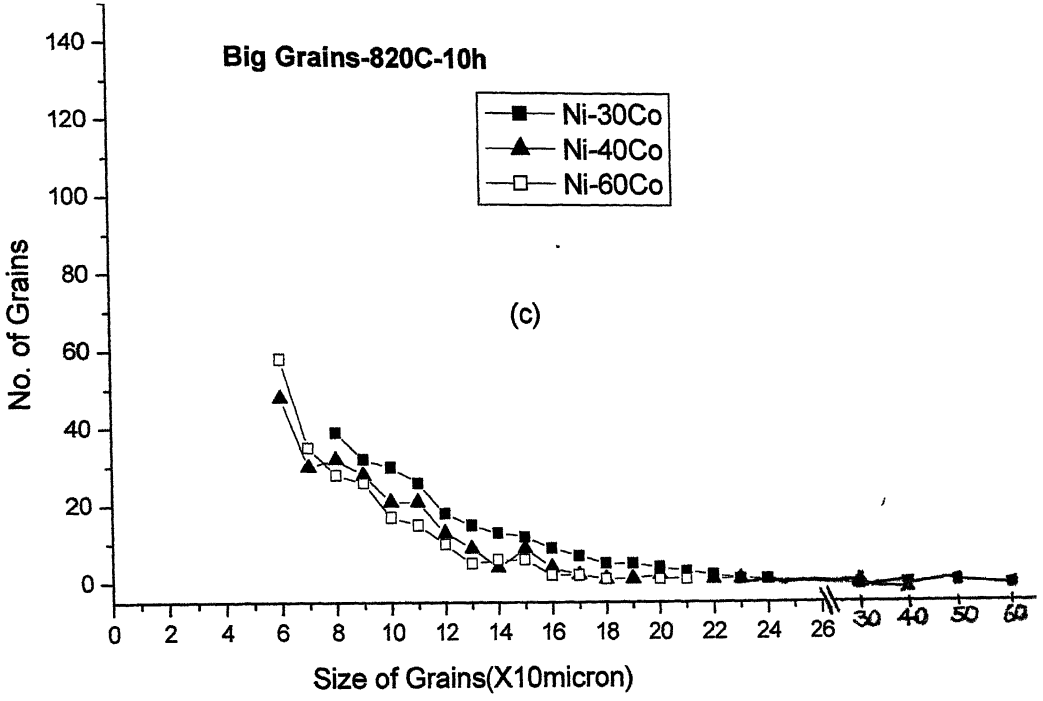

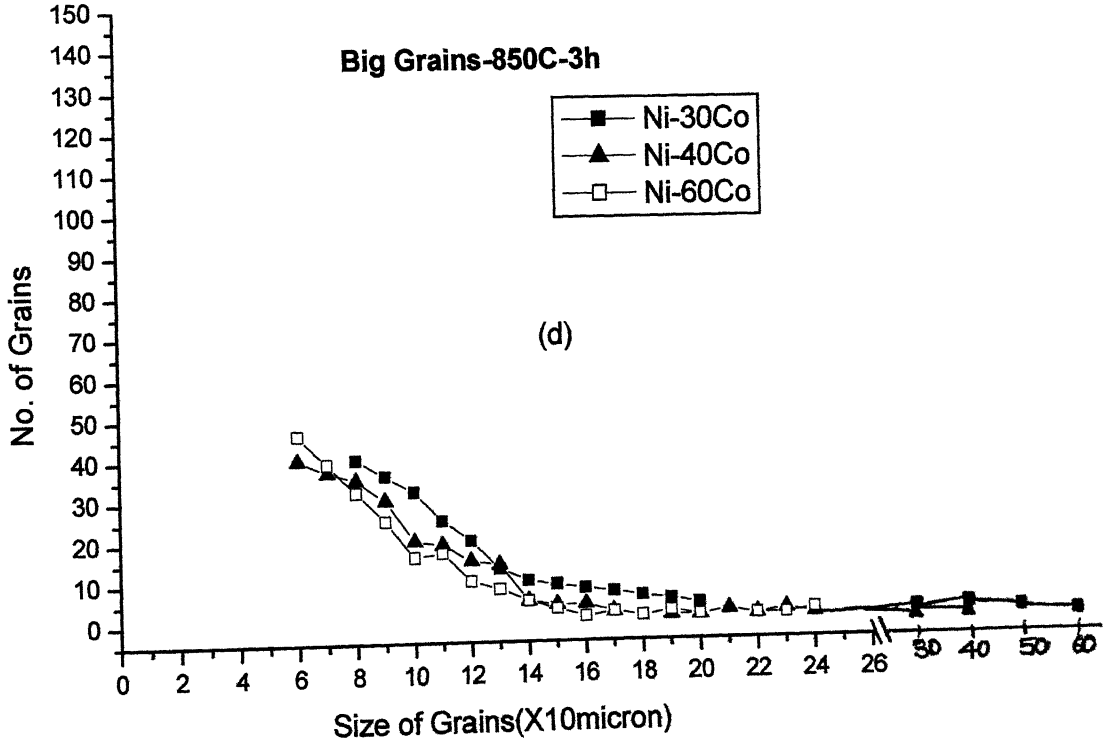

Fig. 54 (c) Plot of Number of grains vs. Size of Grains for the big grains for the heat treatment, Annealed-820°C-10h, for the three alloys
(d) Plot of Number of grains vs. Size of Grains for the big grains for the heat treatment ,Annealed-850°C-3h, for the three alloys

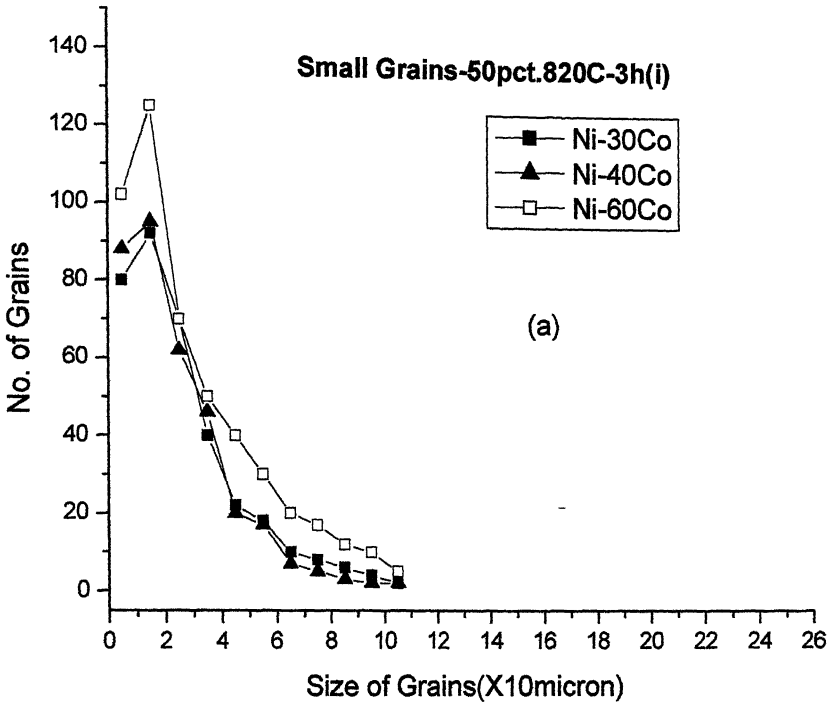

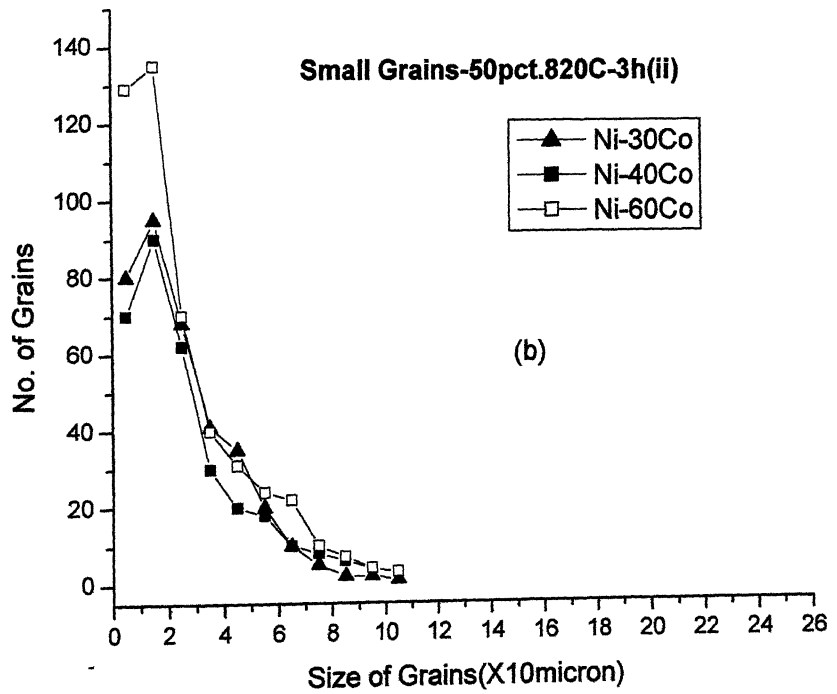

Fig. 55 (a) Plot of Number of grains vs. Size of Grains for the small grains for the heat treatment, 50pct.820°C-3h(i), for the three alloys
(b) Plot of Number of grains vs. Size of Grains for the small grains for the heat treatment , 50pct.820°C-3h(ii), for the three alloys

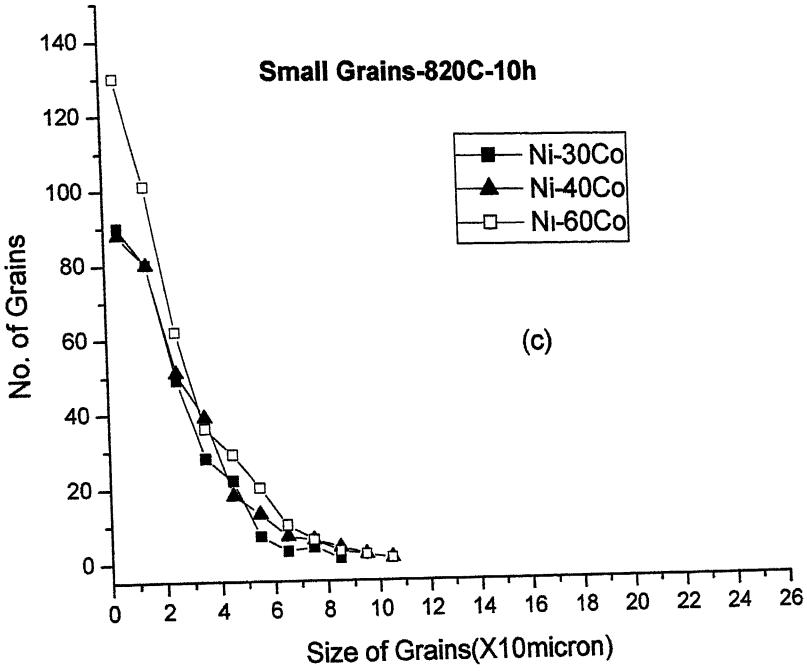

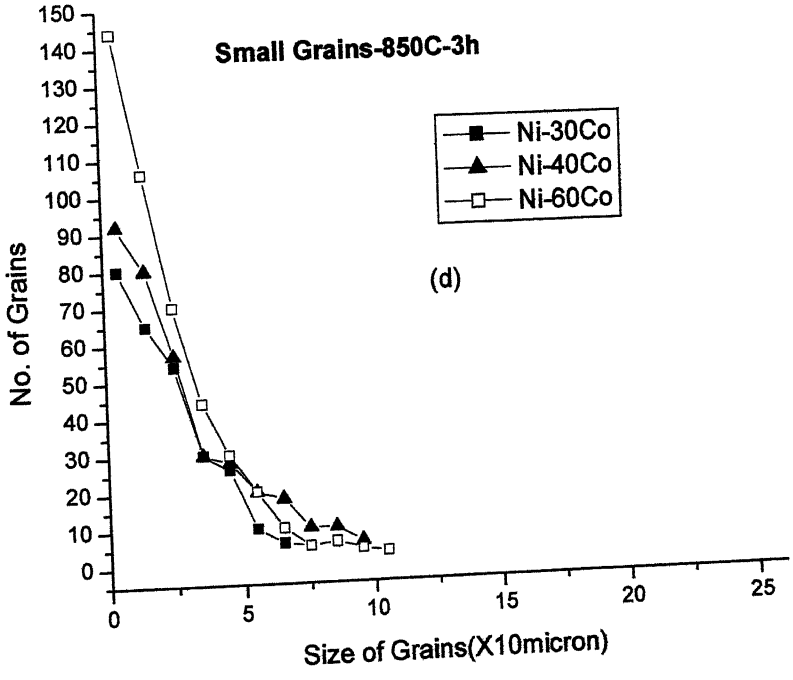

Fig. 55 (c) Plot of Number of grains vs. Size of Grains for the small grains for the heat treatment, Annealed-820°C-10h, for the three alloys
(d) Plot of Number of grains vs. Size of Grains for the small grains for the heat treatment ,Annealed-850°C-3h, for the three alloys

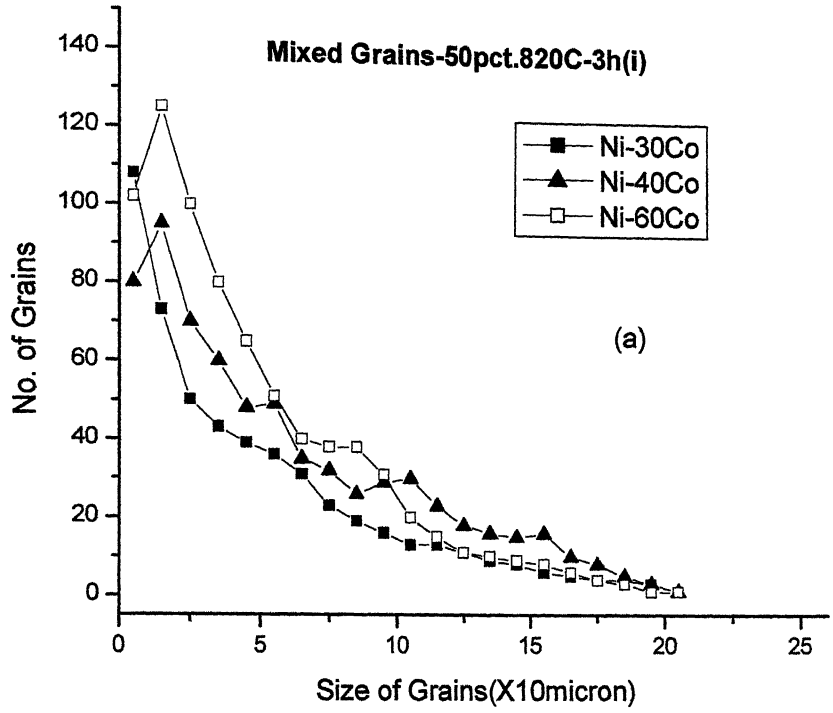

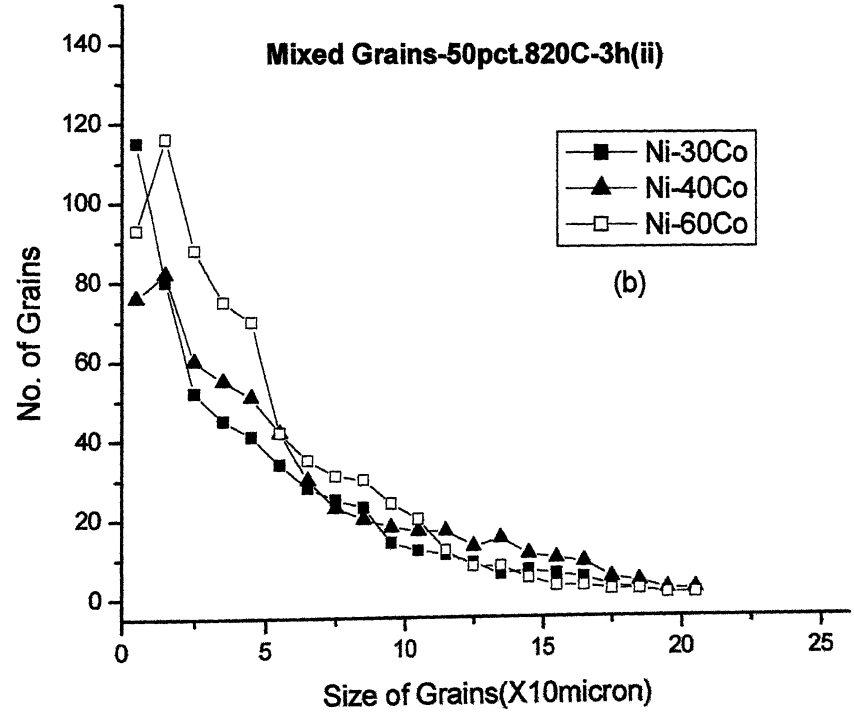

Fig. 56 (a) Plot of Number of grains vs. Size of Grains for the mixed grains for the heat treatment, 50pct.820°C-3h(i), for the three alloys
(b) Plot of Number of grains vs. Size of Grains for the mixed grains for the heat treatment, 50pct.820°C-3h(ii), for the three alloys

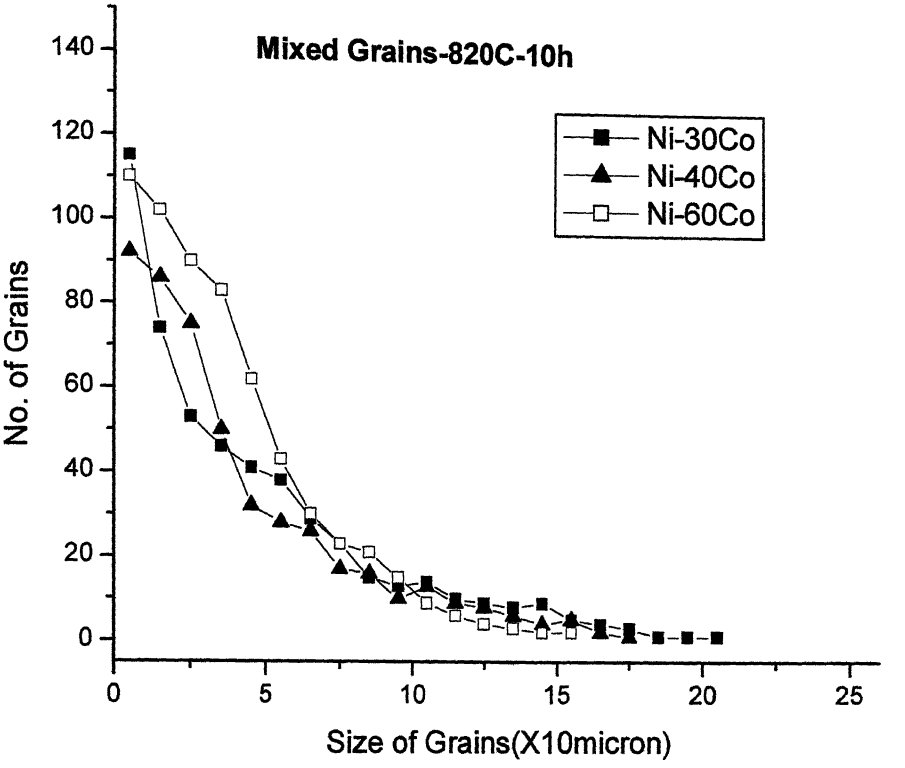

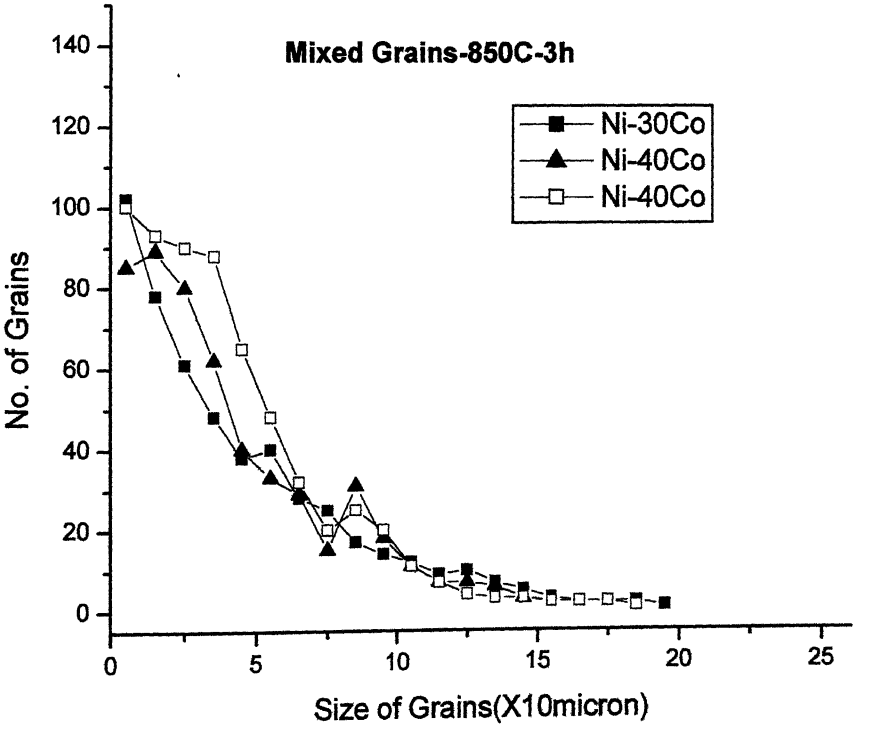

Fig. 56 (c) Plot of Number of grains vs. Size of Grains for the mixed grains for the heat treatment, Annealed-820°C-10h, for the three alloys

(d) Plot of Number of grains vs. Size of Grains for the mixed grains for the heat treatment ,Annealed-850°C-3h, for the three alloys

Chapter 5

DISCUSSION

The above results indicate that for all the three alloys and for all heat treatments, the small grains are persistent and it is almost impossible to remove them. Although in Ni-30Co alloy , the volume fraction of the small grains is least than in other alloys for all the heat treatments, still their fraction is significant.

For any alloy, it was expected that on increasing annealing time and annealing temperature, the volume fraction of big grains because of their size advantage will increase, however, it has been observed that reverse is the case indicating that smaller grains growing at the expense of big grains. This kind of phenomenon is normally observed during 'tertiary recrystallisation'. Tertiary recrystallisation refers to the situation where growth of small grains in a favorable orientation takes place at the expense of a matrix consisting of much larger grains. The driving force for this phenomenon to occur is the difference in surface energies. However the temperature regime and the time periods involved are on the lower side and therefore the occurrence of secondary and tertiary recrystallisation is precluded. On the other hand, a possible explanation of this behavior could be the orientation dependence of grain boundary mobility of the grains. It is known that in fcc metals and alloys, an oriented relationship giving maximum growth rate is characterized by $30^0 - 40^0$ rotation about a common <111> direction.
It should be possible to verify this using 'Orientation imaging microscope' where both microstructural details and the corresponding orientations can be simultaneously determined.

The grain size distribution plots for the Ni-30Co alloy- whether for big, small or mixed grains (Figures 45,46,47) do not show much of a variation as a function of heat treatment. The differences in the distribution plots, as a function of heat treatment, is more in Ni-40Co alloy (mixed grains) and Ni-60Co alloy (big and mixed grains). Figures 54(a), (b) and (c) clearly indicate that the secondary recrystallisation process

[50pct.820°C-3h(ii)] or longer annealing time [Annealed-820°C-10h] leads to a definite increment in the sizes of big grains for the Ni-30Co alloy. The same figures and Fig.54(d) again show that for the Ni-60Co alloy the sizes of big grains increase both with longer annealing times and higher annealing temperature. However, in both these alloys no significant increase in the overall size of the small grains was observed [Figures55(a) to (d)] as function of annealing temperature or time. These results taken with the results of table4.5, where the volume fractions of the small grains increase substantially with higher annealing time and temperature, clearly indicate that within the colonies of small grains, the ones with the largest grain size do not enlarge. It is the grains having the smaller sizes in the colonies must be increasing in size, causing an overall increase in the volume fractions of small grain colonies. This means that within the small grain colonies also their could be a competition between the smaller sized and bigger sized grains for growth, and it appears as though the smaller sized grains in the colonies have a better chance of growing. Therefore, what has been observed on a macroscopic scale, between the big grains in the matrix and small grains in the colonies, seems to persist on a micro-scale within the colonies of the small grains also.

Figures 55(a) to (d) show an interesting phenomenon. It appears that the plots of grain size distribution (for the smaller grains) for Ni-60Co alloy always lie above these for the other two. The differences between the corresponding plots for the Ni-30Co and Ni-40Co alloy are not that significant, although the plots of the former lie somewhat below the plots of the latter. This clearly shows that the grains in the small grain colonies are much finer in the Ni-60Co alloy, as compared to the other two. The sizes of the grains in the small grain colonies of Ni-30Co and Ni-40Co alloy are only marginally different and these are larger than in the case of the Ni-60Co alloy. The above differences persist for all the four different heat treatments. Evidently this phenomenon can be ascribed to the effect of the solute Co in these alloys.

Figures 54(a) to (d) indicate, however, that the above is not the case, so far as the big grains are concerned. The grain sizes in this regime are definitely finer in the case of the

Ni-30Co alloy than in the other two. In face, within this regime, the grain sizes of other two alloys, Ni-40Co and Ni-60Co, are coarser than in Ni-30Co.

Considering the plots for the mixed grains, however, [Figures 56(a) to (d)] it is at once clear that overall grain sizes are finest for the Ni-60Co alloy, followed by Ni-40Co alloy. The Ni-30Co alloy appears to have the coarsest overall grain size, as compared to the other two irrespective of the heat treatment. Clearly, this is an effect of solute content, i.e. Co concentration in these alloys. Higher amount of Co in the alloys tends to make the grain size finer. An explanation of this phenomenon can be given on the basis of stored energy during cold work. On increasing alloying i.e. Co content, the energy stored in the alloy after cold work increases. As we know that larger is the stored energy, more will be the nucleation rate, and so in the Ni-60Co alloy the rate of nucleation will be the largest and it will have largest number of small grains.

So far as the effect of heat treatment on the overall grain size distribution is concerned, Figure 47, 50 and 53 clearly show that these distributions are affected much more in Ni-40Co and Ni-60Co alloy, where higher annealing temperature and time seem to increase the grain size perceptibly. This increase, however is much less in case of Ni-30Co alloy, which to start with, has largest grain size among the three alloys.

CONCLUSIONS

1. For all the three alloys, and for all the heat treatments used, the microstructures are of duplex type, comprised of colonies of small grains embedded in the matrix of big grains.
2. It was observed that for all the heat treatments, the number of the grains are the largest for Ni-30Co alloy. The grain size is decidedly finer for the other two alloys, the grain size of the Ni-60Co alloy being the least.
3. The effects of annealing time or the annealing temperature , within the range used in the investigation, have no major effect on the grain size distribution in these three alloys.
4. Close observations of the results indicate that the grains with finer sizes in the small grain colonies grow faster than their counterparts in the colonies with relatively coarse sizes.
5. On a somewhat macro scale, the volume fractions of colonies of small grains increase, in comparison to the big matrix grains, as temperature or time of annealing increase.
6. The above two phenomena could be due to the orientation dependence of grain boundary mobility. This aspect could not be verified in the present work.
7. Addition of Co to Ni seems to decrease the grain size of recrystallised grains as well as their rate of growth during annealing.

REFERENCES

1. G. Wassermann, Z.Metallk., 54, 61(1963)

2. G.Gordan, Trans. A.I.M.E, 289, 23, (1954)

3. A.S.Keh , Direct Observation of Imperfections in Crystals, NY, (Interscience) (1962)

4. J.C.M.Li, Recrystallisation ,Grain Growth and Textures, 45, ASM Metals Park, Ohio (1966)

5. E. Orwan , Comm. To Congress de La Societe Francies de La Metallurgie d'Octobre (1947)

6. R.W.Cahn, Progress in Metal Physics, 2, 151, (1950)

7. C.G.Dunn and F.Lionetti, Trans. A.I.M.E. , 185, 125, (1949)

8. C.G.Dunn, F.W.Daniels & M.J.Bolton, Trans. A.I.M.E., 188, 1245 (1950)

9. J.J.Gilman, Acta Metallurgica ,3, 277 (1955)

10. R.W.Cahn, Proc. Phy. Soc. , 63a, 323 (1950)

11.N.A.Bryshko, V.V.Gubernatarov, B.K.Sokolov, I.V.Gertvaseva and V.N.Gundyrev, Dokl.Akad.Nauk. SSSR, 255(6), 1367-1369

12. H.Hu, Textures in Research and Practice, (Proc. Of International Symposium at Clausthal – Zellerfeld), Ed. J.Grewen & G.Wasserman , 200 (1968)

13. H.Hu, Electron Microscopy and Strength of Crystals, 564, (1963) , London & Newyork (Interscience)

14. R.W.Cahn , Acta Met. , 10, 789, (1962)

15. B.B.Rath & H.Hu, Trans. A.I.M.E, 236, (1966)

16. R.W.Cahn , Recrystallisation of Metallic Materials, Ed. F.Hassener, 43, (1971)

17. J.C.M.Li , Journal of Applied Physics, 33, 2958 (1962)

18. W.T.Read , Dislocations in Crystals (1953), Newyork (Mc-Graw Hill)

19. N.A.Gjastein & F.N.Rhines, Acta Metallurgica, 7, 319 (1959)

20. J.E.Burke & D.Turnbull, Progress in Metal Physics, 3, 220 (1952)

21.F.B.Hirsch , Phil. Mag. , 7, 67 (1963)

22. J.E.Bailey & P.B.Hirsch, Proc. Royal Society, 267A (1962)

23. M.L. Kronberg & F.H.Wilson, Trans. A.I.M.E, 185, 501 (1949)

24. G.h.Bishop & B.Chalmers, Scripta Metallurgica, 2, 133 (1968)

25. J.W.Cahn , Acta Metallurgica , 10, 789 (1962)

26. R.K.Ray, PhD Thesis, March 1973, Univ. of Bermingham.

27. W.R.Hibbard and C.G.Dunn, 'Creep and Recovery', A.S.M., Clevel (1957)

28. H.Hu & A.Szurmae, Trans. A.I.M.E. , 221, 839 (1961)

29.H.Ahlborn, J.Grewen and G.Wassermann, Z.Metallkunde, 55, 598 (1964)

30.J.Grewen, A.Segmullar & G.Wassermann, Arch. Eisenhuttenwesen, 29, 119 (1958)

31. R.K.Ray, Trans. IIM, 38, No.3, 187 (1985)

32. R.K.Ray, "Rolling Textures of pure Nickel, Ni-Fe, & Ni-Co alloys', Acta Metall. ,43, No.10, 3861-3872, (1995)

33. R.D.Doherty, Metal Odlew, 5(2), 179-196, (1979)